

MODEL IMPROVEMENT AND
SUPERSATURATION CONTROL OF
CRYSTALLIZATION PROCESS FOR THE
CASE OF AGGLOMERATION AND
BREAKAGE

ZAKIRAH BT MOHD ZAHARI

UMP

MASTER OF SCIENCE

UNIVERSITI MALAYSIA PAHANG

UNIVERSITI MALAYSIA PAHANG

DECLARATION OF THESIS AND COPYRIGHT

Author's Full Name : Zakirah Bt Mohd Zahari

Date of Birth : 23rd September 1992

Title : Model Improvement and Supersaturation Control of
Crystallization Process For The Case of Agglomeration and
Breakage

Academic Session : 2017/2018

I declare that this thesis is classified as:

- CONFIDENTIAL (Contains confidential information under the Official Secret Act 1997)*
- RESTRICTED (Contains restricted information as specified by the organization where research was done)*
- OPEN ACCESS I agree that my thesis to be published as online open access (Full Text)

I acknowledge that Universiti Malaysia Pahang reserves the following rights:

1. The Thesis is the Property of Universiti Malaysia Pahang
2. The Library of Universiti Malaysia Pahang has the right to make copies of the thesis for the purpose of research only.
3. The Library has the right to make copies of the thesis for academic exchange.

Certified by:

(Student's Signature)

(Supervisor's Signature)

920923036020
New IC/Passport Number
Date: 15 August 2018

Noor Asma Fazli Bin Abdul Samad
Name of Supervisor
Date: 15 August 2018

SUPERVISOR'S DECLARATION

I/~~We~~* hereby declare that I/~~We~~* have checked this thesis/~~project~~* and in my/~~our~~* opinion, this thesis/~~project~~* is adequate in terms of scope and quality for the award of the degree of *~~Doctor of Philosophy/ Master of Engineering/~~ Master of Science

(Supervisor's Signature)

Full Name : DR NOOR ASMA FAZLI BIN ABDUL SAMAD

Position : SENIOR LECTURER

Date : 15 AUGUST 2018



UMP

STUDENT'S DECLARATION

I hereby declare that the work in this thesis is based on my original work except for quotations and citations which have been duly acknowledged. I also declare that it has not been previously or concurrently submitted for any other degree at Universiti Malaysia Pahang or any other institutions.

(Student's Signature)

Full Name : ZAKIRAH BT MOHD ZAHARI

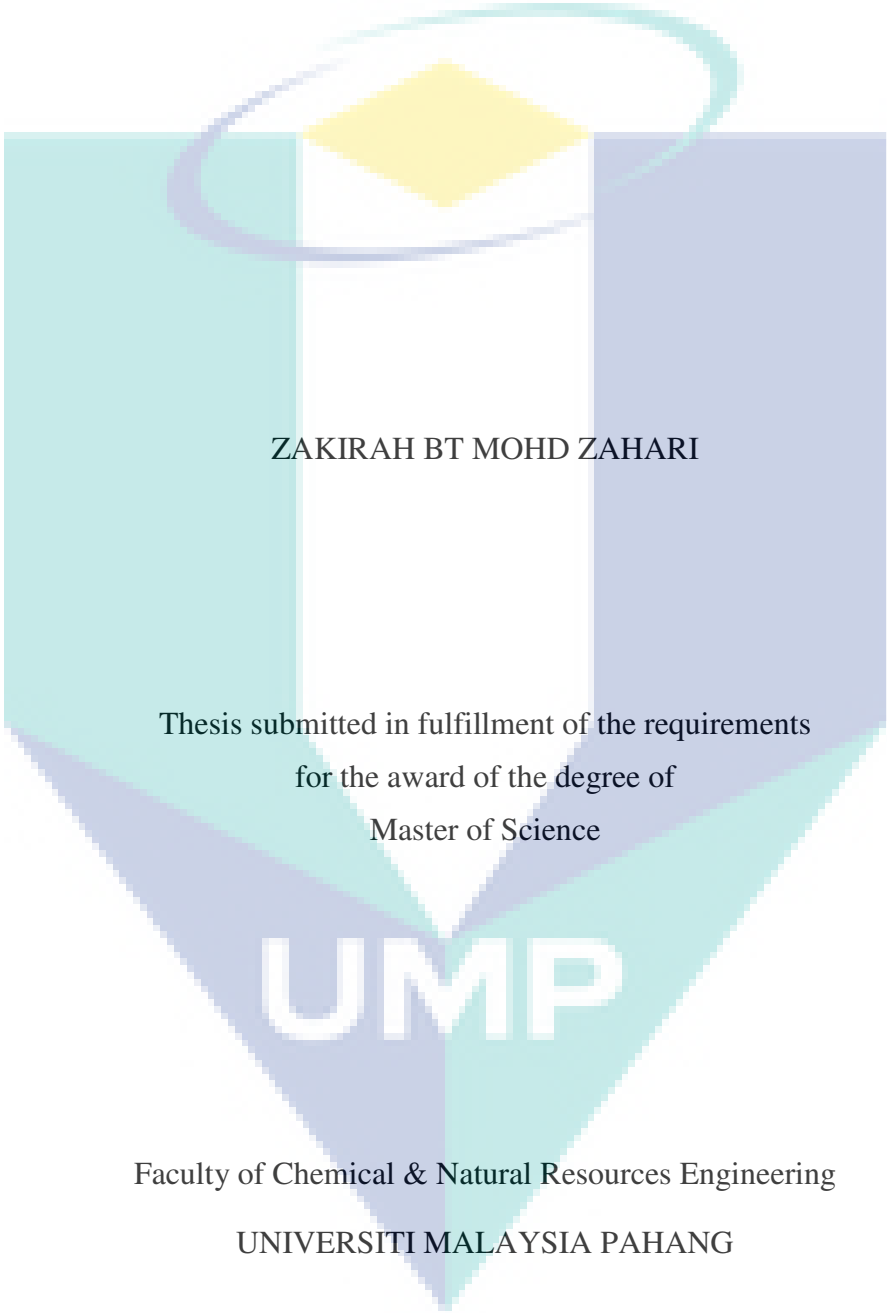
ID Number : MKC15035

Date : 15 AUGUST 2018



UMP

MODEL IMPROVEMENT AND SUPERSATURATION CONTROL OF
CRYSTALLIZATION PROCESS FOR THE CASE OF AGGLOMERATION AND
BREAKAGE



ZAKIRAH BT MOHD ZAHARI

Thesis submitted in fulfillment of the requirements
for the award of the degree of
Master of Science

UMP

Faculty of Chemical & Natural Resources Engineering

UNIVERSITI MALAYSIA PAHANG

AUGUST 2018

ACKNOWLEDGEMENTS

I would first like to express my special gratitude to my thesis advisor and my supervisor Dr. Noor Asma Fazli Bin Abdul Samad for his thoughtful guidance and motivation, his warm encouragement and unlimited knowledge sharing throughout this journey and for the useful comments, remarks and engagement through the learning process of this master thesis.

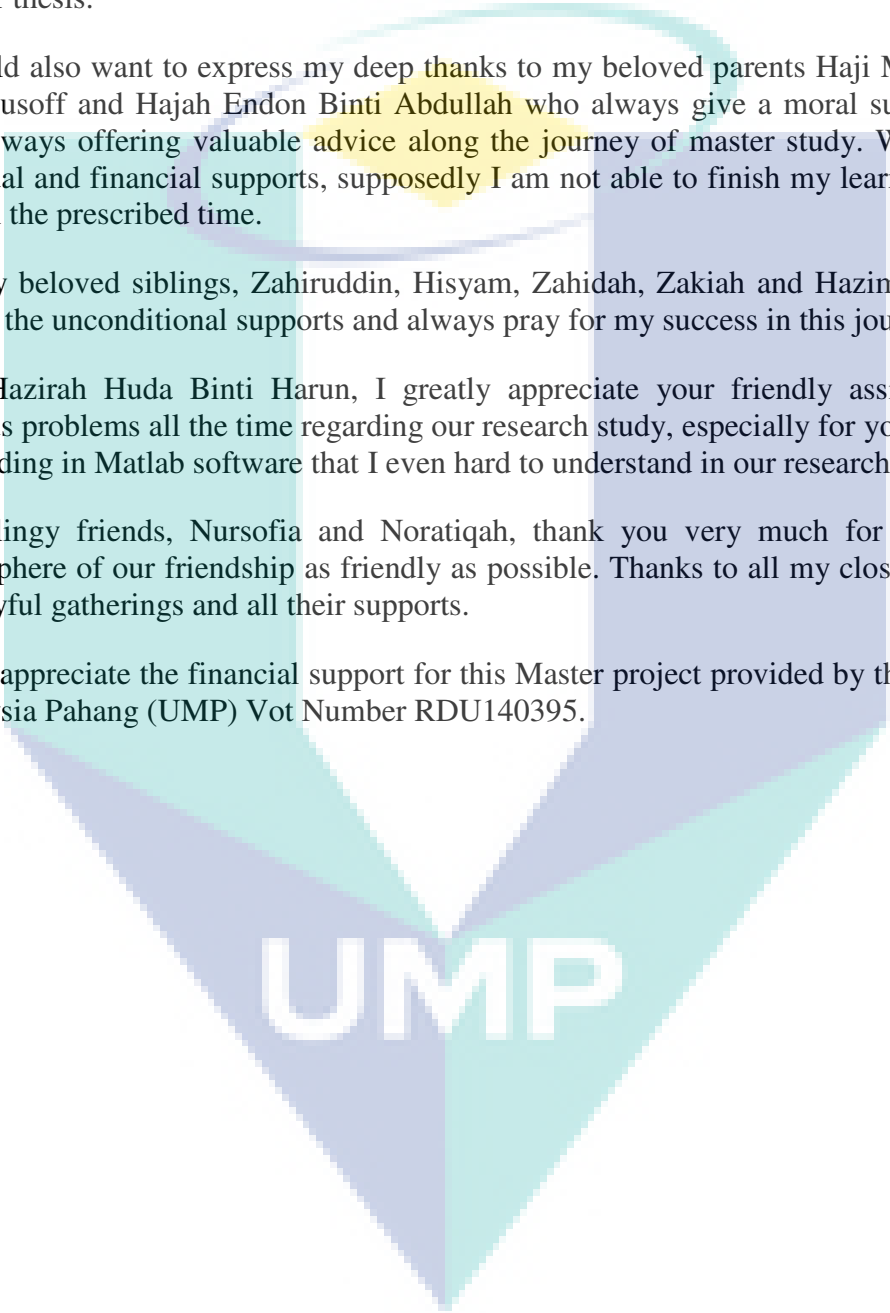
I would also want to express my deep thanks to my beloved parents Haji Mohd Zahari Bin Yusoff and Hajah Endon Binti Abdullah who always give a moral support, trust, and always offering valuable advice along the journey of master study. Without their spiritual and financial supports, supposedly I am not able to finish my learning process within the prescribed time.

To my beloved siblings, Zahiruddin, Hisyam, Zahidah, Zakiah and Hazim, thank you for all the unconditional supports and always pray for my success in this journey.

Nur Hazirah Huda Binti Harun, I greatly appreciate your friendly assistance with various problems all the time regarding our research study, especially for your help with the coding in Matlab software that I even hard to understand in our research area.

My clingy friends, Nursafia and Noratiqah, thank you very much for making the atmosphere of our friendship as friendly as possible. Thanks to all my close friends for the joyful gatherings and all their supports.

I also appreciate the financial support for this Master project provided by the Universiti Malaysia Pahang (UMP) Vot Number RDU140395.



UMP

ABSTRAK

Proses penghabluran adalah salah satu kaedah untuk memisahkan komponen pepejal-cecair dalam industri kimia dan farmaseutikal kerana hasil hablur yang berkualiti tinggi dapat dihasilkan. Kriteria utama bagi hasil hablur selalunya dinilai dari segi taburan saiz hablur. Bagi mendapatkan taburan saiz hablur yang dikehendaki, kawalan lebih tepuan boleh digunakan untuk mengawal komposisi pada set titik yang ditetapkan. Selalunya, kaedah yang digunakan adalah berdasarkan kaedah cuba dan jaya bagi mendapatkan trajektori set titik tetapi ia tidak menjamin untuk mendapatkan taburan saiz hablur yang diperlukan. Selain itu operasi penghabluran hanya melibatkan fenomena penghasilan nuklei dan tumbesaran hablur dengan mengabaikan kesan percantuman dan pemecahan. Oleh itu, objektif utama kerja ini adalah untuk membina gerak kerja berdasarkan model yang sistematik bagi keupayaan kawalan dalam proses penghabluran secara penyejukan berkelompok. Melalui gerak kerja ini, ia mampu untuk meramal parameter setiap kinetik untuk mewakili proses penghabluran, menghasilkan set titik melalui peramal taburan saiz hablur yang telah dilanjutkan secara analitikal dan menguji kemampuan kawalan seperti penjejakan set titik, penolakan gangguan dan analisis ketidakpastian untuk mencapai kawalan yang jitu. Aplikasi bagi gerak kerja secara model ini dijalankan menggunakan dua kajian kes yang berbeza. Kajian kes yang pertama melibatkan penghabluran potassium sulfat bagi kes yang melibatkan kebergantungan suhu pada penghasilan nuklei dan tumbesaran hablur. Selain itu kesan percantuman dan pemecahan dikaji dalam kes kajian kedua iaitu penghabluran sukrosa. Bagi kedua-dua kajian kes, parameter untuk setiap kinetik telah diramal dengan ketepatan yang baik semasa simulasi gelung terbuka. Berdasarkan set titik yang telah dihasilkan daripada peramal CSD secara analitikal yang telah dilanjutkan, kawalan yang digunakan berjaya memastikan operasi berada pada set titik yang diperlukan dan sasaran taburan saiz hablur berjaya di capai semasa simulasi gelung tertutup. Kawalan yang telah dibina untuk kedua-dua kajian kes kemudiannya menjalani penjejakan set titik dan penolakan gangguan. Pencapaian yang baik telah diperolehi berdasarkan kemampuan kawalan untuk menjejaki perubahan set titik dan menolak gangguan yang diperkenalkan semasa operasi dijalankan. Keupayaan kawalan dinilai seterusnya melalui analisis ketidakpastian. Dalam analisis ini, 6 input parameter tidak pasti bagi penghasilan nuklei dan tumbesaran hablur dipilih dalam kajian kes potassium sulfat dan 11 input parameter tidak pasti bagi penghasilan nuklei, tumbesaran hablur, percantuman dan pemecahan digunakan dalam kajian kes sukrosa. Melalui analisis ketidakpastian ini, kawalan yang dicadangkan bertindak secara agresif untuk mengekalkan operasi dan pada akhirnya variasi taburan saiz hablur yang rendah telah diperolehi untuk kedua-dua kajian kes. Ini menunjukkan proses kawalan yang dibina telah berjaya diuji untuk kes kebergantungan suhu pada penghasilan nuklei dan tumbesaran hablur serta kes kesan percantuman dan pemecahan yang membuktikan keupayaan dan kebolehpercayaan kawalan yang telah dibina untuk proses penghabluran ini.

ABSTRACT

Crystallization process is one of the methods for separating solid-liquid components in the chemical and pharmaceutical industries due to the fact that high quality of crystal products can be obtained. The main specifications of the crystal product are usually given in terms of crystal size distribution (CSD). In order to obtain the desired CSD, the supersaturation control can be applied to maintain the concentration at the desired set-point. Usually current practices point to trial and error method in order to find the set-point trajectory but it does not guarantee the achievement of the desired CSD. In addition, the crystallization operation usually involves only nucleation and crystal growth phenomena by neglecting the effects of agglomeration and breakage. Therefore, the main objective of this work is to develop a systematic model-based framework for robust supersaturation control in batch cooling crystallization. Through this framework, it is possible to predict the kinetic parameters for representing the crystallization operation, to generate set-point using extended analytical CSD estimator and to perform robustness testing such as set-point tracking, disturbance rejection and uncertainty analysis for achieving robust control. The applications of the model-based framework have been demonstrated through two different case studies. The first case study involves the potassium sulphate crystallization for the case of temperature dependence in nucleation and crystal growth. Meanwhile the effects of agglomeration and breakage is investigated on the sucrose crystallization case study. For both case studies, the necessary kinetic parameters are accurately predicted under open-loop simulation. Based on set-points generated from the extended analytical CSD estimator, the controller is successfully maintained the operation at the required set-point and the desired target CSD is achieved under closed-loop simulation. The developed controller for both case studies are then undergoing set-point tracking and disturbance rejection testing where a good performance has been obtained by judging the ability of the developed controller to adapt the set-point changes and its ability to reject the disturbance introduced to the operation. The robustness of the controller is further evaluated using uncertainty analysis. In this analysis, 6 uncertain input parameters of nucleation and crystal growth are used for potassium sulphate case study and 11 uncertain input parameters of nucleation, crystal growth, agglomeration and breakage are employed for sucrose crystallization. Through uncertainty analysis, it is shown that the proposed controller is performed aggressively to maintain the operation and in the end less variability of the CSD is obtained for both case studies. This shows that supersaturation control has been successfully developed and tested for the case temperature dependence in nucleation and crystal growth as well as the effects of agglomeration and breakage indicating a robust and reliable of the developed controller for this crystallization process.

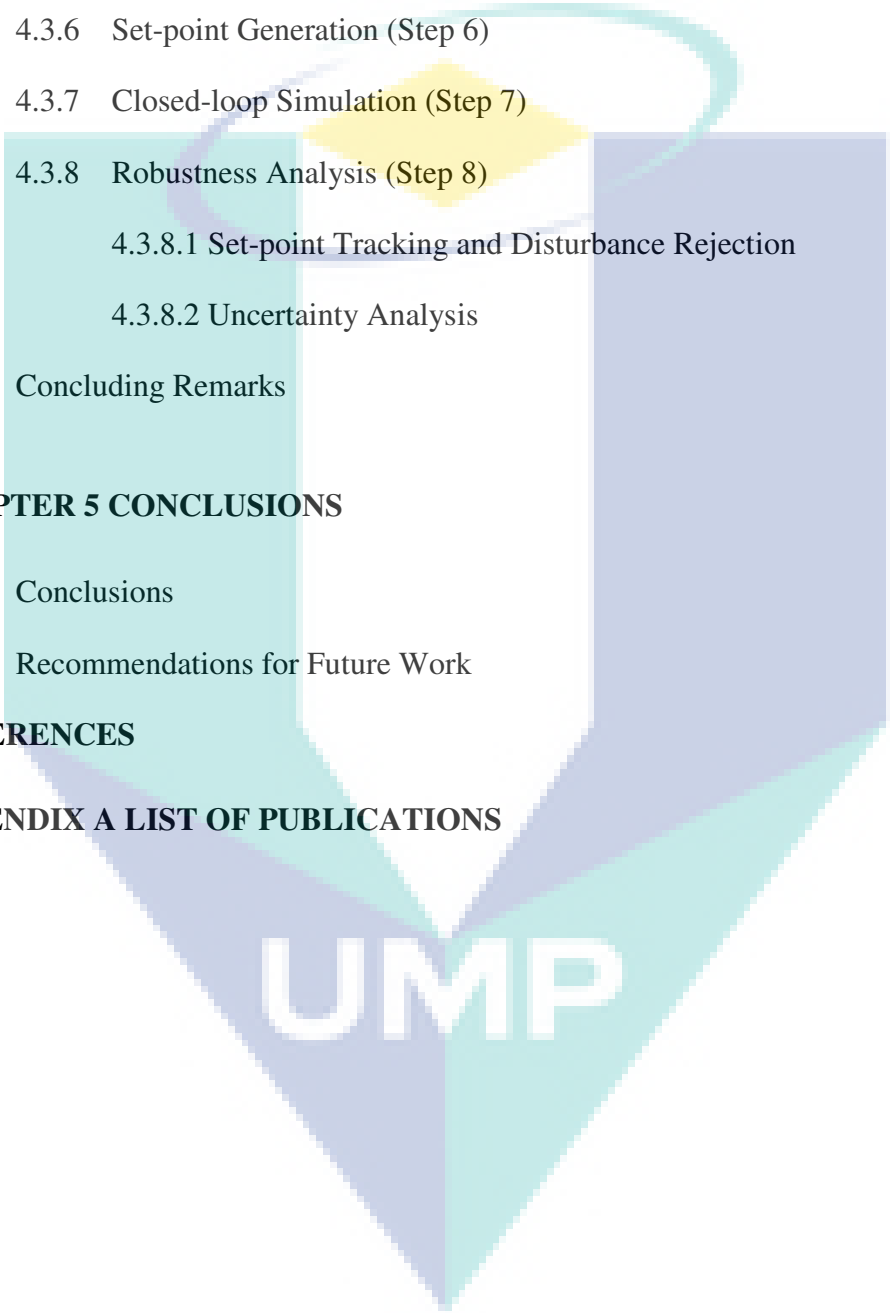
TABLE OF CONTENT

| | |
|--|------------|
| DECLARATION | |
| TITLE PAGE | i |
| ACKNOWLEDGEMENTS | ii |
| ABSTRAK | iii |
| ABSTRACT | iv |
| TABLE OF CONTENT | v |
| LIST OF TABLES | ix |
| LIST OF FIGURES | xi |
| LIST OF SYMBOLS | xiv |
| LIST OF ABBREVIATIONS | xix |
| CHAPTER 1 INTRODUCTION | 1 |
| 1.1 Motivation and Problem Statement | 1 |
| 1.2 Objectives of this Work | 4 |
| 1.3 Scopes of Work | 5 |
| 1.4 Significance of the Study | 6 |
| 1.5 Thesis Layout | 6 |
| CHAPTER 2 LITERATURE REVIEW | 8 |
| 2.1 Fundamental of Crystallization Process | 8 |
| 2.2 Phenomena in Crystallization Process | 11 |
| 2.2.1 Nucleation | 11 |
| 2.2.2 Crystal Growth | 14 |

| | | |
|--|--|-----------|
| 2.2.3 | Agglomeration and Breakage | 15 |
| 2.3 | Types of Operation in Crystallization Process | 17 |
| 2.4 | Modeling of Crystallization Process | 19 |
| 2.4.1 | Population Balance Equation | 19 |
| 2.4.1.1 | Method of Moments | 21 |
| 2.4.1.2 | Method of Classes | 21 |
| 2.4.2 | Overall Mass Balance | 22 |
| 2.4.3 | Energy Balances | 22 |
| 2.5 | Operation and Control | 23 |
| 2.6 | Robustness Issue | 29 |
| 2.7 | Concluding Remarks | 31 |
| CHAPTER 3 METHODOLOGY FOR ROBUST SUPERSATURATION CONTROL IN BATCH COOLING CRYSTALLIZATION PROCESS | | 33 |
| 3.1 | Introduction | 33 |
| 3.2 | Systematic Model-based Framework for Robust Supersaturation Control in Batch Cooling Crystallization Process | 33 |
| 3.2.1 | Problem Definition (Step 1) | 35 |
| 3.2.2 | Process and Product Specifications (Step 2) | 35 |
| 3.2.3 | Development of Mathematical Model (Step 3) | 36 |
| 3.2.3.1 | Population Balance Equation (PBE) Formulation | 36 |
| 3.2.3.2 | Overall Mass Balance Formulation | 38 |
| 3.2.3.3 | Energy Balance Formulation | 38 |
| 3.2.3.4 | Cooling Jacket Energy Balance Formulation | 39 |
| 3.2.3.5 | Selection of Constitutive Equations | 39 |

| | | |
|---|--|-----------|
| 3.2.4 | Model Identification (Step 4) | 40 |
| 3.2.5 | Open-loop Simulation (Step 5) | 41 |
| 3.2.6 | Set-point Generation (Step 6) | 42 |
| 3.2.7 | Closed-loop Simulation (Step 7) | 46 |
| 3.2.8 | Robustness Analysis (Step 8) | 47 |
| 3.2.8.1 | Set-point Tracking and Disturbance Rejection | 47 |
| 3.2.8.2 | Uncertainty Analysis | 47 |
| 3.3 | Concluding Remarks | 49 |
| CHAPTER 4 APPLICATION OF ROBUST SUPERSATURATION CONTROL IN BATCH COOLING CRYSTALLIZATION PROCESS | | 50 |
| 4.1 | Overview | 50 |
| 4.2 | Application of the Model-based Framework: Potassium Sulphate Crystallization Process | 50 |
| 4.2.1 | Problem Definition (Step 1) | 50 |
| 4.2.2 | Process and Product Specifications (Step 2) | 51 |
| 4.2.3 | Development of Mathematical Model (Step 3) | 51 |
| 4.2.4 | Model Identification (Step 4) | 54 |
| 4.2.5 | Open-loop Simulation (Step 5) | 55 |
| 4.2.6 | Set-point Generation (Step 6) | 60 |
| 4.2.7 | Closed-loop Simulation (Step 7) | 61 |
| 4.2.8 | Robustness Analysis (Step 8) | 66 |
| 4.2.8.1 | Set-point Tracking and Disturbance Rejection | 67 |
| 4.2.8.2 | Uncertainty Analysis | 69 |
| 4.3 | Application of Model-based Framework: Sucrose Crystallization Process | 76 |
| 4.3.1 | Problem Definition (Step 1) | 76 |

| | | |
|--|--|------------|
| 4.3.2 | Process and Product Specifications (Step 2) | 77 |
| 4.3.3 | Development of Mathematical Model (Step 3) | 77 |
| 4.3.4 | Model Identification (Step 4) | 79 |
| 4.3.5 | Open-loop Simulation (Step 5) | 81 |
| 4.3.6 | Set-point Generation (Step 6) | 84 |
| 4.3.7 | Closed-loop Simulation (Step 7) | 86 |
| 4.3.8 | Robustness Analysis (Step 8) | 92 |
| | 4.3.8.1 Set-point Tracking and Disturbance Rejection | 92 |
| | 4.3.8.2 Uncertainty Analysis | 94 |
| 4.4 | Concluding Remarks | 99 |
| CHAPTER 5 CONCLUSIONS | | 101 |
| 5.1 | Conclusions | 101 |
| 5.2 | Recommendations for Future Work | 103 |
| REFERENCES | | 105 |
| APPENDIX A LIST OF PUBLICATIONS | | 112 |



UMP

LIST OF TABLES

| | | |
|-----------|---|----|
| Table 2.1 | Summary of supersaturation constitutive model | 8 |
| Table 2.2 | Summary of nucleation kinetic model equation in crystallization process | 13 |
| Table 2.3 | Summary of crystal growth kinetic model equation in crystallization process | 14 |
| Table 2.4 | Production-reduction model in crystallization process | 16 |
| Table 2.5 | Comparison between batch and continuous process | 18 |
| Table 2.6 | Analytical CSD estimator expressions for one- and two-dimensional crystallization | 27 |
| Table 3.1 | Generic equation for one-dimensional PBE | 36 |
| Table 3.2 | Solution equations of one-dimensional PBE using method of moments | 36 |
| Table 3.3 | Solution equations of one-dimensional PBE using method of classes | 37 |
| Table 3.4 | Overall mass balance for one-dimensional crystallization | 38 |
| Table 3.5 | Energy balance for one-dimensional crystallization | 39 |
| Table 3.6 | Cooling jacket energy balance for one-dimensional crystallization | 39 |
| Table 3.7 | List of constitutive equations for the one-dimensional model of crystallization | 40 |
| Table 3.8 | New extension of analytical CSD estimator expressions for one-dimensional crystallization | 44 |
| Table 4.1 | List of model equations for the one-dimensional model of potassium sulphate crystallization | 52 |
| Table 4.2 | Parameter values of potassium sulphate in batch cooling crystallizer | 53 |
| Table 4.3 | Estimated kinetic parameters for potassium sulphate crystallization | 55 |
| Table 4.4 | Analytical CSD estimator equation for potassium sulphate crystallization | 60 |
| Table 4.5 | Total number of crystals generated from different cooling strategies | 66 |

| | | |
|------------|---|----|
| Table 4.6 | Input uncertainties on nucleation and crystal growth rate parameters for potassium sulphate crystallization | 70 |
| Table 4.7 | Monte Carlo error for different number of samples | 71 |
| Table 4.8 | New PI controller parameters for potassium sulphate crystallization | 74 |
| Table 4.9 | List of model equations for the one-dimensional model for sucrose crystallization | 78 |
| Table 4.10 | Parameter values for sucrose crystallization | 79 |
| Table 4.11 | Estimated nucleation kinetic parameters for sucrose crystallization | 80 |
| Table 4.12 | Estimated crystal growth kinetic parameters for sucrose crystallization | 81 |
| Table 4.13 | Estimated production-reduction kinetic parameters for sucrose crystallization | 81 |
| Table 4.14 | Analytical CSD estimator for sucrose crystallization | 84 |
| Table 4.15 | Supersaturation set-point values for the seeded sucrose batch cooling crystallizer | 86 |
| Table 4.16 | Input uncertainties for sucrose crystallization | 94 |
| Table 4.17 | Monte Carlo error for different number of samples in the sucrose crystallization case study | 95 |
| Table 4.18 | New PI controller parameters for sucrose crystallization | 98 |

UMP

LIST OF FIGURES

| | | |
|-------------|--|----|
| Figure 1.1 | Example of crystal product | 1 |
| Figure 1.2 | Solubility curve and metastable zone | 2 |
| Figure 2.1 | Supersaturation in crystallization processes | 9 |
| Figure 2.2 | Growth of nuclei | 12 |
| Figure 2.3 | Nucleation phenomena classification | 12 |
| Figure 2.4 | Jacketed batch cooling crystallization process | 17 |
| Figure 2.5 | PBE solution techniques based on process operation characteristics | 21 |
| Figure 2.6 | Operating region for crystallization process | 24 |
| Figure 2.7 | Cooling policy for crystallization process | 25 |
| Figure 3.1 | Systematic model-based framework for robust supersaturation control in batch cooling crystallization process | 34 |
| Figure 3.2 | Specification of one-dimensional crystallization process | 35 |
| Figure 4.1 | Target CSD for potassium sulphate crystallization | 51 |
| Figure 4.2 | Initial seed distribution for potassium sulphate crystallization | 54 |
| Figure 4.3 | Temperature profiles under open-loop condition | 56 |
| Figure 4.4 | Potassium sulphate concentration profiles under open-loop condition | 56 |
| Figure 4.5 | Supersaturation profiles under open-loop condition | 56 |
| Figure 4.6 | Comparison of CSD under method of classes with linear cooling control for potassium sulphate | 58 |
| Figure 4.7 | Comparison standard method of moments and method of classes for zeroth moment | 59 |
| Figure 4.8 | Comparison standard method of moments and method of classes for third moment | 59 |
| Figure 4.9 | Potassium sulphate crystallization diagram | 61 |
| Figure 4.10 | Potassium sulphate concentration profiles in the closed-loop simulation | 62 |
| Figure 4.11 | Solution temperature profiles in the closed-loop simulation | 63 |
| Figure 4.12 | Supersaturation profiles in the closed-loop simulation | 63 |
| Figure 4.13 | Total crystal mass obtained in the closed-loop simulation | 63 |

| | | |
|-------------|---|----|
| Figure 4.14 | Evolution of CSD at (a) start of the operation, (b) 10 minutes, (c) 20 minutes and (d) end of operation | 64 |
| Figure 4.15 | CSD comparison using different cooling strategies | 65 |
| Figure 4.16 | Performance of PI controller based on set-point tracking in potassium sulphate crystallization process | 67 |
| Figure 4.17 | Performance of PI controller based on disturbance rejection in potassium sulphate crystallization process | 69 |
| Figure 4.18 | Example of the CSD model output based on 50 samples | 71 |
| Figure 4.19 | Effects of input uncertainties on the temperature for potassium sulphate crystallization | 72 |
| Figure 4.20 | Effects of input uncertainties on the concentration for potassium sulphate crystallization | 72 |
| Figure 4.21 | Effects of input uncertainties on the inlet water temperature for potassium sulphate crystallization | 73 |
| Figure 4.22 | Effects of input uncertainties on the CSD for potassium sulphate crystallization | 74 |
| Figure 4.23 | Effects of input uncertainties on (a) CSD obtained from old controller parameter, (b) CSD obtained from new controller parameter, (c) CSD representation from old controller parameter and (d) CSD representation from new controller parameter using mean, 10th percentile and 90th percentile | 75 |
| Figure 4.24 | Target CSD for sucrose crystallization | 77 |
| Figure 4.25 | (a) Temperature (b) Concentration (c) Mean size diameter (d) Agitation rate (e) Supersaturation (f) Total crystal mass profile of sucrose in water. | 82 |
| Figure 4.26 | Crystal size distribution at final time of 180 minutes | 84 |
| Figure 4.27 | Initial seed distribution for sucrose crystallization | 85 |
| Figure 4.28 | Sucrose crystallization diagram | 87 |
| Figure 4.29 | Sucrose concentration profiles in the closed-loop simulation for operational time of (a) 150 min, (b) 180 min, (c) 210 min. | 88 |
| Figure 4.30 | Temperature profiles of sucrose crystallization | 89 |
| Figure 4.31 | Final CSD of sucrose crystallization based on different operation times | 89 |

| | | |
|-------------|---|----|
| Figure 4.32 | Final CSD of sucrose crystallization using 180 minutes operation times | 91 |
| Figure 4.33 | Total crystal mass obtained for sucrose crystallization | 91 |
| Figure 4.34 | Mean size diameter for sucrose crystallization | 92 |
| Figure 4.35 | Performance of PI controller based on set-point tracking in sucrose crystallization process | 93 |
| Figure 4.36 | Performance of PI controller based on disturbance rejection in sucrose crystallization process | 93 |
| Figure 4.37 | Effects of input uncertainties on the temperature for sucrose crystallization | 96 |
| Figure 4.38 | Effects of input uncertainties on the concentration for sucrose crystallization | 96 |
| Figure 4.39 | Effects of input uncertainties on the inlet water temperature for sucrose crystallization | 97 |
| Figure 4.40 | Effects of input uncertainties on the CSD for sucrose crystallization | 97 |
| Figure 4.41 | Effects of input uncertainties on the CSD for sucrose crystallization before (left) and after retuning (right) | 98 |
| Figure 4.42 | Evaluation of input uncertainties on the CSD for sucrose crystallization in terms of mean, 10th percentile and 90th percentile before (left) and after (right) retuning | 99 |

UMP

LIST OF SYMBOLS

| | |
|-----------|--|
| A_1 | crystallizer's internal area (cm^2) |
| A_2 | crystallizer's external area (cm^2) |
| A_c | total area of particles (cm^2) |
| Ab | production-reduction order |
| a_i | tailor development coefficient |
| a_{i1} | polynomial coefficient for saturation concentration |
| a_{i2} | polynomial coefficient for metastable concentration |
| a_{i3} | polynomial coefficient for heat of crystallization |
| a_{xf} | tailor development coefficient |
| B | birth rate (number of particles/ $\text{cm}^3 \cdot \text{min}$) |
| B_{agg} | birth rate due to agglomeration (number of particles/ $\text{cm}^3 \cdot \text{min}$) |
| B_{br} | birth rate due to breakage (number of particles/ $\text{cm}^3 \cdot \text{min}$) |
| B_{nuc} | birth rate due to nucleation (number of particles/ $\text{cm}^3 \cdot \text{min}$) |
| $B_{n,1}$ | primary nucleation (number of particles/ $\text{cm}^3 \cdot \text{min}$) |
| $B_{n,2}$ | secondary nucleation (number of particles/ $\text{cm}^3 \cdot \text{min}$) |
| b | nucleation order |
| b_i | coefficient of the response model |
| b_{i1} | polynomial coefficient for saturation concentration |
| b_{i2} | polynomial coefficient for metastable concentration |
| b_{i3} | polynomial coefficient for heat of crystallization |
| b_{xi} | tailor development coefficient |
| c | solute concentration (g solute/g solvent) |
| c^{sat} | saturation concentration (g solute/g solvent) |
| c^{met} | metastable concentration (g solute/g solvent) |
| c_i | tailor development coefficient |
| c_{i1} | polynomial coefficient for saturation concentration |
| c_{i2} | polynomial coefficient for metastable concentration |
| c_{i3} | polynomial coefficient for heat of crystallization |
| C_p | heat capacity ($\text{J/g} \cdot ^\circ\text{C}$) |
| C_{pw} | water heat capacity ($\text{J/g} \cdot ^\circ\text{C}$) |
| C_{yj} | tailor development coefficient |

| | |
|-------------------------------|---|
| D | diffusivity of the solute (cm ² /min) |
| Diam | stirrer diameter (cm) |
| Diam _T | tank diameter (cm) |
| D | mean size diameter (μm) |
| D _{br} | death rate due to breakage (number of particles/cm ³ .min) |
| d _i | tailor development coefficient |
| d _{i1} | polynomial coefficient for saturation concentration |
| d _{i2} | polynomial coefficient for metastable concentration |
| d _{i3} | polynomial coefficient for heat of crystallization |
| d _{yj} | tailor development coefficient |
| F _{obj} | objective function |
| F _{win} | cooling water flow rate (cm ³ /min) |
| f | relative shape function of crystals |
| f _{ij} ^I | inlet crystal number flow in the length direction |
| f _{ij} ^{I'} | inlet crystal number flow in the width direction |
| f _{ij} ^O | outlet crystal number flow in the length direction |
| f _{ij} ^{O'} | outlet crystal number flow in the width direction |
| f _n | final population density function (number of particles/μm) |
| f _{n0} | initial population density function (number of particles/μm) |
| G _x | crystal growth rate in length direction (μm/sec) |
| G _y | crystal growth rate in width direction (μm/sec) |
| g _x | growth order in length direction |
| g _y | growth order in width direction |
| j | mass order at nucleation |
| k | number of considered variables (factors) |
| k _a | agglomeration rate constant in the diffusional growth regime (min) |
| k _b | kinetic coefficient for nucleation (number of particles/cm ³ .min.(g/cm ³) ^j (rpm) ^p) |
| k _{b0} | frequency factor of nucleation rate |
| k _d | mass transfer coefficient (cm/min) |
| k _{gx} | kinetic coefficient for crystal growth in length direction (μm/sec) |
| k _{g0} | frequency factor of crystal growth rate |
| k _{gy} | kinetic coefficient for crystal growth in width direction (μm/sec) |

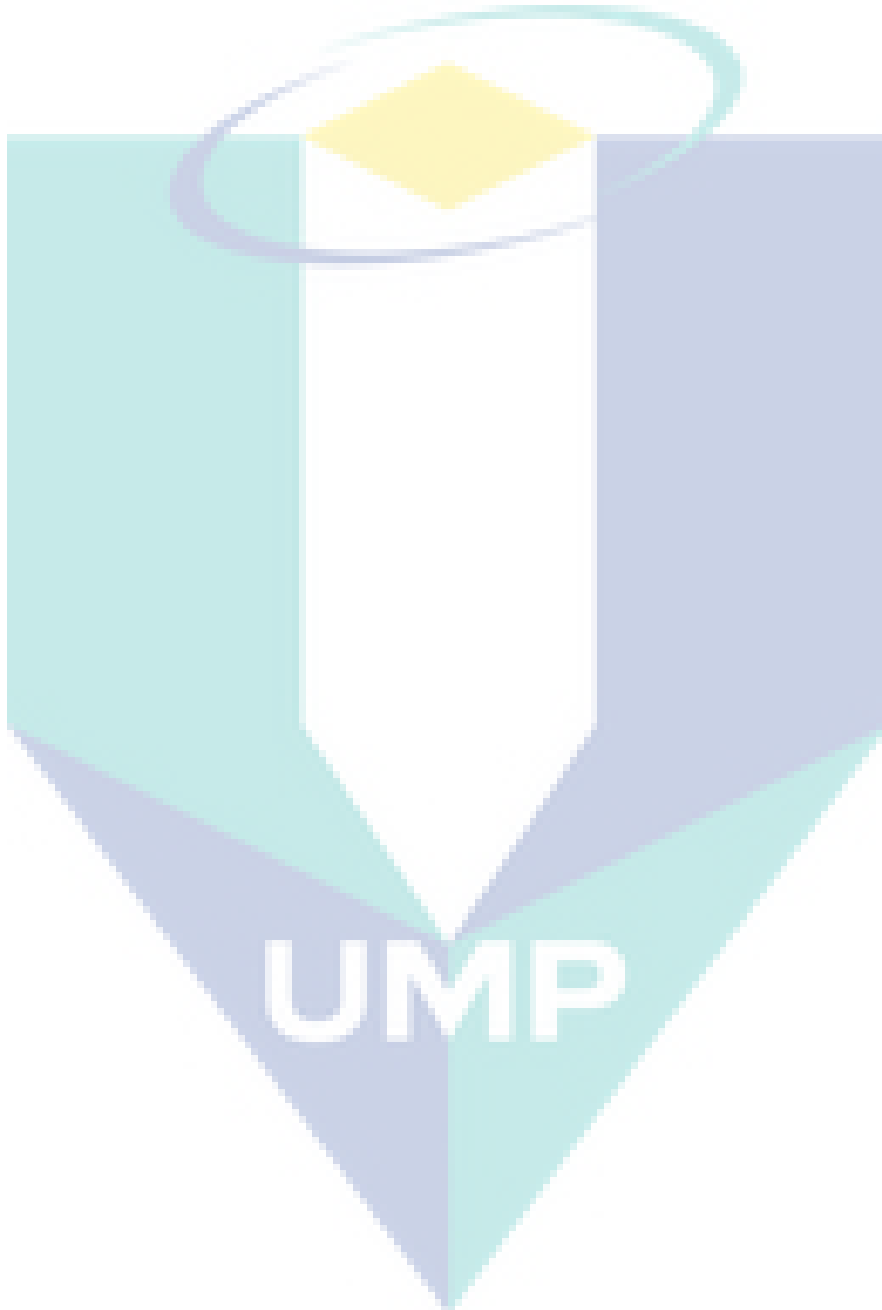
| | |
|------------------|--|
| k_A | crystal shape factor |
| k_L | crystal shape factor |
| k_{pr} | mass order at production-reduction |
| k_r | surface shape factor |
| k_v | crystal shape factor |
| L_x | length of crystal particles (μm) |
| L_{x0} | initial length of crystal particles (μm) |
| L_y | width of crystal particles (μm) |
| L_{y0} | initial width of crystal particles (μm) |
| L_c | total length of crystal particles (μm) |
| M_c | total crystal mass (g) |
| m | molal concentration of solute (moles solute/g solvent) |
| m^{sat} | molal concentration of solute at saturated solution (moles solute/g solvent) |
| m_w | mass of solvent (g) |
| N_c | total number of particles (number of particles) |
| N | number of classes |
| N_i | number of crystals per unit volume of suspension for class i (number of particles/ cm^3) |
| N_{ij} | number of crystals per unit volume of suspension for class i and j (number of particles/ cm^3) |
| N_{rpm} | agitation rate (rpm) |
| p | agitation order at nucleation |
| p_x | size dependent growth constant for length direction |
| p_y | size dependent growth constant for width direction |
| q | agitation order at crystal growth |
| R | ideal gas constant (J/mol.K) |
| r | agitation order at production-reduction |
| S | normal supersaturation (g solute/ g solvent) |
| S_r | Supersaturation ratio |
| S_{sp} | supersaturation set point (g solute/ g solvent) |
| S | mean crystal size (μm) |
| S_{xi} | mean size of class i (μm) |

| | |
|------------------|--|
| S_{yj} | mean size of class j (μm) |
| T | solution temperature ($^{\circ}\text{C}$) |
| T_{ex} | exterior temperature ($^{\circ}\text{C}$) |
| T_w | cooling water temperature ($^{\circ}\text{C}$) |
| T_{win} | inlet cooling water temperature ($^{\circ}\text{C}$) |
| t_c | total crystallization time (sec) |
| U_1 | heat transfer coefficient for internal crystallizer ($\text{J}/^{\circ}\text{C}\cdot\text{min}\cdot\text{cm}^2$) |
| U_2 | heat transfer coefficient for external crystallizer ($\text{J}/^{\circ}\text{C}\cdot\text{min}\cdot\text{cm}^2$) |
| V | solution volume (cm^3) |
| \bar{V} | mean crystal volume (cm^3) |
| V_c | crystal volume (cm^3) |
| V_w | cooling water volume (cm^3) |
| ν | kinematic viscosity (m^2/s) |
| x | mole fraction of solute |
| x^{sat} | mole fraction of solute at saturated solution |

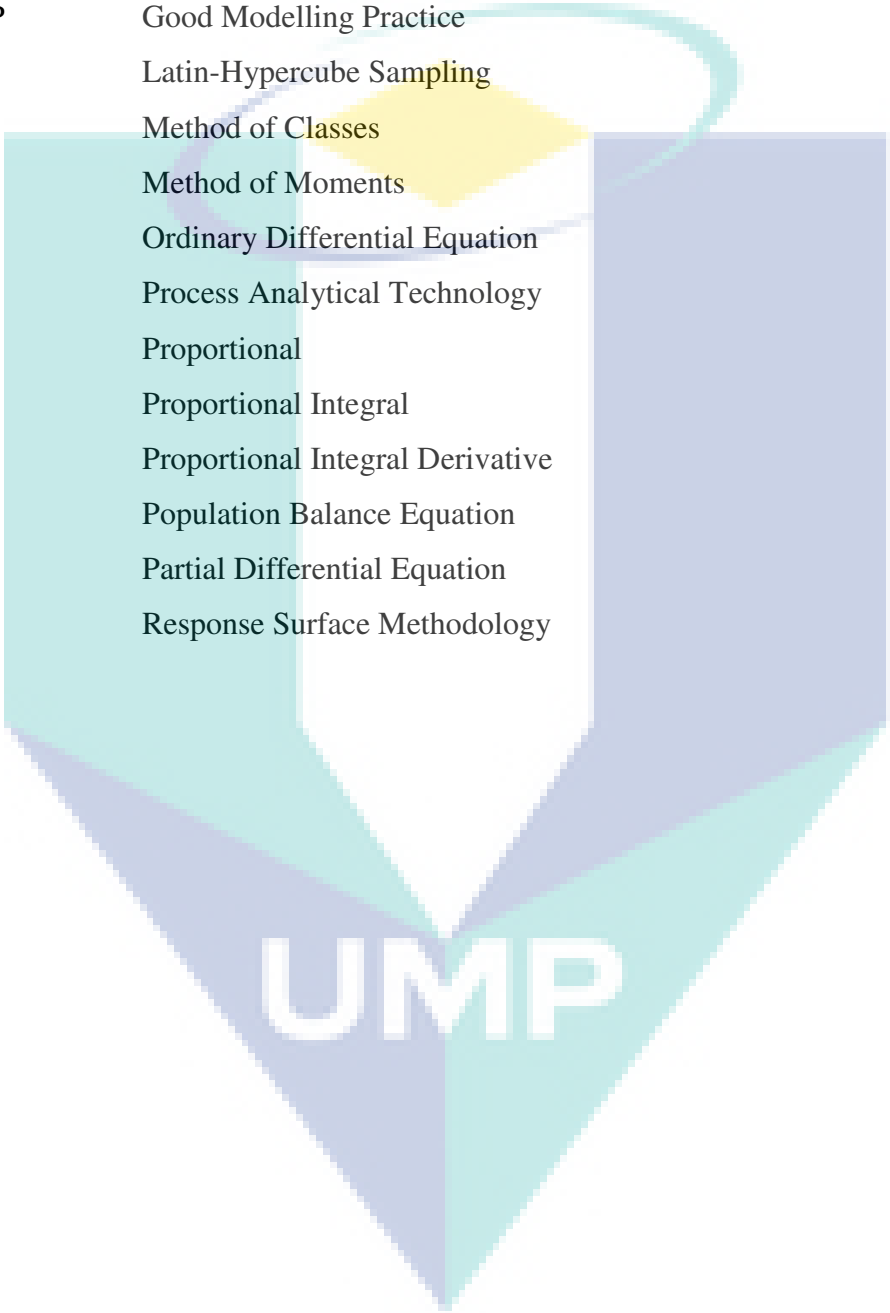
Greek letters

| | |
|--------------|--|
| α | production-reduction term (number of particles/ $\text{cm}^3\cdot\text{min}$) |
| μ_0 | zero th moment for one-dimensional PBE |
| μ_m | m^{th} for one-dimensional PBE |
| Δc_i | extent of i^{th} classes (μm) |
| Δc_j | extent of j^{th} classes (μm) |
| ΔE_b | activation energy for nucleation rate |
| ΔE_g | activation energy for crystal growth rate |
| ΔH_c | heat of crystallization (J/g) |
| Δc | concentration difference ($\text{g solute}/\text{g solvent}$) |
| σ | relative supersaturation |
| σ_x | standard deviation for length direction |
| σ_y | standard deviation for width direction |
| ζ | activity coefficient |
| ρ_c | crystal density (g/cm^3) |

| | |
|---------------|---|
| ρ_w | water density (g/cm^3) |
| γ_x | size dependent growth constant for length direction |
| γ_y | size dependent growth constant for width direction |
| η_r | effectiveness factor |
| ε | power dissipation per unit of mass ($\text{W}\cdot\text{m}^2/\text{kg}\cdot\text{s}^3$) |



LIST OF ABBREVIATIONS



| | |
|------|--|
| API | Active Pharmaceutical Ingredients |
| CSD | Crystal Size Distribution |
| ECDF | Empirical Cumulative Distribution Function |
| GMoP | Good Modelling Practice |
| LHS | Latin-Hypercube Sampling |
| MOC | Method of Classes |
| MOM | Method of Moments |
| ODE | Ordinary Differential Equation |
| PAT | Process Analytical Technology |
| P | Proportional |
| PI | Proportional Integral |
| PID | Proportional Integral Derivative |
| PBE | Population Balance Equation |
| PDE | Partial Differential Equation |
| RSM | Response Surface Methodology |

CHAPTER 1

INTRODUCTION

1.1 Motivation and Problem Statement

Crystallization is a solid-liquid separation process in which mass transfer of a solute from a liquid solution to a pure solid crystalline phase occurs (Myerson, 2002). Crystallization is a homogenous process where the solid particles are formed at the end of the process. Homogenous phase refers to a substance that contains only one kind of compounds or one element. The main specifications of the crystal product is high purity, a specific crystal size distribution (CSD), crystal size and shape as shown in Figure 1.1 (Zarabad and Rezvani, 2018; Perez-Calvo et al., 2016; Aamir, 2010).



Figure 1.1 Example of crystal product

Source: Aamir (2010)

At the industrial level, crystallization is often applied in the chemical industries as a method for purification and as a method for producing the crystalline materials at the desired size and shape (Wang et al., 2018). In addition the crystallization process is also applicable in the production of salts and active pharmaceutical ingredients (API) (Baino and Fiume, 2018; Gao et al., 2017; Derdour et al., 2017). Technically,

crystallization process can be divided into three methods which are cooling, evaporation, and anti-solvent addition (Lenka and Sarkar, 2018). The most common approach is by using the cooling method. The main advantage of cooling method is quality of the end product particularly the crystal size can be achieved consistently and thus it is widely used in the chemical and pharmaceutical industries (Artusio and Pisano, 2018; Ghadipasha et al., 2018; Abbas and Romagnoli, 2007). In crystallization process, batch cooling operation is often conducted rather than continuous because this allows greater operation flexibility and shorter process development (Powell et al., 2016). The main driving force in the crystallization process is the supersaturation which drives the solid phase out of the crystallization solution. During the crystallization process there are also nucleation and crystal growth phenomena which have direct influences on the final crystal product. Both nucleation and crystal growth are function of supersaturation and thus maintaining the supersaturation level is the main challenge in the crystallization process.

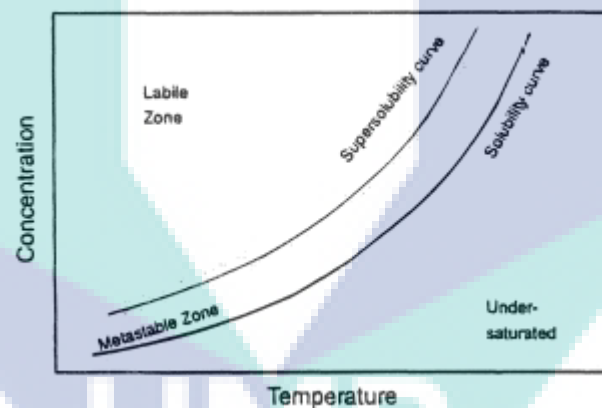


Figure 1.2 Solubility curve and metastable zone

Source: Myerson (2002)

In many crystallization processes, the main problem is how to obtain a uniform and reproducible crystal size distribution (CSD) (Perez-Calvo et al., 2016; Vetter et al., 2014; Park and Yeo, 2012; Widenski et al., 2010). In order to achieve a uniform and a desired CSD, it is essential to maintain the crystallization operation at its set-point. Usually the set-point is targeted within the metastable zone which is bounded by the saturation (solubility curve) and metastable concentrations (supersolubility curve) as shown in Figure 1.2. This is due to the fact that if the crystallisation operation exceeds the metastable concentration then, the high supersaturation is expected which results in

excessive nucleation. The excessive nucleation is undesirable in the crystallisation operation because the new crystals produced usually are considered fine particles at relatively small size. The production of these new crystals also affect the downstream process which is fouling problem. If the crystallization operation is operated below or near saturation line then the low or zero supersaturation is achieved and low crystal growth is expected. As consequence a crystal product at relatively small size is obtained by the end of operation.

For the purpose of maintaining the operation, a supersaturation control is often applied to drive the process within the metastable zone in order to enhance the control of the CSD (Gao et al., 2017; Amini et al., 2016; Gernaey et al., 2012). In order to implement the supersaturation control in the crystallization process, the set-point trajectory needs to be designed to lie within the metastable zone. Here the set-point trajectory, which in fact consists of both the supersaturation and the total batch time needed to complete the crystallization operation, can be determined using an analytical CSD estimator (Samad et al., 2013). Analytical CSD estimator is used to generate supersaturation set-point that yields a target CSD, given the initial seed distribution and growth kinetics of the crystallization system. The analytical CSD estimator is computationally efficient and can be applied for size independent and size dependent growth for one-dimensional processes. However, the main drawback of this approach is it only applicable for the crystallization process dominated by the crystal growth phenomena and neglecting the effect of agglomeration or breakage. In crystallization process, it is important to consider the agglomeration or breakage phenomena because the crystal particles tend to merge with other crystal particles due to stirring and may break due to the collision between particles during the operation. As a result major fundamental problems like limited operation flexibility, non-linear behaviour and inconsistent product quality cannot be addressed and solved adequately (Acevedo et al., 2018; Wohlgemuth and Schembecker, 2013).

Robustness of the controller is another issue that needs to be considered in achieving a consistent crystal product. The robust control usually can be defined as a controller that is able to work and adapt to the uncertain input ranges for the process (Cao et al., 2018). Based on the uncertain input ranges, the dynamic behaviour of the operation is changed and as consequence the product variability is expected. Therefore

a robust control needs to counteract this change and still achieve the target product by the end of operation. For example the uncertain input presence in the crystallization process may come from the kinetic parameters. Usually the exact value of kinetic parameters for nucleation and crystal growth expressions are estimated from model identification together with confidence interval. This confidence interval provides the possible range of each parameters where the use of these values will ultimately causing the variability of the CSD obtained in the end of the crystallization operation. Therefore there is a degree of uncertainty around the values of nucleation and crystal growth that needs to be considered for developing a robust control in order to achieve consistent product quality.

In this study, the agglomeration and breakage are included in the crystallization model in order to study the effects of agglomeration and breakage on the crystal size distribution. Thus a full mathematical model consists of the population balance equations (PBE), overall mass balance, energy balances as well as nucleation, crystal growth, agglomeration and breakage models are needed for simulation of crystallization process. The analytical CSD estimator is extended for covering the effects of agglomeration and breakage. This estimator is then used to generate the set-point trajectory for crystallization process. A Proportional-Integral (PI) controller is then employed to maintain the supersaturation at the set-point trajectory. In order to study the robustness of controller, Monte Carlo simulation is applied for evaluating the uncertainty analysis based on the input uncertainties from nucleation, crystal growth agglomeration and breakage.

1.2 Objectives of this Work

The objectives of this work consists of:

- a) To perform open-loop simulation for predicting crystallization operations and estimating kinetic parameters such as nucleation, crystal growth, agglomeration and breakage.
- b) To extend the analytical CSD estimator for covering the effects of agglomeration and breakage in crystallization operation and the temperature dependence case in nucleation and crystal growth phenomena.

- c) To control supersaturation using Proportional-Integral (PI) controller in the closed-loop simulation based on the set-point generated from the extension of analytical CSD estimator.
- d) To evaluate the robustness of supersaturation control that is capable to deal with set-point tracking and disturbance rejection as well as to counteract the effects of input uncertainties in the nucleation, crystal growth, agglomeration and breakage parameters.

1.3 Scopes of Work

The following is the scopes of this work:

- a) Identifying suitable mathematical model for representing crystallization operations and phenomena such as nucleation, crystal growth, agglomeration and breakage.
- b) Development of model identification for predicting kinetic parameters such as nucleation, crystal growth, agglomeration and breakage.
- c) Performing open-loop simulation of crystallization process for understanding the crystallization operation and validating the estimated kinetic parameters.
- d) Extension of original analytical CSD estimator for covering the effects of agglomeration and breakage in crystallization operation and the temperature dependence case in nucleation and crystal growth phenomena.
- e) Development of model-based optimization incorporating the extended analytical CSD estimator for generating the optimal set-point.
- f) Simulation, analysis and validation of the optimal set-point obtained from the analytical CSD estimator for achieving the desired CSD using supersaturation control in the closed-loop simulation.
- g) Robustness analysis of the developed supersaturation control in terms of set-point tracking and disturbance rejection
- h) Uncertainty analysis using Monte Carlo simulation on the closed-loop simulation of crystallization process in order to analyze controller robustness in counteracting the effect of input uncertainties and reducing the variability of the CSD.

1.4 Significance of the Study

The main specification of crystal product usually is evaluated based on the CSD. In this work, the effects of agglomeration and breakage are included together with nucleation and crystal growth phenomena. Thus the final CSD obtained by including all of the phenomena are more accurate which is essential particularly in pharmaceutical crystallization. The extended analytical CSD estimator covering the effects of all phenomena is important in order to generate the required set-point trajectory. This extended analytical CSD estimator is generic and can be widely applied for the case of agglomeration and breakage in crystallization operation as well as the temperature dependence case in nucleation and crystal growth phenomena. The supersaturation control preferable PI controller is then developed for maintaining the supersaturation at the desired set-point which subsequently producing the target CSD.

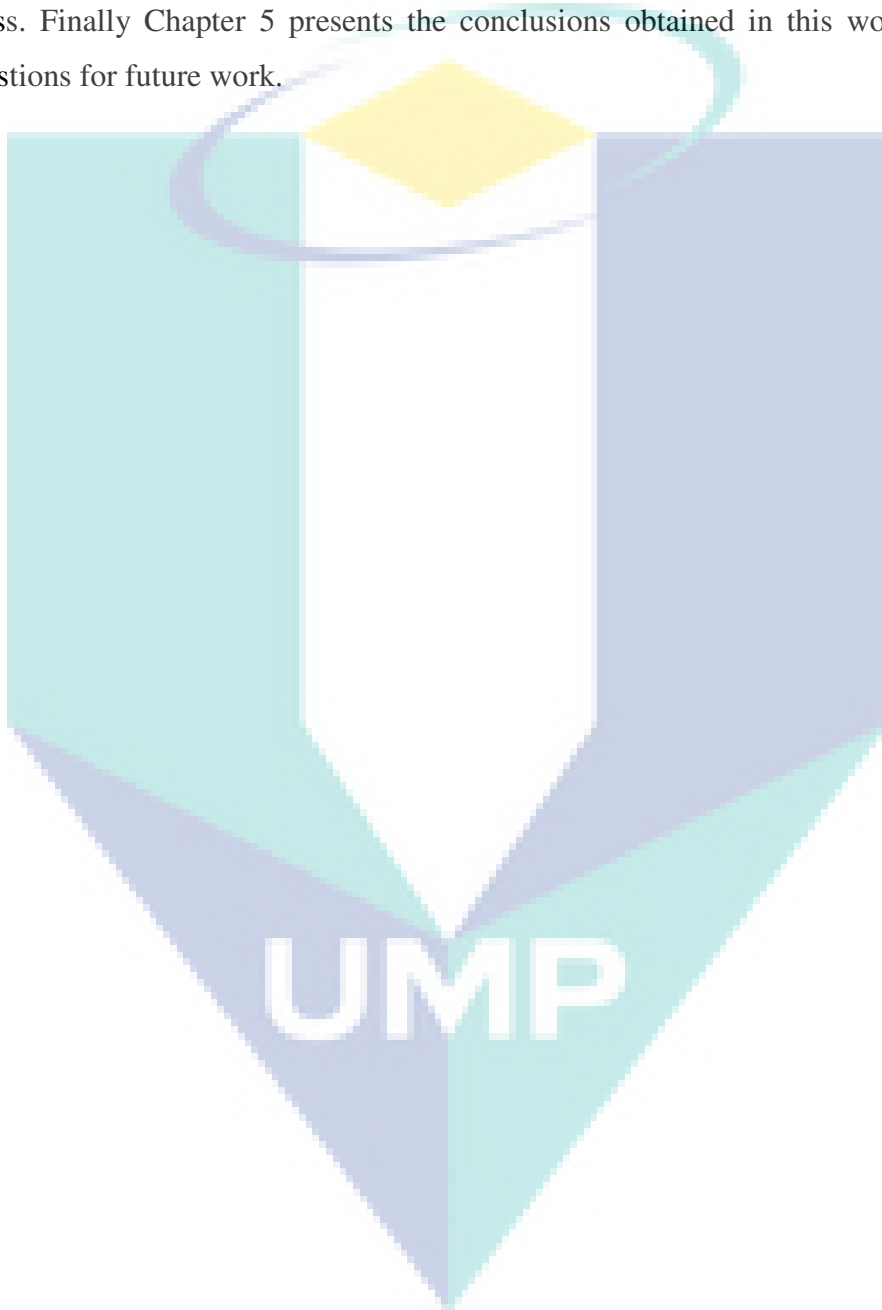
In addition, the robustness of controller in crystallization process is also included in this work. Two different analyses are used. Firstly the common testing in the forms of set-point tracking and disturbance rejection. In this setting, the ability of the controller to follow the changes of set-point and to adapt the introduction of disturbance are evaluated for base case controller performance. Secondly the robustness of controller is tested using uncertainty analysis based on Monte Carlo method. Through uncertainty analysis, the effects of input uncertainties such as nucleation, crystal growth agglomeration and breakage are evaluated and its impact on the final CSD is assessed. Thus the robustness of controller is judged based on its ability to maintain the supersaturation at its set-point and counteract the effects of input uncertainties in order to consistently produce the desired CSD.

1.5 Thesis Layout

The structure of the remainder of the thesis is outlined as follows:

Chapter 2 provides a review of literature studies involving the fundamental of crystallization process, mathematical modelling of the crystallization process and finally the operation and control of crystallization process. Chapter 3 provides the systematic model-based framework for robust supersaturation control in batch cooling crystallization process. In this chapter, a step-by-step procedure of the model-based framework is explained in detailed in terms of development of mathematical model,

model identification, generation of set-point using extended analytical CSD estimator, closed-loop control and uncertainty analysis. Chapter 4 discussed the application of the systematic model-based framework for robust supersaturation control in batch cooling crystallization process. Two case studies are selected for demonstrating the model-based framework which consists of potassium sulphate and sucrose crystallization process. Finally Chapter 5 presents the conclusions obtained in this work and some suggestions for future work.



CHAPTER 2

LITERATURE REVIEW

2.1 Fundamental of Crystallization Process

Crystallization process is a separation process to form solid crystals from a liquid solution (Geankoplis, 2003). It is one of the widely used method for purification of substances (Gao et al., 2017). The fundamental to drive solid crystals from a liquid solution is supersaturation which is defined as the state where the concentration of substance exceeds the solubility of the substance solution at the given temperature. In crystallization process, the supersaturation behaviour is essential in determining the quality of crystal products in terms of final CSD, the shape and the crystal size obtained at the end of the operation. The constitutive model for measuring supersaturation usually is divided into three types namely the degree of supersaturation, supersaturation ratio and relative supersaturation. The expressions for all supersaturation model are shown in Table 2.1. The saturation concentration (solubility) is represented in the polynomial form as:

$$c^{sat} = a_{i1} + b_{i1}T + c_{i1}T^2 + d_{i1}T^3 \quad 2.1$$

Table 2.1 Summary of supersaturation constitutive model

| Phenomena | Equations | References |
|---------------------------|-----------------------------------|-----------------------|
| Degree of supersaturation | $\Delta c = c - c^{sat}$ | Myerson (2002) |
| Supersaturation ratio | $S_r = \frac{c}{c^{sat}}$ | Myerson (2002) |
| Relative supersaturation | $S = \frac{c - c^{sat}}{c^{sat}}$ | Nagy and Aamir (2012) |

Usually the supersaturation condition is obtained by manipulating the temperature in the liquid solution which can be achieved through cooling, evaporation, anti-solvent addition or combination cooling and anti-solvent addition (Myerson, 2002). Cooling crystallization is defined as the formation of solid with sensible and consistent properties of a solution, where its parameter, the solubility line is highly sensitive to decrease the temperature. It is widely used in pharmaceutical, petrochemical and semiconductor industry. It is often conducted in batch operation rather than continuous operation because it allows flexibility for changing product demand and product scheduling (Yamba et al., 2008). In this case, the physical system consists of one or more solute dissolve in a solvent. For a crystallization process to occur, the system must be in supersaturated condition where the entire solvent is no longer able to dissolve in a solution and reach the solubility limit. Figure 2.1 shows the supersaturation generated by cooling method. The crystallization process usually takes place in the metastable region where this region is bounded by saturation (solubility) curve (indicated as curve AB in Figure 2.1) and the metastable (nucleation) curve (represented as CD).

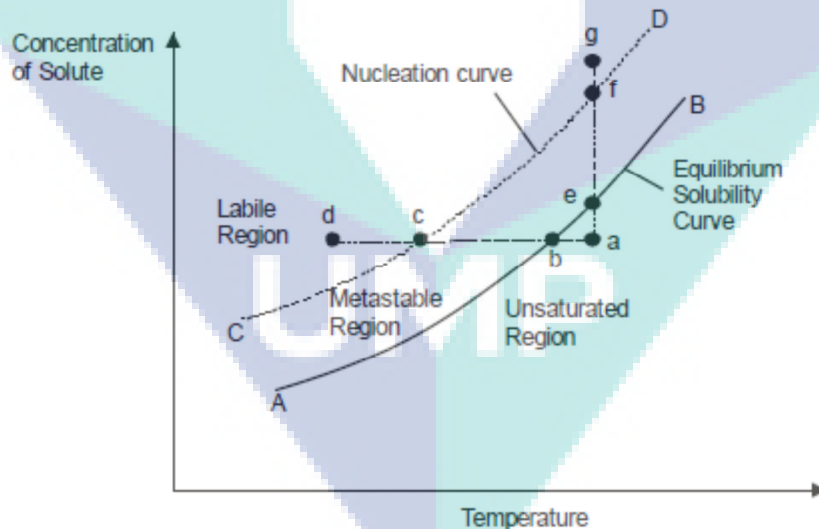


Figure 2.1 Supersaturation in crystallization processes

Source: Geankoplis (2003)

Initially the solution begins at point 'a' in the unsaturated condition. Due to the cooling, the temperature of crystallization process is decreased and the solution is then

moved from point 'a' to 'b' on the saturation curve where the solution now become saturated condition. The solution is then past the saturation curve due to the further cooling and move to the metastable region where the solution is now under supersaturated condition. In the metastable region, the crystal particles will be produced and start to grow where the supersaturation acts as the main driving force to move the solute in the solution into crystal particles. In order to achieve a specified crystal products, it is important to maintain the operation inside the metastable region. This is due to the further cooling which subsequently reducing the crystallization temperature, the solution tends to reach metastable curve at point 'c' and past beyond point 'c' to 'd' under labile region. Once the solution in the labile region, it is not possible to obtain a desired crystal products anymore because in this region the crystallization occurs spontaneously where a various size and shape of crystal particles are generated from nucleation and crystal growth. Based on the cooling method, the temperature profile of cooling crystallization process is much easier to be obtained since the compound (solute) tends to be more soluble in hot liquid (solvent) than they are in cold liquids.

Evaporation is another method to create supersaturation. Unlike cooling method where the temperature is decreased slowly to reach supersaturation condition, the evaporation method employ the concept of solvent removal. As shown in Figure 2.1, the solution starts at point 'a', move to point 'e' to become saturated and enters the metastable region due to the solvent removal from the solution by evaporation method. Normally the solution is measured by its concentration where there will be two components available in the solution namely the solute and the solvent. When the solvent in the solution is starting to evaporate, then solute concentration is definitely increased. This is the concept used in the evaporation method. Nevertheless the solution needs to be kept under metastable region similar as cooling method to promote the growth of crystal particles. Once the solution past beyond point 'f' and move to point 'g', the solution usually will be dissolved again and back to the point 'a' for recrystallization process.

The supersaturation can be generated using addition of another solvent in the solution. This method is called anti-solvent addition. In this method, the solubility of the solute concentration is reduced by using the anti-solvent. Assuming the initial solution at point 'a' in the Figure 2.1 where only solute and one solvent available in the

solution. The solute in the solution is able to crystallize when the saturation (AB) and metastable (CD) curves is moved downwards in Figure 2.1. Both curves are possible to be moved by adding anti-solvent into the solution where the solubility of the solution is reduced gradually. In order to achieve this condition the anti-solvent should be miscible with the other solvent in the solution, have a direct influence on the solubility of the solute and different polarity with the other solvent in the solution. Anti-solvent crystallization has been widely used to crystallize pharmaceutical products, which are generally sensitive to degradation by heating and frequently have polymorphism occurrence (Giulietti et al., 2001). However this approach is suitable only for thermally sensitive product in pharmaceutical application when it needs to be conducted at low operating temperature. In addition the use of additional solvent also involves the cost of anti-solvent separation at the end of the crystallization operation (Konstantakou et al., 2017).

2.2 Phenomena in Crystallization Process

The solute in the solution starts to crystallize once the solution in the metastable region. In this region there will be several phenomena occurring such as nucleation, crystal growth, agglomeration or breakage during the operation. The details of all phenomena occurring during crystallization are explained in the next section.

2.2.1 Nucleation

Nucleation can be defined as the formation of new crystal particles (which subsequently grow). Nucleation is a phenomena whereby a dust particle, a tiny seed crystal starts a crystallization process. Nucleation can occur in the labile zone, where there is no crystal growth occurring in that zone. It poses a large energy barrier, which is easier to overcome at a higher level of supersaturation (Mesters, 2007). In the metastable region, when the solution become supersaturated condition, the solute in the solution begins to form a solid state. The molecules of solute starts to appear and merge to form clusters. This clusters then form a nuclei due to the nucleation phenomena as shown in Figure 2.2. This nuclei is usually stable and will be growth into bigger size due to the crystal growth.

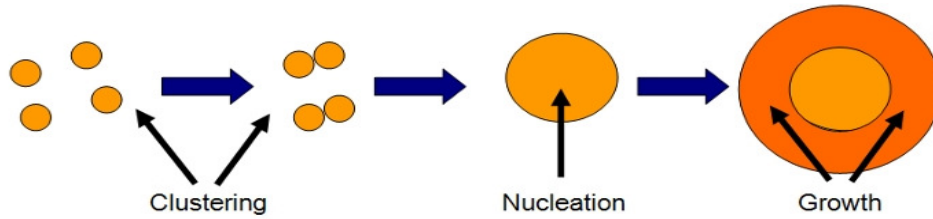


Figure 2.2 Growth of nuclei

Source: Myerson (2002)

The nucleation phenomena can be classified as primary and secondary nucleation as shown in Figure 2.3. A primary nucleation occurs when new solids are formed from clear liquid at high supersaturation whereas secondary nucleation is a new crystal formed that are generated from seed crystals at low supersaturation (Geankoplis, 2003).

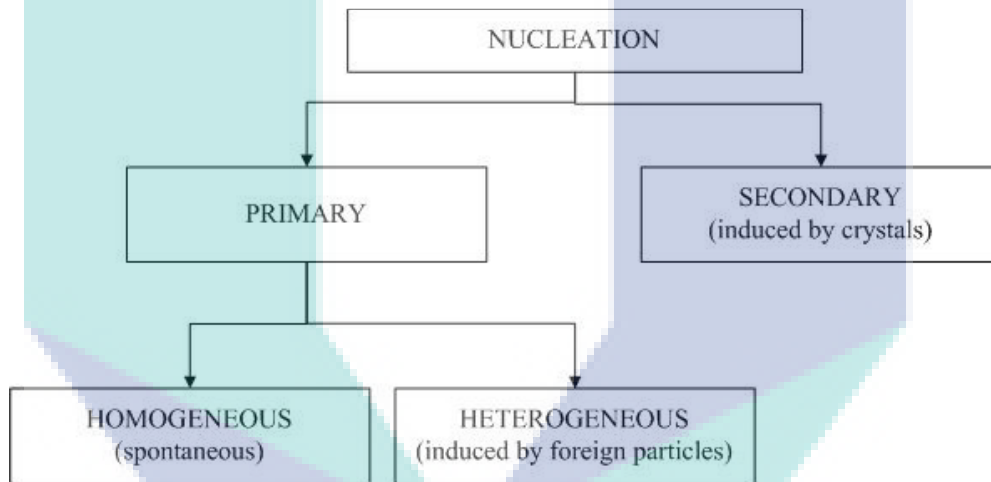


Figure 2.3 Nucleation phenomena classification

A primary nucleation can be divided into two types namely homogeneous and heterogeneous. The homogeneous primary nucleation occurs under pure bulk solution where no other particles are present and nucleation occur as a result of fluctuation of the concentration in the liquid. The heterogeneous primary nucleation occurs when the nuclei are produced from the presence of foreign particles due to the effect of impurities in the liquid. Meanwhile, secondary nucleation is production of new crystals that are induced by seed crystals at low supersaturation level in the case of seeded crystallization where the seed crystals are added once the solution in the supersaturated condition. In addition the secondary nucleation can be generated due to collisions with the impeller in the pump, vessel wall, initial breeding, fluid shear and contact with other crystals (Yamba et al., 2008). In order to achieve the desired CSD, usually the seeded

crystallization is preferred where the seed crystals are able to grow until they reach the desired crystal particles. Thus, secondary nucleation is normally used to determine the production of new crystals during the seeded crystallization process. The summary of model equations to represent nucleation in crystallization processes is shown in Table 2.2. Based on Table 2.2, the primary nucleation used by Marchal et al. (1988) is only for unseeded crystallization. For the seeded crystallization process, secondary nucleation models need to be employed. Based on Table 2.2, there are many types of secondary nucleation models, and the selection of a secondary nucleation model depends on the level of supersaturation, consideration of agitation rate, and total crystal mass. In this work, the level of supersaturation is based on the normal supersaturation (S) and the effect of agitation rate is included in order to cover the effects of agglomeration and breakage. Thus, the secondary nucleation model as suggested by Quintana-Hernandez et al. (2004) is the most suitable model to be used in this work.

Table 2.2 Summary of nucleation kinetic model equation in crystallization process

| Phenomena | Equations | References |
|----------------------|--|----------------------------------|
| Primary Nucleation | $B = k_b \exp \left(- \frac{B_p}{\ln \left(\frac{c}{c_{sat}} \right)^2} \right)$ | Marchal et al. (1988) |
| Secondary Nucleation | $B = k_b (\Delta C)^b$ | Yamba et al. (2008) |
| | $B = k_b S^b$ | Aoun et al. (1999) |
| | $B = k_b S_b M_c^j N_{rpm}^p$ | Quintana-Hernandez et al. (2004) |
| | $B = k_b e^{-\frac{E_a}{RT}} S^b \mu_3$ | Shi et al. (2006) |
| | $B = k_b \sigma^\pi M_t^i$ | Zumstein and Rousseau (1987) |
| | $B = A e^{\frac{k}{\ln 2 \cdot s}}$ | Dirksen and Ring (1991) |
| | $B = P_3 \left[n(L, t) L^{P_5} dL \right]^{P_1} (C - C_3)^{P_3}$ | Eek (1995) |

2.2.2 Crystal Growth

Crystal growth is the series of processes where an atom or a molecule is incorporated into the surface of a crystal, causing an increase in size of crystal particles. These different processes can be summarized into four steps (Cubillas and Anderson, 2010): (1) the transport of atoms through the liquid solution; (2) attachment of atoms to the surface; (3) movement of atoms on the surface; and (4) attachment of atoms to edges and kinks. Since these different steps normally occur in series, the slowest process will control the overall crystal growth. Growth is also referred to the deposition of solid material on existing crystals. Growth together with nucleation can determine the number of crystals and their size distribution even without the consideration of another two phenomena such as agglomeration and breakage (Rao et al., 2007). Growth and nucleation can take place through several mechanisms and their rate can be directly related to the degree of supersaturation (Everett, 1976). There are several kinetic models for crystal growth rate in the crystallization processes used by other researchers as summarized in Table 2.3.

Table 2.3 Summary of crystal growth kinetic model equation in crystallization process

| Phenomena | Equations | References |
|---|---|----------------------------------|
| Crystal growth rate (size independent growth) | $G = k_g (\Delta C)^g$ | Wibowo et al. (2006) |
| | $G = k_g N \exp\left(\frac{-E}{RT}\right) \Delta C^g$ | Canning and Randolph (1967) |
| | $G = k_g \sigma^g$ | Jones et al. (2008) |
| | $G = k_g S^g N_{rpm}^q$ | Quintana-Hernandez et al. (2004) |
| Crystal growth rate (size dependent growth) | $G = k_g S^g (1 + \chi L)^p$ | Aamir et al. (2010) |

Based on Table 2.3, there are two types of crystal growth models which consist of size independent growth and size dependent growth. In this work the crystal particles are assumed to be grown independently and thus the size independent growth model is selected. Similar to the nucleation model, the selection of crystal growth model is depending on the level of supersaturation, consideration of agitation rate and total crystal mass. Thus size independent crystal growth model as suggested by Quintana-Hernandez et al. (2004) is the most suitable model to be used in this work.

2.2.3 Agglomeration and Breakage

Another two phenomena take place in the crystallization process is agglomeration and breakage. Agglomeration is formed when the growing crystals collide with each other, then the particles will stick together to form a new particle. Generally, agglomeration is related to higher supersaturation and can be operated in the unstable zone. For example, if they are more particle in the batch crystallization, the probability of collision will be increased, and thus agglomeration will be more extensive (Yamba et al., 2008). To minimize agglomeration, supersaturation should be limited. There are two approaches to describe the effect of agglomeration in the crystallization process (Wang and Dong, 2006): (1) agglomeration as a kind of crystal growth (disobey the McCabe's ΔL law); and (2) differences of agglomeration from crystal growth (obey the McCabe's ΔL law). The McCabe's ΔL law refers to the states that geometrically similar crystals of the same material suspended in the same solution grow at similar linear rate (Canning and Randolph, 1967). In a kinetic model of the crystallization process, agglomeration has been expressed as shown in Equation (2.2) (Yamba et al., 2008).

$$\beta = (L_i + L_j)^3 \quad 2.2$$

Where β is the agglomeration rate of the crystals and L is the crystal length. Agglomeration is rarely discussed in the literature that is involved together with nucleation and crystal growth due to the lack of available models and phenomena understanding in the literature. However, agglomeration phenomena is equally important in the crystallization process because the crystal particles tend to merge with other crystal particles due to stirring effect. Therefore the number of crystal particles will be reduced and the size of crystal particles will be increased due to the merging of

crystal particles. As a result, the CSD obtained in the end of crystallization process will be different in the case of agglomeration. Meanwhile breakage also defined as erosion describes the phenomena where particles split up into a smaller pieces (Laloue et al., 2007). Particle breakage creates fine crystal fragments and can affect the products crystal size distribution. The breakage process is determined by two opposing factors which are the mechanical strength of the crystals and the applied breaking forces. Usually the breakage function provides the fragment sizes of the broken particle as reported by Borsos and Lakatos (2012) and the kinetic model can be expressed in the following form:

$$b_{br}^1(L_1, \lambda_1) b_{br}^2(L_2, \lambda_2) = 2\lambda \left(L_1 - \frac{\lambda_1}{2} \right) \delta(L_2 - \lambda_2) \quad 2.3$$

Where b is the exponent of secondary nucleation rate, L is the crystal length, δ is delta function and λ is the sizes of parent crystals. Based on Equations (2.2) and (2.3), the rates of agglomeration and breakage are determined based on the individual crystal particles and there is a need to measure the length of each crystal particles for rate calculation which makes the calculation becomes complex and complicated. Usually, the agglomeration and breakage occur simultaneously in the crystallization process due to its kinetic relationship in the process. In the work of Quintana - Hernandez et al. (2004), the agglomeration and breakage phenomena is quantified as one kinetic model as a function of a kinetic constant, supersaturation, total crystal mass generated in the operation and the effects of agitation as shown in Table 2.4. The kinetic model is called as the production-reduction term which represents the birth and death rates that are generated by the agglomeration, breakage, aggregation, crystal contact, crystal shaft contact and attrition.

Table 2.4 Production-reduction model in crystallization process

| Phenomena | Equations | References |
|---------------------------|------------------------------------|----------------------------------|
| Production-reduction term | $\alpha = k_a S^a M_c^k N_{rpm}^r$ | Quintana-Hernández et al. (2004) |

2.3 Types of Operation in Crystallization Process

Production process in the chemical industry can be carried out in several ways which are batch, continuous or semi-continuous (in which certain parts are done continuously and some in batch form). The selection of operation mode is very important to meet specified product requirements and changing market demands. The batch process is a single or multi-stage (batch-to-batch) process in which a certain quantity of inputs such as raw materials are fed into the reactor unit under specified operating conditions that is suitable for obtaining the desired product. In the batch reactor, the solution is prepared before the process takes place where no feed or product removal during the crystallization operation as shown in Figure 2.4. At the end of the operation the product is removed from the reactor and it then undergoes the suitable separation and processing stages to achieve the required level of purity (Spina et al., 2018; Zhang et al., 2017). The quality of the end product can also be controlled by the addition of appropriate separation stages between the various other stages as required.

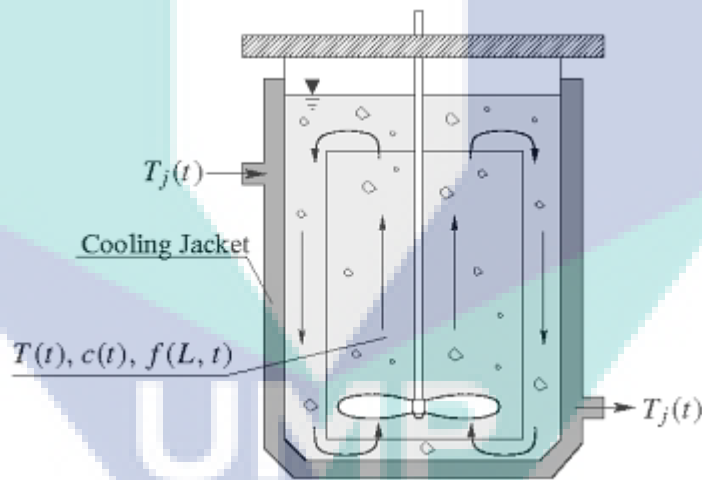


Figure 2.4 Jacketed batch cooling crystallization process

Source: Zhang et al. (2017)

The continuous process is where the raw materials are fed into the system at a constant rate and at preset ratios and at the same time a constant extraction of outputs (product) is implemented. This process is characterized by a constant process taking place in each section of the processing stage. Thus, the concentration of reactants and products at every stage in the system is in a durable state and control of the process is done by maintaining the concentrations (Wang et al., 2017). In the continuous process,

all the stages are carried out simultaneously and the overall time required for the process is shortened (Zhang et al., 2017). In summary, the batch and continuous processes can be compared as shown in the Table 2.5.

Table 2.5 Comparison between batch and continuous process

| Specification | Batch process | Continuous process |
|------------------------------|---|--|
| Types of materials | Can be used with all types of materials | Easier for use with flowing materials |
| Installation size | Small installations with significant savings in land | Large installations and big investment in land |
| Reactor | Changes occur in the concentration of materials with time | Conditions are constant with time at all locations (durable conditions) |
| Feeding raw materials | Raw materials are fed before the start of the reaction | Constant feeding of raw materials during the entire reaction process |
| Control system | Manual and automatic control can be applied | Manual and automatic control must be used. |
| Products | Extraction of materials can be done after finishing all the actions in the reactions | Continuous extraction of products at all times during the entire process |
| Trouble shooting | A fault or dealing with a batch requiring "repair" does not cause problems in the other stages. | The installations are interconnected, so a fault in one causes a stoppage in all the others. |
| Quantities produced | Preferable when production of small quantities of a specific material is planned. | Preferable for large scale production. |
| Variety of products in plant | Preferable when the plant produces a wide variety of materials. | Preferable for a central and permanent product. |
| Product development stage | Preferable when the process is relatively new and still unfamiliar. | Preferable after the conclusion of all the stages of grossing-up and economic feasibility tests. |

Based on the comparison in Table 2.5, the batch process is preferable due to its ability to reflect changing product demand, a proper control can be used to maintain the operation, operation feasibility and its flexibility on the process condition.

2.4 Modeling of Crystallization Process

In the simulation work, mathematical model is widely used to represent the necessary process. In the crystallization process, usually the mathematical model consists of dynamic balance equations which are combined with constitutive models describing the phenomena such as nucleation, crystal growth, agglomeration and breakage as well as saturation concentration, mass and heat transfers involved with the crystallization process (Samad et al., 2011). Generally, the dynamic balance equations involve the population balance equation for representing the CSD, mass balance for predicting the change of solute concentration and energy balance for estimating the dynamic behavior of temperature in the solution.

2.4.1 Population Balance Equation

The main equations used to model the crystallization process is the population balance equation, which describes the state of the CSD (Hu et al., 2005). The type of population balance equation (PBE) engaged is usually a hyperbolic partial differential equation (PDE), which also includes the crystallization kinetics phenomena. The general form of PBE is shown below (Hulburt and Katz, 1964):

$$\frac{\partial f_n(L,t)}{\partial t} = -\frac{\partial f_n(L,t)G(L,T)}{\partial L} + (B - D) \quad 2.4$$

Where f_n is the population density, L is the length scales of crystal, G refer to the crystal growth rate phenomena, B represent the birth rate of crystal and D is the death rate of crystals. The terms birth (B) and death rate (D) can be represented as:

$$B - D = B_{nuc} + B_{agg} - D_{agg} + B_{br} - D_{br} \quad 2.5$$

Where the birth rate of crystal, B usually is formed by nucleation, B_{nuc} , agglomeration of crystal particles, B_{agg} or from the breakage of crystal particles, B_{br} . Meanwhile the

death of crystals are usually caused by agglomeration, D_{agg} and breakage, D_{br} . In the work of Quantina-hernandez et al. (2004), the birth and death rates of crystal generated by agglomeration and breakage can be represented as production-reduction term, α . Thus, Equation (2.5) can be simplified as

$$\frac{\partial f_n(L,t)}{\partial t} = -\frac{\partial f_n(L,t)G(L,T)}{\partial L} + B_{nuc} + \alpha \quad 2.6$$

Where the production-reduction term, α as shown in Table 2.4 can be substituted in Equation (2.6) as shown in Equation (2.7).

$$\frac{\partial f_n(L,t)}{\partial t} = -\frac{\partial f_n(L,t)G(L,T)}{\partial L} + B_{nuc} + k_a S^a M_c^k N_{rpm}^r \quad 2.7$$

If there is no agglomeration and breakage is assumed in the crystallization process, Equation (2.7) is simply reduced to Equation (2.8) as shown below:

$$\frac{\partial f_n(L,t)}{\partial t} = -\frac{\partial f_n(L,t)G(L,T)}{\partial L} + B_{nuc} \quad 2.8$$

Usually the solution of the generic PBE requires numerical solution techniques and the most common solution of these PBE is using standard method of moments and method of classes techniques (Samad et al., 2011) as shown in Figure 2.5. The population balance equations (PBE) are transformed to a system of ordinary differential equation (ODE) by applying the standard method of moments and the method of classes. Both methods are capable to perform the operation for unseeded and seeded crystallization process as well as size independent and size dependent crystal growth except standard method of moments only capable to solve for the case of size independent growth rate only.

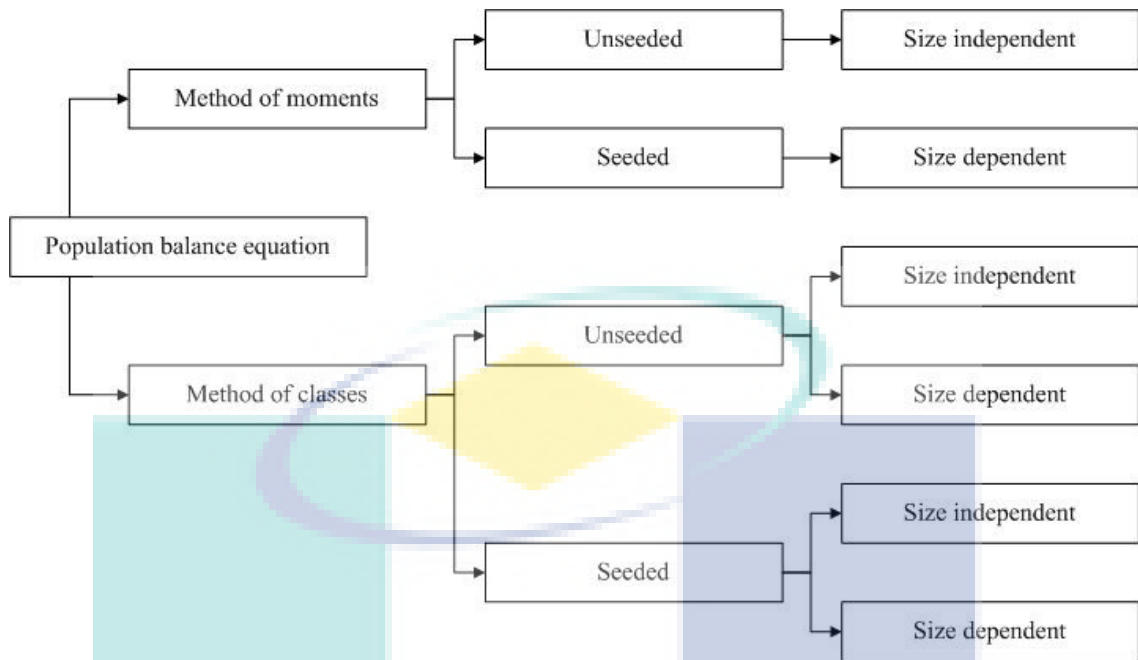


Figure 2.5 PBE solution techniques based on process operation characteristics

Source: Samad et al. (2011)

2.4.1.1 Method of Moments

The standard method of moments is originally developed by Hulburt and Katz (1964) is very popular and its application has been reported by many researchers (Nagy et al., 2008; Paengjuntuek et al., 2008; Fujiwara et al., 2002; and Shi et al., 2006). The approach of this method is to convert the partial differential equations (PDE) that represent the population balance into a set of coupled ordinary differential equations (ODEs) for the n -moments considered (Samad et al., 2011). The advantage of this method is the ease of solution, since the ODE solvers are readily available (Samad et al., 2011). However, the PBE including the size dependent growth functions or agglomeration and breakage terms may cause convergence problems because of closure of the respective moment equations (Gimbun et al., 2009). In addition the size distribution of crystal particles cannot be obtained from this method which represent the major lacking point of this method.

2.4.1.2 Method of Classes

The methods of classes are different compared to method of moments where the partial differential equations (PDE) are sectioned along the size domains into finite classes. This method overcomes the problem encountered with the standard method of

moments as it permits the discretization of the growth functions along the size domains and thereby able to deal for case of size independent and size dependent crystal growth. Moreover, this method allows phenomena such as agglomeration and breakage to be implemented within the solution of PBE (Samad et al., 2011). In addition the distribution of crystal particles at various size can be estimated using this method. A disadvantage of this method is the accuracy of the simulated behavior depends on the number of discretization points and also the computational effort. The higher number of discretization points used to construct the CSD then the higher accuracy of CSD is obtained but high computational time is also expected. However, this problem can be overcome with the availability of faster computers and more efficient numerical solvers (Amini et al., 2016; Abbas and Romagnoli, 2007; Puel et al., 2003).

2.4.2 Overall Mass Balance

The overall mass balance used in the crystallization process is developed to determine the rate of change of the solute concentration as shown in Equation (2.9).

$$\frac{dc}{dt} = -\frac{\rho_c k_v V}{m_w} \left(3 \int_0^{\infty} G_n(L, t) L^2 dL \right) \quad 2.9$$

Where ρ_c is crystal density, V is volume m_w is the mass of solvent and L is the characteristic length. Meanwhile k_v is the shape factor where the value is depending on crystal shape (Samad et al., 2011). For example the value for sphere shape is $\pi/6$ and for cube shaped crystal is 1. The Equation (2.9) is in the form of integro-differential equation and can be solved using standard method of moments and method of classes (Samad et al., 2011) as shown in Equations (2.10) and (2.11).

$$\frac{dc}{dt} = -\frac{\rho_c k_v V}{m_w} (3G\mu_2) \quad 2.10$$

$$\frac{dc}{dt} = -\frac{\rho_c k_v V}{m_w} \left(\sum_{i=1}^{i=N} S_i^3 N_i \right) \quad 2.11$$

2.4.3 Energy Balances

The energy balances for the crystallization process can be divided into the energy balance inside the crystallizer and the energy balance for the cooling jacket. The

energy balance for accounting the rate of change of crystallizer temperature is shown in Equation (2.12).

$$\rho V c_p \frac{dT}{dt} = -\Delta H_c \rho_c k_v V \left(3 \int_0^{\infty} G_n(L, t) L^2 dL \right) - U_1 A_1 (T - T_w) \quad 2.12$$

Where ΔH_c is the heat of crystallization, U_1 is the heat transfer coefficient and A_1 is crystallizer internal area. Similar to the overall mass balance, the energy balance inside the crystallizer is also in the form of integro-differential equation. The solution of this equations using standard method of moments and method of classes (Samad et al., 2011) are shown in Equations (2.13) and (2.14).

$$\rho V c_p \frac{dT}{dt} = -\Delta H_c \rho_c k_v V (3G\mu_2) - U_1 A_1 (T - T_w) \quad 2.13$$

$$\rho V c_p \frac{dT}{dt} = -\Delta H_c \rho_c k_v V \left(\sum_{i=1}^{i=N} S_i^3 N_i \right) - U_1 A_1 (T - T_w) \quad 2.14$$

Meanwhile the energy balance for cooling jacket is shown in Equation (2.15) as suggested by Quantina-hernandez et al. (2004).

$$\rho_w V_w c_{pw} \frac{dT_w}{dt} = \rho_w F_{win} c_{pw} (T_{win} - T_w) + U_1 A_1 (T - T_w) + U_2 A_2 (T_{ex} - T_w) \quad 2.15$$

2.5 Operation and Control

In order to achieve high purity and uniform crystal size distribution (CSD), normally the operation of crystallization process must lies within the metastable zone which is bounded with saturation (solubility) curve and metastable (nucleation) curve as shown in the Figure 2.6. In order to crystallize the solution, the system must be in the supersaturated condition where the entire solute is no longer able to dissolve in the solution. In the metastable zone, the crystal will be formed and grow due to the supersaturation that occurs during the process. However in many crystallization processes, the main problem is to determine the control trajectory (set-point) inside the metastable zone. This is due to the fact that if the crystallization is operated near to the saturation (solubility) curve then low supersaturation is obtained. Supersaturation have a direct relationship on the nucleation and crystal growth rate. A low supersaturation

level will result into low nucleation rate which is preferable because less production of new crystals at relatively low size. However a longer operational time is required to obtain the desired size of crystal particles because of the low rate of crystal growth. Another scenario is when the crystallization is operated near the metastable curve, then a high level of supersaturation is expected. Thus the crystal particles will grow steadily according to the rate of crystal growth but excessive nucleation is also expected where a large number of crystal particles will be produced which is not preferable in the crystallization process. Therefore a suitable approach to generate the necessary set-point is needed in order to obtain a uniform and reproducible crystal size distribution (CSD).

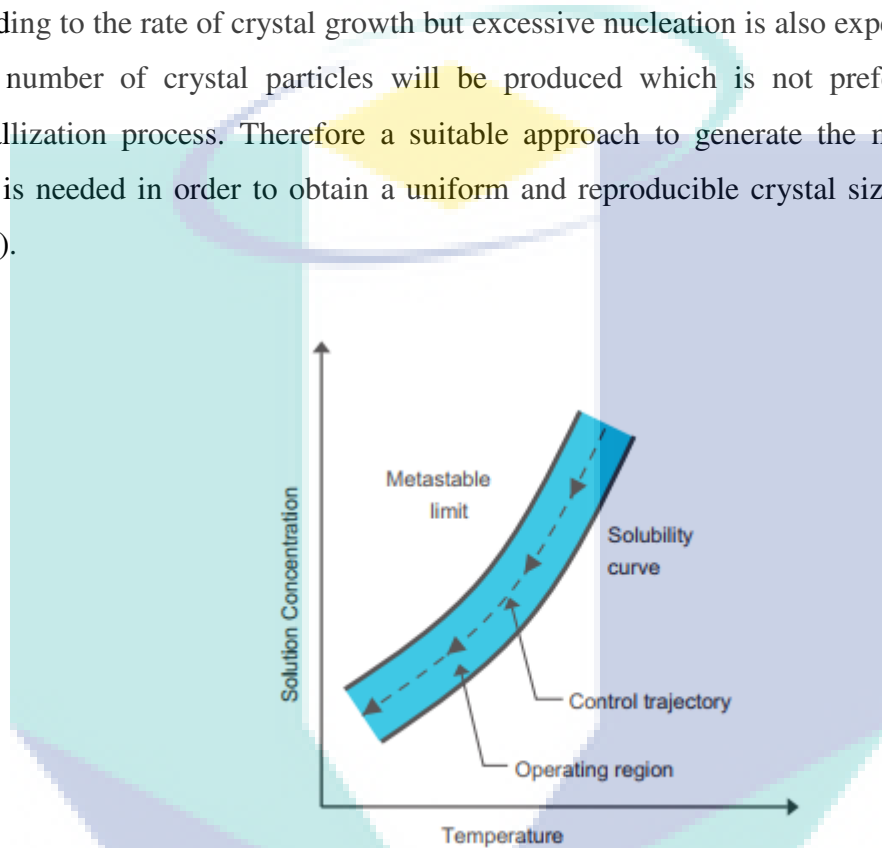


Figure 2.6 Operating region for crystallization process

Source: Fujiwara et al. (2005)

One of the early works for generating the desired trajectory in batch cooling crystallization process is using the cooling policy as shown in Figure 2.7 (Hojjati and Rohani, 2005; Myerson, 2002; Jones and Mullin, 1974). The cooling policy which includes natural, linear and controlled cooling policy is often applied to generate temperature profile for producing the crystal products (Bohlin and Rasmuson, 1992; Nakamura et al., 2007). In the natural cooling policy, the temperature of the solution is cooled down steadily until the end of operation. Although natural cooling mode is very easy to operate but it has never been able to obtain product crystals at the desired size (Dunuwila and Berglund, 1997). This is because in the natural cooling policy usually a high supersaturation is obtained in the beginning of the operation since the temperature

is dropped quickly but low supersaturation level is achieved by the end of the operation. Therefore a large number of crystal particles will be generated in the beginning but in the end all of these particles will not be grown sufficiently due to the low supersaturation during the end of operation which contributing to the low crystal growth rate. In addition a high supersaturation usually happens when the solute concentration is crossing the metastable limit into the labile region, thereby promoting uncontrolled crystallization and the formation of fines which is often undesirable since they may be difficult to filter, dry and package. In order to overcome a large production of crystal particles, linear cooling policy is introduced where the cooling rate is decreased linearly. This approach is able to reduce the production of crystal particles at relatively low size but the supersaturation obtained using this method is low which contributing to the low size of crystal particles.

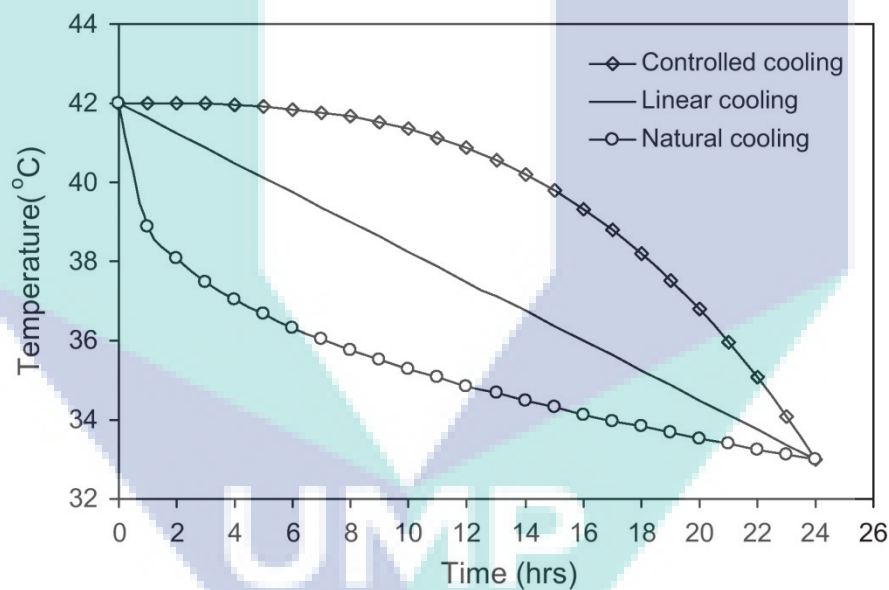


Figure 2.7 Cooling policy for crystallization process

Source: Myerson (2002)

Previous works have shown that through the use of a controlled cooling policy, as opposed to a natural or linear cooling policy, a larger mean size diameter size of crystal particles can be obtained and less number of crystal particles due to the nucleation can be achieved. This is due to the cooling rate for this policy is decreased based on the cubic function. The low supersaturation in the beginning of the operation and a sufficient supersaturation level for adequate growth of crystal in the middle of

operation makes this approach better than natural or linear cooling policy. Therefore controlled cooling policy is commonly applied for optimization of batch crystallization (Simone et al., 2017; Shiau and Lu, 2004; Jones and Mullin, 1974). In order to reflect the changes of product specification this policy is combined with optimization techniques to generate the optimal model-based design approach. In this approach usually the objective function for optimization is specified for example to maximize the mean crystal size of crystal particles or to reduce the production of crystal particles due to the nucleation (Amini et al., 2016; Fujiwara et al., 2005). Then the optimization algorithm is implemented together with a detailed mathematical model for crystallization process to generate the optimal temperature profiles for achieving the specified objective function (Wang and Ward, 2016).

However most of the works only concern with the objective to maximize mean crystal size and mean size diameter or to minimize production of new crystal particles (Hemalatha et al., 2018; Bhoi et al., 2017; Amini et al., 2016, Nagy et al., 2008). Only limited works in literature can be found on achieving the distribution of crystal particles in the form of CSD. Usually the mean crystal size and mean size diameter can be calculated using standard method of moments considering it is a simple method and easier to solve. However the CSD cannot be determined using the standard method of moments and it requires discretization method such as method of classes. The CSD from method of classes is depending on the number of discretized equations. The higher the number of discretized equations then the higher accuracy of the CSD. The major drawback using this method is if the optimization algorithm is performed together with the mathematical model using method of classes, then high computational times is expected which sometimes leads to failure of reaching the specified objective function. Therefore the performance of optimal model-based approach depends on the mathematical model equations (Cao et al., 2017; Nagy et al., 2008).

Alternative to optimal model-based approach is by using model-free (or direct design) approach where analytical CSD estimator can be employed to generate the set-point trajectory (Aamir, 2010). The analytical CSD estimator originally developed by Aamir (2010) and further extended by Samad et al. (2013) is based on the assumption of constant supersaturation throughout the entire batch operation and can be applied for size independent and size dependent growth for one- and two-dimensional

crystallization processes as shown in the Table 2.6. The analytical CSD estimator is selected based on the characteristic selection for example size independent growth or size dependent growth. There are two main equations in the analytical CSD estimator namely final CSD and final characteristic length in the case of one-dimensional crystallization process. Notes that the final characteristic width is only applicable for two-dimensional case.

Table 2.6 Analytical CSD estimator for one- and two-dimensional crystallization

| Characteristic | Analytical model equations |
|--|--|
| Size independent growth: $G_x = k_{gx} s^{gx}$ | Final CSD: $f_{n,i} = f_{n0,i} \quad i = 1, 2, \dots, N$ Final characteristic length: $L_{x,i} = L_{x0,i} + k_{gx} s_{sp}^{gx} t_c, \quad i = 1, 2, \dots, N$ Final characteristic width: $L_{y,i} = L_{y0,i} + k_{gy} s_{sp}^{gy} t_c, \quad i = 1, 2, \dots, N$ |
| Size dependent growth: $G_x = k_{gx} s^{gx} (1 + \gamma_x L_x)^{p_x}$ | Final CSD: $f_{n,i} = f_{n0,i} \left[\frac{(1 + \gamma_x L_{x0,i})^{1-p_x} + k_{gx} s_{sp}^{gx} \gamma_x t_c (1 - p_x)}{(1 + \gamma_x L_{x0,i})^{1-p_x}} \right]^{\frac{p_x}{p_x - 1}}$ $+ f_{n0,i} \left[\frac{(1 + \gamma_y L_{y0,i})^{1-p_y} + k_{gy} s_{sp}^{gy} \gamma_y t_c (1 - p_y)}{(1 + \gamma_y L_{y0,i})^{1-p_y}} \right]^{\frac{p_y}{p_y - 1}}$ |
| $G_y = k_{gy} s^{gy} (1 + \gamma_y L_y)^{p_y}$ | Final characteristic length: $L_{x,i} = \frac{[(1 + \gamma_x L_{x0,i})^{1-p_x} + k_{gx} s_{sp}^{gx} \gamma_x t_c (1 - p_x)]^{1/(1-p_x)} - 1}{\gamma_x}$ |
| For the case of: $(\gamma_x = \gamma_y \neq 0; p_x = p_y \neq 1)$ | Final characteristic width: $L_{y,i} = \frac{[(1 + \gamma_y L_{y0,i})^{1-p_y} + k_{gy} s_{sp}^{gy} \gamma_y t_c (1 - p_y)]^{1/(1-p_y)} - 1}{\gamma_y}$ |
| Size dependent growth: $G_x = k_{gx} s^{gx} (1 + \gamma_x L_x)$ $G_y = k_{gy} s^{gy} (1 + \gamma_y L_y)$ | Final CSD: $f_{n,i} = f_{n0,i} \exp^{-(\gamma_x k_{gx} s_{sp}^{gx} t_c + \gamma_y k_{gy} s_{sp}^{gy} t_c)}, \quad i = 1, 2, \dots, N$ Final characteristic length: $L_{x,i} = \frac{(1 + \gamma_x L_{x0,i}) \exp^{\gamma_x k_{gx} s_{sp}^{gx} t_c} - 1}{\gamma_x}, \quad i = 1, 2, \dots, N$ |
| For the case of: $(\gamma_x = \gamma_y \neq 0; p_x = p_y = 1)$ | Final characteristic width: $L_{y,i} = \frac{(1 + \gamma_y L_{y0,i}) \exp^{\gamma_y k_{gy} s_{sp}^{gy} t_c} - 1}{\gamma_y}, \quad i = 1, 2, \dots, N$ |

Source: Samad et al. (2013)

Based on the informations of target final CSD, initial seed of CSD and the growth kinetics of the crystallization process, the possible candidates of set-point which consists of supersaturation and total crystallization time can be estimated. In the analytical CSD estimator, the optimal supersaturation set-point (S_{sp}) and the total crystallization time (t_c) can be obtained by minimizing the sum of squares of relative errors between the predicted CSD obtained from the analytical estimator and the desired target CSD (Samad et al., 2013) as shown in Equations (2.16) - (2.19).

Minimize

$$F_{obj} = \sum_{i=1}^N \left(\frac{f_{n,i} - f_{n,i_{target}}}{f_{n,i_{target}}} \right)^2 \quad 2.16$$

Subject to: S_{sp}, t_c

$$S_{sp,min} \leq S_{sp} \leq S_{sp,max} \quad 2.17$$

$$t_{min} \leq t_c \leq t_{max} \quad 2.18$$

$$c_{t_{batch}} \leq c_{f_{max}} \quad 2.19$$

Where N is the number of discretization points, $f_{n,i}$ is the predicted CSD that is obtained from the analytical CSD estimator and $f_{n,i_{target}}$ is the desired target CSD, $c_{t, batch}$ is the expected solute concentration at the end of the batch and $c_{f, max}$ represents the maximum acceptable solute concentration at the end of the batch to achieve the required yield. Subsequently the optimal supersaturation set-point is used as a trajectory that needs to be maintained during the entire batch operation using a suitable feedback control in order to achieve the desired target CSD. This approach is relatively simple and efficient. The main advantage is the set-point generated by analytical CSD estimator is directly corresponding to the target CSD indicating that by maintaining the operation at its set-point by feedback control then the desired CSD can be achieved. This reduces the needs for trial-and-error approach which is often applied during experimentation works. However, the main drawback of this approach is it is only applicable for the crystallization process dominated only by the crystal growth

phenomena and thus neglecting the effect of agglomeration or breakage. In addition the crystal growth kinetic (k_g) in the estimator neglects the dependence of temperature and thus the parameters are assumed constant. In some cases, particularly in the pharmaceutical crystallisation, the crystal growth kinetic is dependent on the temperature of crystallisation operation and thus the kinetic must be extended. Therefore there is a need to extend the current analytical CSD estimator in order to overcome these limitations.

2.6 Robustness Issue

Although a proper feedback control system can be developed to maintain the operation at the set-point trajectory in crystallization process but usually the developed control is sometimes capable to work only under specific crystallization operation (Yang et al., 2014). Also often the controller needs to be designed again when the specification of the operation or the product is changing indicating the controller is not robust enough to adapt the changes (Sin et al., 2009). Therefore robustness issue of controller is one of the problem in crystallization process where a suitable approach needs to be implemented for producing robust control. One of the simplest method is to test the control based on set-point tracking and disturbance rejection (Saengchan et al., 2011). Through set-point tracking, a various of set-points are introduced at different times during the crystallization operation then the performance of the developed controller is observed based on its ability to follow and maintain the operation based on the changes of set-points. Meanwhile for the disturbance rejection, a change of input is implemented on the crystallization operation. For example the input of cooling jacket temperature is disturbed during the crystallization operation. This change will ultimately change the crystallization operation particularly the behavior of crystallizer temperature, solute concentration and CSD of crystal product. Therefore the controller must good enough to adapt this change and rectify the operation back to the set-point trajectory. If the controller is not able to handle both of these changes then the controller needs to undergo a tuning procedure until the performance of the controller is satisfied.

Another factor which can be considered for testing the robustness of controller is parameter uncertainty (Samad and Saleh, 2016; Saengchan et al., 2011, Sin et al., 2009). Usually the parameter uncertainty in crystallization process presences in the

kinetic model equations such as nucleation, crystal growth rate, agglomeration and breakage (Saengchan et al., 2011). The kinetic coefficients of these equations normally are estimated based on experimental data such as solubility data, solute concentration data or crystallizer temperature data. All of these data are collected during experiment works and sometimes there are considerable errors during the data measurement. In order to consider these errors, a confidence interval can be calculated during parameter estimation which the acceptable range of values is determined as a good estimates of the unknown parameter. For example, the coefficient of crystal growth kinetic (k_g) is estimated as 1.44 ± 0.08 from parameter estimation. The good estimate of this parameter is 1.44 and the confidence interval which is based on 95% reliability is 0.08. This indicates that the reliable value for this parameter is in the range of 1.36 – 1.52 where this range provides the uncertainty of the parameter. As consequence, the use of this range will contribute to the variability of the CSD by the end of the operation (Forgione et al., 2015). Therefore the developed controller needs to be able to handle the effect of this range and to reduce the variation of the CSD.

For considering the parameter uncertainty in the crystallization process, uncertainty analysis can be applied in order to measure the uncertainties and minimize the risk of not achieving the target CSD specifications. This is actually a part of good modeling practice (GMoP) to allow improvement of the usage and the reliability of the model within process monitoring and control applications (Sin et al., 2009). In the uncertainty analysis, the input uncertainty which consists of estimated parameters used in the mathematical model will be propagated and the effects on the model output will then be evaluated. The uncertainty analysis leads to probability distributions of model predictions, which are then used to infer the mean, variance and percentiles of model predictions (Sin et al., 2009). One of the widely used methods to perform uncertainty analysis is Monte Carlo method (Samad and Saleh, 2016). Monte Carlo method or probability method is a technique used to understand the impact of uncertainty in many areas such as financial, project management, and costing as well as engineering area. In some cases such as crystallization process, it is possible to estimate a range of values for input parameters during parameter estimation. Based on the range of estimated values, random value is selected for each parameters and the Monte Carlo simulation is performed to generate the model output. Here the required number of Monte Carlo simulation will be set by the user. Usually the higher number of Monte Carlo simulation

will produce more accurate propagation of input data on the model output. The advantages of Monte Carlo analysis is the extensive sampling from the ranges of the uncertain variables, and a surrogate model is not needed to obtain the uncertainty results unlike the other uncertainty techniques such as Taylor series in differential analysis or Response Surface Methodology (RSM) (Sin et al., 2009).

2.7 Concluding Remarks

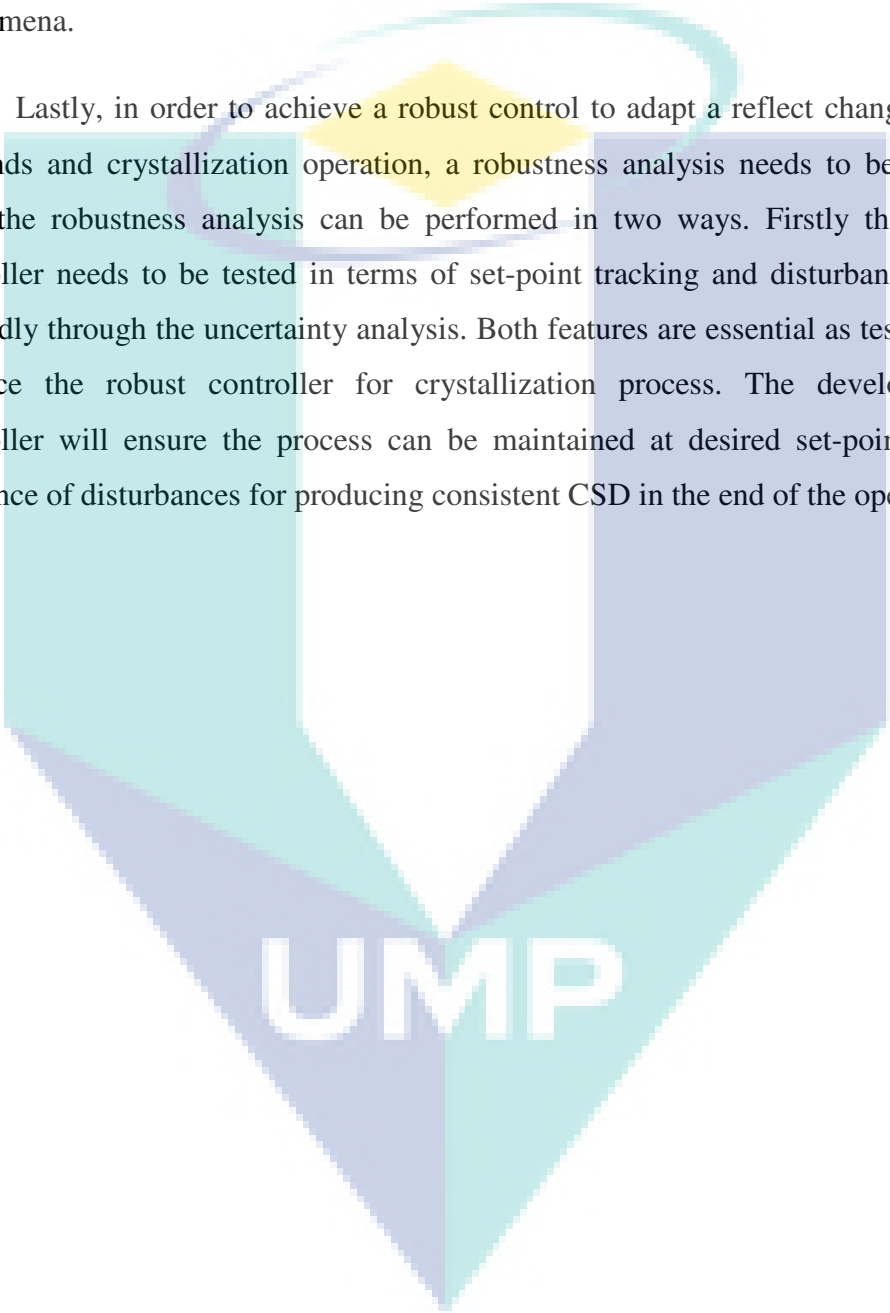
Crystallization is a widely used technique in various chemical-based product industries especially in the production of pharmaceutical and chemicals. The driving force for crystallization process is supersaturation. It can be achieved by different operating approaches which are cooling, evaporation and anti-solvent addition. Some of the techniques can be combined to achieve the supersaturation in the crystallization operation. In this work, batch cooling of crystallization method is chosen instead of evaporation and anti-solvent addition since the process offer flexibility compared to the another methods.

Population balance equation (PBE) has been accepted as the most fundamental model for constructing CSD of crystal particles. The PBE is a balance that has been used for distribution in particle size, location and other state variables. A lot of methods are available to solve the PBE. The most suitable method is the method of classes (MOC) which is able to solve the problem related to size independent or dependent growth, agglomeration and breakage phenomena. The PBE together with overall mass and energy balances can be combined with the desired phenomena such as nucleation, crystal growth agglomeration and breakage to represent the crystallization process and be used as a tools for simulation, operation and control of the crystallization process.

Usually in many crystallization processes the main problem is to obtain a uniform and reproducible crystal size distribution (CSD). Thus, supersaturation control is often applied to drive the process that lies in the metastable zone in order to enhance the control of the CSD. In order to implement supersaturation control in the crystallization process, the set-point trajectory needs to be designed to lie within the metastable zone. Here the set-point trajectory, which in fact consists of both the supersaturation and the total batch time needed to complete the crystallization operation, can be determined using an analytical CSD estimator as highlighted in the

work of Samad et al. (2013) and Nagy and Aamir (2012). The analytical CSD estimator is computationally efficient in kinetic mathematical model equation and can be applied for size independent and size dependent growth for one-dimensional crystallization. However the current estimator needs to be extended for covering the effects of temperature dependency in the kinetic rates as well as agglomeration and breakage phenomena.

Lastly, in order to achieve a robust control to adapt a reflect changing product demands and crystallization operation, a robustness analysis needs to be performed. Here the robustness analysis can be performed in two ways. Firstly the developed controller needs to be tested in terms of set-point tracking and disturbance rejection. Secondly through the uncertainty analysis. Both features are essential as testing tools to produce the robust controller for crystallization process. The developed robust controller will ensure the process can be maintained at desired set-point under the influence of disturbances for producing consistent CSD in the end of the operation.

The logo for UMP (Université de Moncton) is a large, stylized shield shape. It is divided into four quadrants by a white vertical line and a white horizontal line. The top-left quadrant is light blue, the top-right is light purple, the bottom-left is light purple, and the bottom-right is light blue. The letters 'UMP' are written in white, bold, sans-serif font across the bottom of the shield.

UMP

CHAPTER 3

METHODOLOGY FOR ROBUST SUPERSATURATION CONTROL IN BATCH COOLING CRYSTALLIZATION PROCESS

3.1 Introduction

In this chapter, the systematic model-based framework for robust supersaturation control in batch cooling crystallization is presented. A general step-by-step procedure has been included in this model-based framework to allow the user to study the crystallization operation under open-loop and closed-loop conditions. In addition, an extension of new generic analytical crystal size distribution (CSD) estimator that is applicable for all necessary phenomena such as nucleation, crystal growth, agglomeration and breakage as well as temperature dependency in the kinetic rate has been included to provide an accurate set-point trajectory for supersaturation controlled in the crystallization process in order to achieve the target CSD. In addition the robustness analysis is also included in the model-based framework to deal with the controller robustness issue.

3.2 Systematic Model-based Framework for Robust Supersaturation Control in Batch Cooling Crystallization Process

A systematic model-based framework for robust supersaturation control in batch cooling crystallization process has been developed as shown in Figure 3.1. The model-based framework consists of eight main steps to allow the systematic development of a wide range of crystallization phenomena for different operational case study.

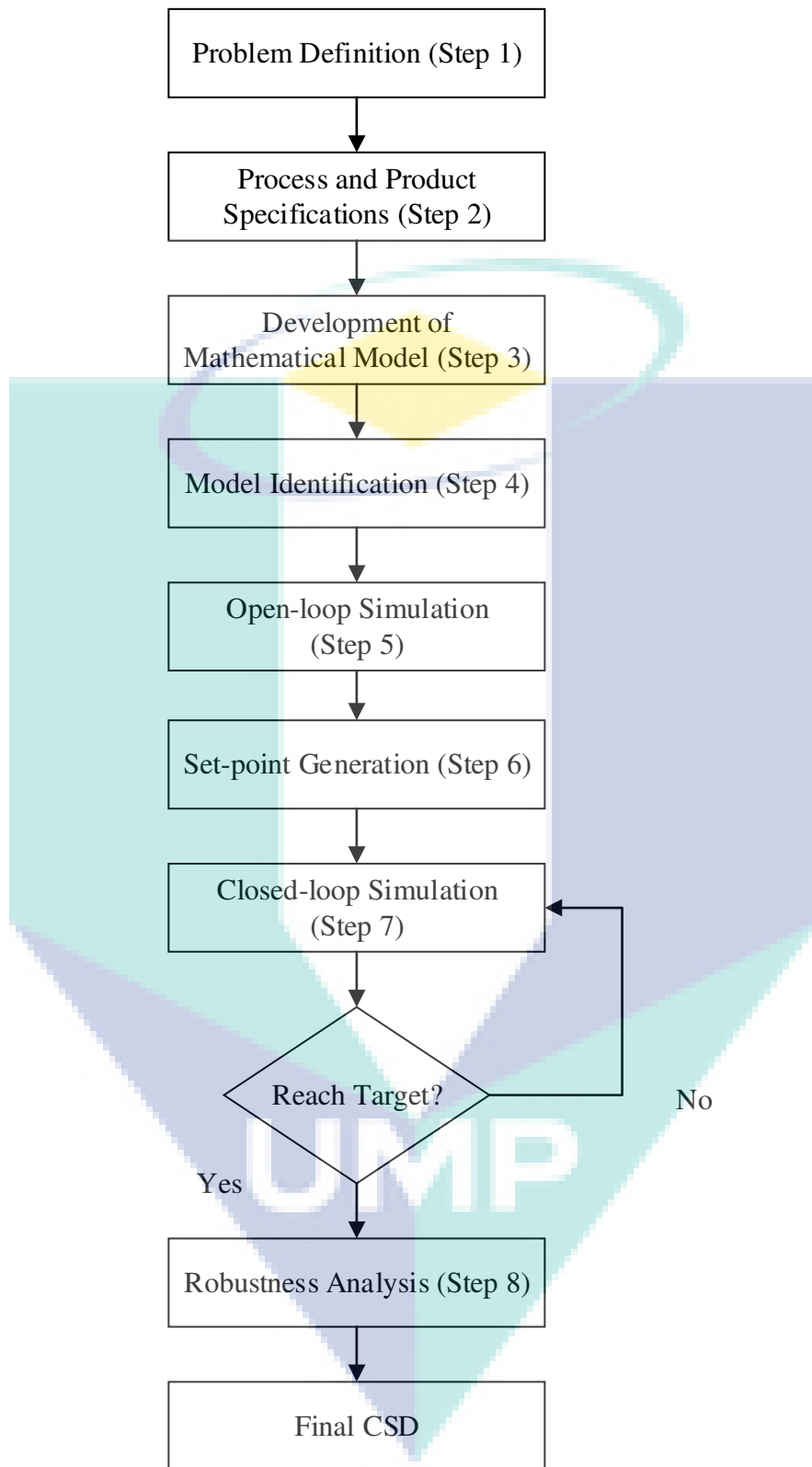


Figure 3.1 Systematic model-based framework for robust supersaturation control in batch cooling crystallization process

3.2.1 Problem Definition (Step 1)

The first step is the problem definition where the specific objective of crystallization process to be studied is defined. For example, the objective could be to study the dynamic behavior of crystallization process, to develop supersaturation control for achieving the desired target CSD or to evaluate the robustness of supersaturation controller.

3.2.2 Process and Product Specifications (Step 2)

The process and product specifications in Step 2 represents the selection of characteristics and specification of the crystallization process. In the process specification as shown in Figure 3.2, the user needs to select three main specifications which consists of to study crystallization process with or without the effects of agglomeration and breakage, in the case of size independent or size dependent crystal growth and finally for temperature independent or dependent study. The product specification is usually the target crystal properties in the form of CSD, mean crystal size and mean size diameter.

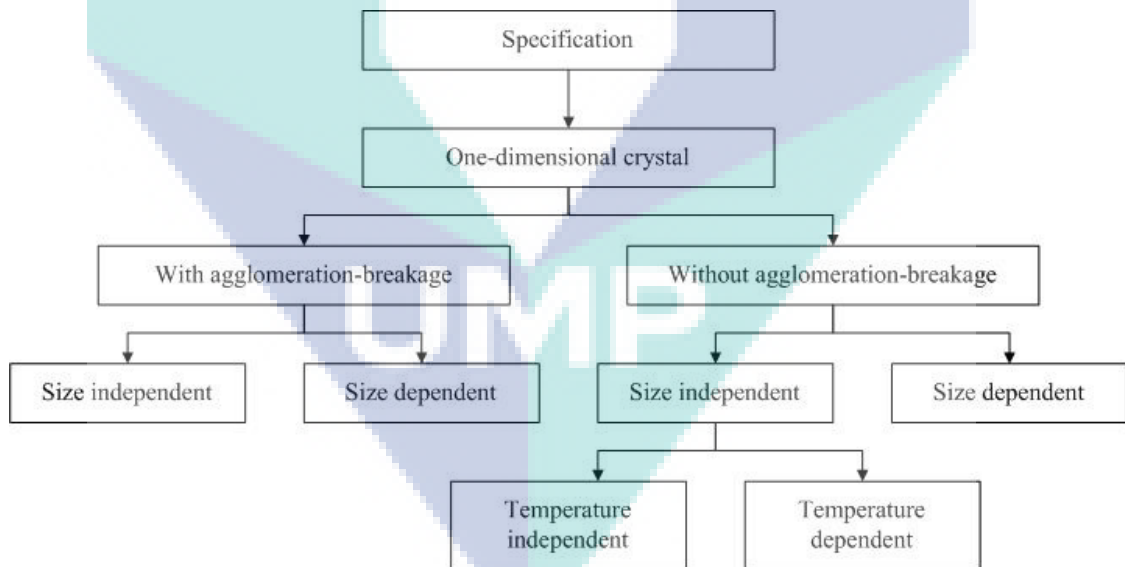


Figure 3.2 Specification of one-dimensional crystallization process

3.2.3 Development of Mathematical Model (Step 3)

In this step, the development of the mathematical model to represent the crystallization operation and phenomena is explained. The mathematical model for crystallization process can be divided into two types which are dynamic balances and constitutive model equations. The dynamic balance equations consists of the crystal population to represent the CSD, overall mass for solute concentration and energy for temperature behavior in crystallization process. The constitutive model equations contain a set of models for describing the crystallization phenomena such as nucleation, crystal growth rate, agglomeration, breakage as well as its chemical and physical properties such as saturation concentration, metastable concentration, total crystal mass and CSD formulation.

3.2.3.1 Population Balance Equation Model (PBE) Formulation

In this study, the population balance equation (PBE) model involves only for one-dimensional cases as shown in Table 3.1. In this step, the PBE is transformed into a system of ODE by applying the standard method of moments and the method of classes. Table 3.2 shows the solution of PBE using standard method of moments.

Table 3.1 Generic equation for one-dimensional PBE

| Equation |
|--|
| $\frac{\partial n(L,t)}{\partial t} = -\frac{\partial n(L,t)G(L,c,T)}{\partial L} + (B - D), \text{ where } (B - D) = B_{nuc} + B_{agg} - D_{agg} + B_{br} - D_{br}$ |

Table 3.2 Solution equations of one-dimensional PBE using method of moments

| Method of moments | |
|-------------------------------|-------------------------------|
| Size independent growth | |
| $\frac{d\mu_0}{dt} = B_{nuc}$ | $\frac{d\mu_3}{dt} = 3G\mu_2$ |
| $\frac{d\mu_1}{dt} = G\mu_0$ | $\frac{d\mu_4}{dt} = 4G\mu_3$ |
| $\frac{d\mu_2}{dt} = 2G\mu_1$ | |

The method of moments consists of 5 equations which are zeroth moment (μ_0) for calculating the total number of crystal particles produced from nucleation phenomena, first moment (μ_1) for estimating the total length of crystal particles, second moment (μ_2) for predicting the total area of crystal particles, third moment (μ_3) for computing the total crystal mass and finally the fourth moment (μ_4) is used for obtaining the mean size diameter of crystal particles. This method is actually calculating the total values of crystal particles at the end of the operation. In this method, it can be used for unseeded and seeded crystallization operation but it is only applicable to size independent characteristic only. Furthermore, the method cannot be used to cover the effects of agglomeration and breakage. In order to overcome these weaknesses, another method is included in this step which is the method of classes as shown in Table 3.3.

Table 3.3 Solution equations of one-dimensional PBE using method of classes

| Method of Classes | |
|--------------------------------|---|
| Size independent growth | |
| For $i = 1$: | $\frac{dN_1}{dt} + \frac{G}{2\Delta Cl_1} N_1 = B_{nuc} + B_{agg,1} - D_{br,1}$ |
| For $1 < i < n$: | $\frac{dN_i}{dt} + \frac{G}{2\Delta Cl_i} N_i - \frac{G}{2\Delta Cl_{i-1}} N_{i-1} = B_{agg,i} - D_{br,i}$ |
| For $i = n$: | $\frac{dN_n}{dt} + \frac{G}{2\Delta Cl_n} N_n - \frac{G}{2\Delta Cl_{n-1}} N_{n-1} = B_{agg,n} - D_{br,n}$ |
| Size dependent growth | |
| For $i = 1$: | $\frac{dN_1}{dt} + \frac{G(L_1)}{2\Delta Cl_2} N_2 + \frac{G(L_1) - G(L_0)}{2\Delta Cl_1} N_1 = B_{nuc} + B_{agg,1} - D_{br,i}$ |
| For $1 < i < n$: | $\frac{dN_i}{dt} + \frac{G(L_i)}{2\Delta Cl_{i+1}} N_{i+1} - \frac{G(L_1) - G(L_{i-1})}{2\Delta Cl_i} N_i - \frac{G(L_{i-1})}{2\Delta Cl_{i-1}} N_{i-1} = B_{agg,i} - D_{br,i}$ |
| For $i = n$: | $\frac{dN_n}{dt} - \frac{G(L_{n-1})}{2\Delta Cl_n} N_n - \frac{G(L_{n-1})}{2\Delta Cl_{n-1}} N_{n-1} = B_{agg,n} - D_{br,n}$ |

The method of classes can be used for size independent or dependent growth, unseeded or seeded operation as well as to include the agglomeration and breakage phenomena. The term classes in this method is referring to the number of discretization point. For example, if the CSD is targeted to be achieved at a characteristic length of 1000 μm . Then by assuming the size of each class is 2 μm then the number of discretization point

is 500 indicating that 500 equations will be used for method of classes. In this method, the number of discretization points need to be selected with caution. If less number of discretization point is selected, then less number of equations in the method of classes is needed but sometimes it will lead to the inaccuracy of CSD obtained by the end of the operation. However, if the number of equations is too high then a long computational time is expected. Therefore the accuracy of this method is measured based on selected number of discretization points and the computational effort to solve the equations. However, this problem can be overcome with the availability of faster computer (Samad et al., 2011; Abbas and Romagnoli, 2007; Costa et al., 2005).

3.2.3.2 Overall Mass Balance Formulation

The overall mass balance equation involves the general balance equation of the total or component mass of any system that is used to describe and design almost every process in the chemical system. The overall mass balance equation will be depending on the PBE solution either using standard method of moments or method of classes as shown in Table 3.4.

Table 3.4 Overall mass balance for one-dimensional crystallization

| Types | Equations |
|-------------------|--|
| Generic equations | $\frac{dc}{dt} = -\frac{\rho_c k_v V}{m_w} \left(3 \int_0^{\infty} Gn(L, t) L^2 dL \right)$ |
| Method of moments | $\frac{dc}{dt} = -\frac{\rho_c k_v V}{m_w} (3G\mu_2)$ |
| Method of classes | $\frac{dc}{dt} = -\frac{\rho_c k_v V}{m_w} \left(\sum_{i=1}^{i=N} S_i^3 N_i \right)$ |

3.2.3.3 Energy Balance Formulation

The concept of energy balance formulation is similar to the mass balance formulation where a balance of energy is important in solving many problems involving the change of temperature during the operation. Similarly like overall mass balance, the final equation for energy balance depends on the solution of PBE. Table 3.5 lists the energy balance equation for one-dimensional case study.

Table 3.5 Energy balance for one-dimensional crystallization

| Types | Equations |
|-------------------|---|
| Generic equations | $\rho V c_p \frac{dT}{dt} = -\Delta H_c \rho_c k_v V \left(3 \int_0^{\infty} G n(L, t) L^2 dL \right) - U_1 A_1 (T - T_w)$ |
| Method of moments | $\rho V c_p \frac{dT}{dt} = -\Delta H_c \rho_c k_v V (3G\mu_2) - U_1 A_1 (T - T_w)$ |
| Method of classes | $\rho V c_p \frac{dT}{dt} = -\Delta H_c \rho_c k_v V \left(\sum_{i=1}^{i=N} S_i^3 N_i \right) - U_1 A_1 (T - T_w)$ |

3.2.3.4 Cooling Jacket Energy Balance Formulation

In the batch cooling crystallization process, it is assumed that the jacketed batch crystallizer is used. Therefore the cooling jacket energy balance equation for one-dimensional case is similar for both method of moments and method of classes as shown in the Table 3.6.

Table 3.6 Cooling jacket energy balance for one-dimensional crystallization

| Generic equation |
|--|
| $\rho_w V_w c_{pw} \frac{dT_w}{dt} = \rho_w F_{win} c_{pw} (T_{win} - T_w) + U_1 A_1 (T - T_w) + U_2 A_2 (T_{ex} - T_w)$ |

3.2.3.5 Selection of Constitutive Equations

The constitutive equations involve the kinetic phenomena and solubility model such as nucleation, crystal growth rate, supersaturation, metastable concentration, saturation concentration, agglomeration, breakage as well as its physical properties of crystallization process such as total crystal mass and CSD. The list of constitutive equations is shown in the Table 3.7.

Table 3.7 List of constitutive equations for the one-dimensional model of crystallization

| Types | Equations | References |
|--|--|----------------------------------|
| Saturation concentration | $c^{sat} = a_{i1} + b_{i1}T + c_{i1}T^2 + d_{i1}T^3$ | Shi et al. (2011) |
| Metastable concentration | $c^{met} = a_{i2} + b_{i2}T + c_{i2}T^2 + d_{i2}T^3$ | Shi et al. (2011) |
| | $\Delta c = c - c^{sat}$ (degree of supersaturation) | |
| Supersaturation | $S = \frac{c - c^{sat}}{c^{sat}}$ (relative supersaturation) $\sigma = \frac{c}{c^{sat}}$ (supersaturation ratio) | Myerson (2002) |
| Nucleation | $B_{nuc} = k_b S_b M_c^j N_{rpm}^p$ | Quantina-hernandez et al. (2004) |
| Crystal growth rate (size independent) | $G_x = k_g S^g N_{rpm}^q$ | Quantina-hernandez et al. (2004) |
| Characteristic size | $S_{xi} = \frac{L_{xi} - L_{xi-1}}{2}$ | Samad et al. (2011) |
| Size of classes | $\Delta Cl_i = S_{xi} - S_{xi-1}$ | Samad et al. (2011) |
| Total number of particles | $N_c = N_1 + N_2 + N_3 + \dots + N_n$ | Myerson (2002) |
| Total crystal mass | $M_c = \rho_c k_v \left(\sum_{i=1} S_{xi}^3 N_i \right)$ | Samad et al. (2011) |
| Crystal size distribution | $f_n(L_{xi}) = \frac{(N_i / \Delta Cl_i) + (N_{i+1} / \Delta Cl_{i+1})}{2}$ | Samad et al. (2011) |
| Production reduction-term | $\alpha = K_a S^a M_c^k N_{rpm}^r$ | Quantina-hernandez et al. (2004) |

3.2.4 Model Identification (Step 4)

The model identification has been included in the model-based framework in order to estimate the kinetic parameters of crystallization operation (nucleation, crystal growth, agglomeration, breakage) and also to calculate the confidence interval for each estimated parameters. For model identification, the objective function for parameter estimation takes the following form:

$$F_{obj} = \min_{\theta} \left\{ w_T \sum_{i=1}^n \left(\frac{T_{calculated} - T_{exp}}{T_{exp}} \right)^2 + w_c \sum_{i=1}^n \left(\frac{c_{calculated} - c_{exp}}{c_{exp}} \right)^2 + w_S \sum_{i=1}^n \left(\frac{S_{calculated} - S_{exp}}{S_{exp}} \right)^2 + w_{Mc} \sum_{i=1}^n \left(\frac{Mc_{calculated} - Mc_{exp}}{Mc_{exp}} \right)^2 \right\} \quad 3.1$$

Where $\theta = [k_b, b, j, p, k_g, g, q, k_a, a, k, r]$ is the sets of parameters for the nucleation, crystal growth, agglomeration and breakage. Meanwhile w is the weightage used for temperature, concentration, supersaturation and total crystal mass. The value of w is assumed in the range of 0.1 to 1 (Nagy and Aamir, 2012). Based on Equation (3.1), it requires the experimental data for temperature, solute concentration, supersaturation and total crystal mass. The experimental data can be obtained from the experimental works or from published literature (for example the potassium sulphate experimental data is taken from Shi et al., 2006). However, in some cases it is not possible to obtain all the necessary data. Therefore the compulsory data needed to perform model identification is temperature and solute concentration experimental datas. In this work, the model identification is developed in the Matlab modelling software using least square method as a solver to estimate the necessary kinetic parameters.

3.2.5 Open-loop Simulation (Step 5)

The mathematical model developed in Step 3 will be combined and simulated with model identification in Step 4 under open-loop condition. In this step the model validation is performed where the predicted dynamic behavior data using estimated kinetic parameters is compared with experimental data taken from literature works. If the data is matching then the model is validated and the estimated kinetic parameters are indeed reliable. In the case of mismatch data, then the model identification is performed again until the simulated data is matching with experimental data or the kinetic model for nucleation or crystal growth rate needs to be changed with other types of model.

3.2.6 Set-point Generation (Step 6)

In this step, a systematic procedure to generate the set-point necessary for achieving the target CSD is introduced. Previously, the original analytical CSD estimator for one-dimensional crystallization process has been developed by incorporating the growth kinetics without considering the effects of agglomeration and breakage phenomena as well as temperature dependence in the kinetic rates. In this work, the original analytical CSD estimator has been extended to cover the effects of agglomeration and breakage as well as temperature dependence case for assessing its influence on the performance of the final CSD. In order to represent the effects of agglomeration and breakage, the production-reduction term (α) as shown in Table 2.4 is used. Meanwhile the Arrhenius expression is employed for covering the effects of temperature dependence. The derivation of the extended analytical CSD estimator is shown below. Population balance equation (f_n) incorporating production-reduction term, α for one-dimensional case is shown in Equation (3.2).

Population balance equation:

$$\frac{df_n(L_x, t)}{dt} + \frac{d[G_x(L_x, t)f_n(L_x, t)]}{dL_x} = \alpha \quad 3.2$$

In the case of size independent growth rate, Equation (3.2) can be rewritten as:

$$\frac{df_n}{dt} + G_x \frac{df_n}{dL_x} = \alpha \quad 3.3$$

The expression for size independent growth with the effects of agitation is given by:

$$G_x = k_g S^g N_{rpm}^r \quad 3.4$$

The supersaturation is assumed to be constant which is possible in a controlled crystallization and supersaturation expression is given by:

$$S = \frac{c - c^{sat}}{c^{sat}} \quad 3.5$$

Notes that relative supersaturation is used in Equation (3.5). However the degree of supersaturation or supersaturation can be used in the same way as relative supersaturation. Differentiating Equation (3.4) with respect to characteristic length gives:

$$\frac{dG_x}{dL_x} = 0 \quad 3.6$$

Introduce $f_n(L_x, t) = f_n(L_x(Z), t(Z))$ and by applying chain rule give:

$$\frac{dL_x}{dZ} \frac{df_n}{dL_x} + \frac{dt}{dZ} \frac{df_n}{dt} = \frac{df_n}{dZ} \quad 3.7$$

Comparing Equation (3.7) and (3.3), gives:

$$\frac{dt}{dZ} = 1 \quad 3.8$$

$$\frac{dL_x}{dZ} = G_x \quad 3.9$$

$$\frac{df_n}{dZ} = \alpha \quad 3.10$$

Integrating Equations (3.8) with limits:

$$dt = dZ \quad 3.11$$

$$\int_{t_0}^t dt = \int_{z_0}^z dZ \quad 3.12$$

$$(t - t_0) = (Z - Z_0) \quad 3.13$$

By assuming $t_0 = Z_0 = 0$, Equation (3.13) can be simplified as:

$$t = Z \quad 3.14$$

Since $dt = dZ$, Equation (3.9) becomes:

$$\frac{dL_x}{dt} = G_x \quad 3.15$$

Substitute Equation (3.4) into (3.15) gives:

$$\frac{dL_x}{dt} = k_g S^g N_{rpm}^r \quad 3.16$$

Integrating Equation (3.16) with limits:

$$dL_x = k_g S^g N_{rpm}^r dt \quad 3.17$$

$$\int_{L_{x0}}^{L_x} dL_x = k_g S^g N_{rpm}^r \int_{t_0}^t dt \quad 3.18$$

$$(L_x - L_{x0}) = k_g S^g N_{rpm}^r (t - t_0) \quad 3.19$$

By assuming $t_0 = 0$, Equation (3.19) can be simplified:

$$(L_x - L_{x0}) = k_g S^g N_{rpm}^r t \quad 3.20$$

Rearranging Equation (3.20) gives:

$$L_x = L_{x0} + k_g S^g N_{rpm}^r t \quad 3.21$$

Equation (3.21) represents the final expression for calculating characteristic length of crystal particles. Since $dt = dZ$, thus:

$$\frac{df_n}{dt} = \alpha \quad 3.22$$

Integrating Equation (3.22) with limits:

$$\int_{f_{n0}}^{f_n} df_n = \alpha \quad 3.23$$

$$(f_n - f_{n0}) = \alpha \quad 3.24$$

$$f_n = f_{n0} + \alpha \quad 3.25$$

Where Equation (3.25) represents the final equation for calculating the CSD. In this derivation, the analytical CSD estimator is successfully developed for considering the effects of agglomeration and breakage in the case of temperature independence. For temperature dependence, the kinetic model for temperature dependence crystal growth rate as shown in Table 3.7 is used and substituted into Equation (3.4). The derivation is then repeated. The extended analytical CSD estimator is summarized in Table 3.8 where it is applicable for the case of with or without agglomeration and breakage as well as temperature independence or temperature dependence.

In order to generate the optimal supersaturation set-point using the extended analytical CSD estimator, three conditions must be taken into accounts which are the initial seed of crystals ($f_{n0,i}$), a target CSD ($f_{n,i \text{ target}}$) and a kinetic data for the growth and agglomeration-breakage must be available. Usually, the initial seed of CSD and target CSD are supplied in the form of normal, lognormal or bimodal distribution (Samad et al., 2013). Meanwhile the kinetic data is obtained from model identification step. Based on analytical CSD estimator, the candidate of set-points which are the supersaturation

set-point (S_{sp}) and total crystallization time (t_c) can be generated and the optimal set-point is obtained based on model-based optimization as shown in Equations (2.16)-(2.19).

Table 3.8 New extension of analytical CSD estimator expressions for one-dimensional crystallization

| | Characteristic | Analytical model equations |
|--|--|---|
| Size independence growth (No agglomeration and breakage) | Temperature independence: $G_x = k_g S^g$ | Final CSD: $f_{n,i} = f_{n0,i} \quad i = 1,2,\dots,N$ Final characteristic length: $L_{x,i} = L_{x0,i} + k_g S_{sp}^g t_c, \quad i = 1,2,\dots,N$ |
| | Temperature dependence: $G_x = k_g e^{\frac{-E_g}{RT}} S^g$ | Final CSD: $f_{n,i} = f_{n0,i} \quad i = 1,2,\dots,N$ Final characteristic length: $L_{x,i} = L_{x0,i} + k_g e^{\frac{-E_g}{RT}} S_{sp}^g t_c, \quad i = 1,2,\dots,N$ |
| Size independence growth (With agglomeration and breakage) | Temperature independence: $G_x = k_g S^g N_{rpm}^q$ | Final CSD: $f_{n,i} = f_{n0,i} + k_a S_{sp}^g M_c^k N_{rpm}^r \quad i = 1,2,\dots,N$ Final characteristic length: $L_{x,i} = L_{x0,i} + k_{gx} S_{sp}^g N_{rpm}^q t_c, \quad i = 1,2,\dots,N$ |
| | Temperature dependence: $G_x = k_g e^{\frac{-E_g}{RT}} S^g N_{rpm}^q$ | Final CSD: $f_{n,i} = f_{n0,i} + k_a S_{sp}^g M_c^k N_{rpm}^r \quad i = 1,2,\dots,N$ Final characteristic length: $L_{x,i} = L_{x0,i} + k_g e^{\frac{-E_g}{RT}} S_{sp}^g N_{rpm}^q t_c, \quad i = 1,2,\dots,N$ |

3.2.7 Closed-loop Simulation (Step 7)

In this step, the mathematical model is then simulated under closed-loop condition. In the closed-loop condition, a Proportional-Integral (PI) control as shown in Equation (3.26) is proposed to maintain the solute concentration based on set-point generated in Step 6. The PI control is the most suitable controller and widely used for maintaining the concentration in crystallization process (Samad et al., 2011, Nagy et al., 2008, Fujiwara et al. 2008). Based on literature, it is proven that the PI controller is performed better than the Proportional (P) controller and also produce similar performance as Proportional-Integral-Derivative (PID) (Fujiwara et al., 2008).

$$y_m = \bar{y}_m + K_c \left[e(t) + \frac{1}{\tau_I} \int_0^t e(t) dt \right] \quad 3.26$$

Where y_m is the current measured variable and \bar{y}_m is the previous measured variable. K_c and τ_I are the controller parameters for proportional and integral actions. Meanwhile $e(t)$ is the error between set-point variable and measured variable. For crystallization process, the set-point variable is supersaturation and the measured variable is solute concentration. In order to calculate the controller parameters for PI controller, dynamic response from open-loop simulation is performed. Based on dynamic response, the process reaction curve in the form of first order plus time delay is constructed. Then the values of K_c and τ_I are calculated using Internal Model Control (IMC) tuning method (Samad et al., 2011; Nagy et al., 2008). The mathematical model of crystallization process is then simulated under closed-loop simulation and the performance of controller is analyzed. Two important criterias are measured in the closed-loop simulation. Firstly the performance of PI controller to follow the given set-point trajectory and secondly the achievement of target CSD. In this closed-loop simulation, the set-point trajectory has been generated from extended analytical CSD estimator where theoretically if the operation is maintained at the set-point, the target CSD could be achieved. Thus the ability of PI controller to maintain the operation at the generated set-point is analyzed. If indeed the operation has been maintained at its set-point then the final CSD obtained is compared with the target CSD. If these two criterias are not met then the controller will undergo the tuning process until both criterias are obtained.

3.2.8 Robustness Analysis (Step 8)

Step 8 introduces the controller testing in terms of its robustness. Two types of testing will be conducted which consists of controller performance based on set-point tracking and disturbance rejection as well as uncertainty analysis involving Monte Carlo procedure.

3.2.8.1 Set-point Tracking and Disturbance Rejection

The performance of PI controller is tested based on its ability to track the changes of set-point and the presence of disturbance. For set-point tracking, three different set-points are employed in order to test the PI controller. Meanwhile two small fluctuations in cooling jacket temperature are introduced during the crystallization operation for disturbance rejection. A good controller must be able to adapt the changes of set-point and to reject the disturbance introduces during the crystallization operation.

3.2.8.2 Uncertainty Analysis

The PI controller is further tested based on uncertainty analysis. In this work, uncertainties are considered in the input parameters of the kinetic models such as nucleation, crystal growth, agglomeration and breakage. The value of each parameters are determined from the model identification step. The suitable range of uncertainty for each parameter is obtained from the upper and lower bound of kinetic parameters which can be obtained from the confidence interval. The Monte Carlo procedure is then implemented in order to propagate different sources of uncertainties in the model prediction. The Monte Carlo procedure involves three sub-steps: (1) sampling of uncertainties; (2) Monte Carlo simulations; and (3) evaluation of output uncertainties.

Sampling of Uncertainties

The next step concerns with the number of sampling specifications. Since there is no suitable approach to determine the appropriate number of sampling, 5 different number of sampling are used in this work for example it may consists of 25, 50, 100 and 150 samples. The combination of input uncertainties are then generated based on 5 different number of sampling. For example, 5 different combination for input uncertainties are generated for 5 number of sampling where these 5 different

combination are then used for Monte Carlo simulation. In order to generate this combination, a Latin-Hypercube sampling method (LHS method) can be applied (Gunawan et al., 2004; Helton and Davis, 2003). Based on each samples, the mean, standard deviation and Monte Carlo error as shown in Equations (3.27)-(3.29) are calculated. Here the best number of sampling is determined based on the lowest Monte Carlo error. Usually the lowest Monte Carlo error indicates that the input uncertainties are successfully propagating on the output prediction.

$$\bar{X} = \frac{\sum_i X_i}{N} \quad 3.27$$

$$SD = \frac{\sqrt{\sum (X - \bar{X})^2}}{N} \quad 3.28$$

$$MC_{error} = \frac{\sigma}{\sqrt{N_{samples}}} \quad 3.29$$

Monte Carlo Simulation

In this step, the Monte Carlo simulation is performed based on the best number of sampling. For example, if the best number of sampling is 100 then the mathematical model of crystallization process is simulated for 100 times using 100 different combination of input uncertainties using Monte Carlo simulation.

Evaluation of Output Uncertainties

The model output from Monte Carlo simulation is then evaluated in terms of the model output variation. In this work, the severity of uncertainty is measured based on the spread of the data. The higher spread of the data indicating the high uncertainty is presence. In the uncertainty analysis, the closed-loop simulation is repeated using different combinations of input uncertainties based on the number of sampling. Thus it will affect the behavior of crystallization process particularly solute concentration, temperature and final CSD. This contributes to the spread of data in the end of operation if the controller not able to counteract the effects of input uncertainties. Thus the influence of input uncertainties is concluded as dominant and high (Sin et al., 2008). The main focus is the impact of input uncertainties on the CSD where the low

variability of the CSD is preferred. In this case, the performance of PI controller is analyzed in terms of its ability to maintain the concentration at the set-point for different combinations of kinetic parameters. Subsequently the variability of the CSD is then checked in this evaluation. If spread of the CSD data is small then it can be concluded that the PI controller is robust enough to counteract the impact of input uncertainties. In the case large variation of CSD is obtained then the PI controller needs to be retuned and Monte Carlo simulation will be performed again in order to improve its robustness.

In the end the outcome of this work is that the final target CSD is achieved with less variability through closed-loop simulation using a robust PI controller developed in this study.

3.3 Concluding Remarks

In this chapter, a model-based framework for robust supersaturation control in batch cooling crystallization process is proposed to achieve the desired target CSD using robust control. This model-based framework is generic where it can be applied on a wide range of crystallization process. The features of this model-based framework consists of mathematical model development, model identification, set-point generation, open- and closed-loop operations as well as robustness analysis for controller. The set-point for achieving the target CSD is generated using analytical CSD estimator where it has been extended to cover the effects of agglomeration and breakage as well as the effects of temperature dependence on kinetic rates. In addition, the robustness of controller to reduce the variation of CSD is also introduced in the model-based framework. This unique feature provides the platform of testing the controller performance for counteracting the impact of input uncertainties and at the same time achieving the desired target of CSD with less variability.

CHAPTER 4

APPLICATION OF ROBUST SUPERSATURATION CONTROL IN BATCH COOLING CRYSTALLIZATION PROCESS

4.1 Overview

The application of the systematic model-based framework for robust supersaturation control of batch cooling crystallization process is tested and evaluated through two case studies involving potassium sulphate and sucrose crystallization processes. The first case study involving potassium sulphate crystallization process has been adopted from Shi et al. (2006) where the target CSD is obtained for the case of temperature dependence in the nucleation and crystal growth kinetics. Meanwhile sucrose crystallization is the selected second case study which has been adopted from Quintana-Hernández et al. (2004). In this second case study, production-reduction term is used to represent the effects of agglomeration and breakage and its impact on achieving the target CSD is discussed.

4.2 Application of the Model-based Framework: Potassium Sulphate Crystallization Process

The application of the model-based framework is highlighted using potassium sulphate crystallization process. Relevant data for this case study is taken from Shi et al. (2006).

4.2.1 Problem Definition (Step 1)

The overall objective for this case study is to design a robust supersaturation control for potassium sulphate crystallization process in order to achieve the desired target CSD. The target CSD used is taken from Shi et al. (2006) as uniform distribution and is expressed as follows:

For $487 \mu\text{m} \leq L \leq 537 \mu\text{m}$:

$$f(L,0) = 0.0032(537 - L)(L - 487) \quad 4.1$$

For $L < 487 \mu\text{m}$, $L > 537 \mu\text{m}$:

$$f(L,0) = 0 \quad 4.2$$

The target CSD generated from Equations (4.1) and (4.2) is shown in Figure 4.1.

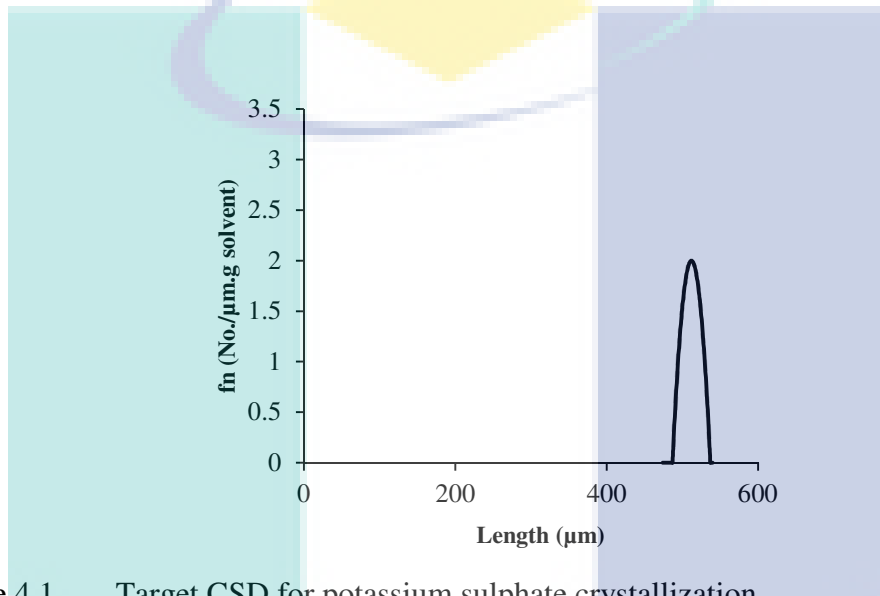


Figure 4.1 Target CSD for potassium sulphate crystallization

4.2.2 Process and Product Specifications (Step 2)

In this step the process specification is one-dimensional crystallization process for size independent crystal growth with temperature dependence. It has been assumed the effects of agglomeration and breakage is neglected. The chemical system involved in this study consists of potassium sulphate as a solute and water as a solvent. The jacketed batch crystallizer is assumed for this operation. For the product specification, the CSD of potassium sulphate is the target product as shown in Figure 4.1 where the mean characteristic length and standard deviation for the target CSD are $512 \mu\text{m}$ and $2.8 \mu\text{m}$ respectively.

4.2.3 Development of Mathematical Model (Step 3)

Based on the process specifications, the necessary mathematical model is then developed. Firstly, the population balance equation (PBE) model is formulated based on

the assumptions of seeded operation with size independent growth (temperature dependence) with neglecting the agglomeration and breakage phenomena. The PBE is solved using the method of classes where the size of class (ΔCl) is set at 0.5 μm and the number of equations used for method of classes are 1200. The number of equations used are based on target CSD in Figure 4.1 where the projected characteristic length for CSD is up to 600 μm . Thus if the size of class is set at 0.5 μm , 1200 total number of equations should be used in order to meet the projected characteristic length. The equations for overall mass and energy balances are selected based on the method of classes solution. For the selection of constitutive equations, secondary nucleation is assumed, relative supersaturation is employed and the temperature dependence is included in the nucleation and crystal growth rate equations. Based on the above information, the complete mathematical model for potassium sulphate crystallization process is summarized in the Table 4.1. Table 4.2 shows some of the known variables taken from Shi et al. (2006) in the mathematical model of potassium sulphate for the seeded batch cooling crystallizer.

Table 4.1 List of model equations for the one-dimensional model of potassium sulphate crystallization

| Types | Equations |
|--|---|
| Population balance equation | $\frac{dN_1}{dt} + \frac{G_x}{2\Delta Cl} N_1 = B_{nuc}, i = 1$ $\frac{dN_i}{dt} + \frac{G_x}{2\Delta Cl} N_i + \frac{G_x}{2\Delta Cl} N_{i-1} = 0, 1 \leq i \leq n$ $\frac{dN_n}{dt} + \frac{G_x}{2\Delta Cl} N_n - \frac{G_x}{2\Delta Cl} N_{n-1} = 0, i = n$ |
| Overall mass balance: solute concentration | $\frac{dc}{dt} = -\frac{\rho_c k_v v}{m_w} \left(\sum_{i=1}^n S_{xi}^3 \frac{dN_i}{dt} \right)$ |
| Energy balance | $\rho V c_p \frac{dT}{dt} = -H_c \rho_c k_v v \left(\sum_{i=1}^n S_{xi}^3 \frac{dN_i}{dt} \right) - U_1 A_1 (T - T_w)$ |
| Cooling jacket energy balance | $\rho_w V_w c_{pw} \frac{dT_w}{dt} = \rho_w F_{win} c_{pw} (T_{win} - T_w) + U_1 A_1 (T - T_w) + U_2 A_2 (T_{ex} - T_w)$ |
| Saturation concentration | $c^{sat} = 6.29 \times 10^{-2} + 2.46 \times 10^{-3} T - 7.14 \times 10^{-6} T^2$ |
| Metastable concentration | $c^{met} = 7.76 \times 10^{-2} + 2.46 \times 10^{-3} T - 8.10 \times 10^{-6} T^2$ |
| Supersaturation | $S = \frac{c - c^{sat}}{c^{sat}}$ |
| Nucleation | $B_{nuc} = k_b \exp(-E_b / RT) S^b \mu_3$ |

Table 4.1 Continued

| Types | Equations |
|---------------------------|---|
| Crystal growth rate | $G_x = k_g \exp(-E_g / RT) S^g$ |
| Characteristic size | $S_{xi} = \frac{L_{xi} - L_{xi-1}}{2}$ |
| Total number of particles | $N_c = N_1 + N_2 + N_3 + \dots + N_n$ |
| Total crystal mass | $M_c = \rho_c k_v \left(\sum_{i=1}^n S_{xi}^3 N_i \right)$ |
| Crystal size distribution | $f_n(L_{xi}) = \frac{(N_i / \Delta Cl) + (N_{i+1} / \Delta Cl)}{2}$ |

Table 4.2 Parameter values of potassium sulphate in batch cooling crystallizer

| Parameter | Value | Units |
|---|------------------------|-----------------------------|
| Overall heat transfer coefficient (internal), U_1 | 1800 | $\text{kJ/m}^2 \text{ h K}$ |
| Total heat-transfer surface area (internal), A_1 | 0.25 | m^2 |
| Overall heat transfer coefficient (internal), U_2 | 2300 | $\text{kJ/m}^2 \text{ h K}$ |
| Total heat-transfer surface area (external), A_2 | 0.45 | m^2 |
| Heat of crystallization, ΔH | 44.5 | kJ/kg |
| Heat capacity of solution, C_p | 3.8 | kJ/ K kg |
| Inlet water flow rate, F_{win} | 5500 | cm^3/min |
| Exterior temperature, T_{ex} | 302 | K |
| Mass of solvent, M | 27.0 | Kg |
| Density of crystals, ρ_c | 2.66×10^{-12} | $\text{g}/\mu\text{m}^3$ |
| Density of water, ρ_w | 1 | g/cm^3 |
| Volumetric shape factor, k_v | 1.5 | - |
| Operation time, t_f | 30 | min |

Source: Shi et al. (2006)

The initial seed distribution used for this seeded operation is based on the uniform distribution as shown in Equations (4.3) – (4.4). Figure 4.2 shows the initial seed distribution obtained from this uniform distribution where the initial mean characteristic length is 275 μm (Shi et al., 2006). Here the idea is to use the initial seed as a starting point and to grow the seed until it reaches the target CSD as shown in Figure 4.1.

For $250 \mu\text{m} \leq L \leq 300 \mu\text{m}$:

$$f(L,0) = 0.0032(300 - L)(L - 250) \quad 4.3$$

For $L < 250 \mu\text{m}$, $L > 300 \mu\text{m}$:

$$f(L,0) = 0 \quad 4.4$$

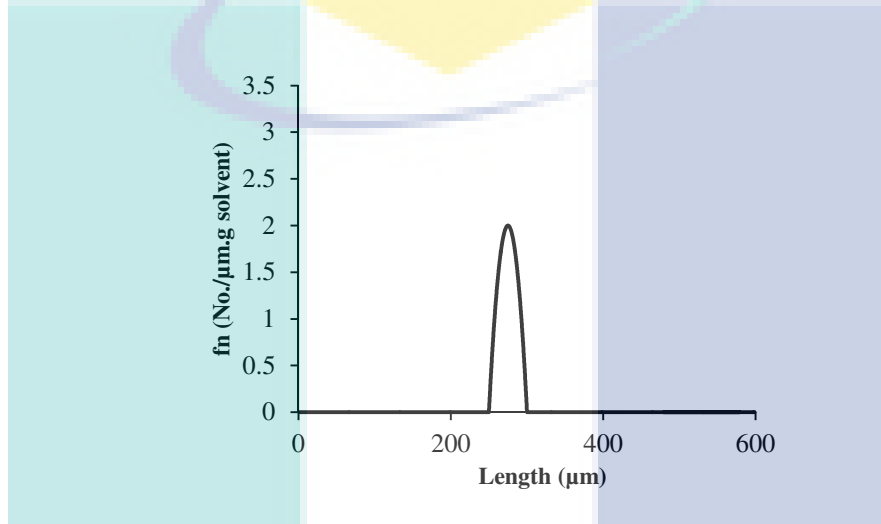


Figure 4.2 Initial seed distribution for potassium sulphate crystallization

4.2.4 Model Identification (Step 4)

In this step the model identification is implemented to predict the kinetic parameters of nucleation and crystal growth rate. There are 6 parameters for nucleation and crystal growth rate to be predicted which consists of k_b , b , E_b/R , k_g , g and E_g/R . In order to estimate all of these parameters, the experimental datas of temperature and potassium sulphate concentration are available which are taken from Shi et al. (2006). The objective function for parameter estimation is shown in Equation (4.5):

$$F_{obj} = \min_{\theta} \left\{ w_T \sum_{i=1}^n \left(\frac{T_{calculated} - T_{exp}}{T_{exp}} \right)^2 + w_c \sum_{i=1}^n \left(\frac{c_{calculated} - c_{exp}}{c_{exp}} \right)^2 \right\} \quad 4.5$$

Subject to: $\theta_{min} < \theta < \theta_{max}$ and model equations in Table 4.1

Where θ represents the 6 parameters to be estimated, θ_{min} is the lower bound of parameters and θ_{max} is the upper bound of parameters. The weightages used for

temperature (w_T) and potassium sulphate concentration (w_c) are 0.5 and 0.2 respectively. The model identification is then performed in Matlab software and based on the simulation the objective function obtained is 4.5×10^{-05} . Table 4.3 shows the estimated kinetic parameter for potassium sulphate crystallization. The estimated kinetic parameters obtained in this work are compared with the value obtained from literature and a good agreement has been achieved where the estimated parameters are very close with the expected value in literature. This indicates that the developed model identification is very reliable and is able to predict the accurate parameters. In addition the confidence interval is also calculated in this step and the interval for each parameters are shown in Table 4.3.

Table 4.3 Estimated kinetic parameters for potassium sulphate crystallization

| Parameter | k_b | b | E_b/R | E_g/R | k_g | g |
|--|--------|------|---------|---------|---------------------|------|
| Literature value (Shi et al., 2006) | 285.01 | 1.45 | 7517 | 4859 | 1.440×10^8 | 1.50 |
| This work | 284.50 | 1.45 | 7515 | 4788 | 1.435×10^8 | 1.49 |
| Confidence interval | 5.1 | 0.09 | 109 | 167.2 | 0.08×10^8 | 0.07 |

4.2.5 Open-loop Simulation (Step 5)

Based on the estimated kinetic parameters, the mathematical model as shown in Table 4.1 is simulated under open-loop condition using the same operating condition from literature to allow model validation. The model is solved using backward differentiation formula (BDF) method known as solver ‘ode15s’ which is available in the Matlab software. Figures 4.3 and 4.4 show the crystallizer temperature and the potassium sulphate concentration profile under the conventional linear cooling strategy where the temperature of crystallizer is cooled down linearly from 323 K to 303 K for 30 minutes operation time. As consequence the potassium sulphate concentration is dropped linearly from 0.1742 g potassium sulphate/g water to 0.1372 g potassium sulphate/g water at the final time. This is due to the fact that potassium sulphate concentration is depends on the temperature behavior.

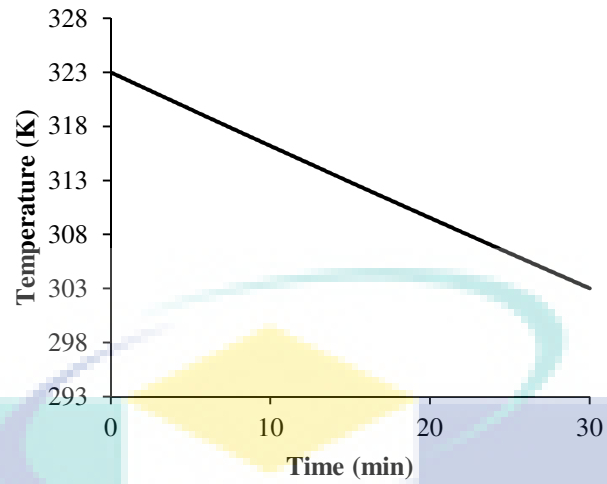


Figure 4.3 Temperature profiles under open-loop condition

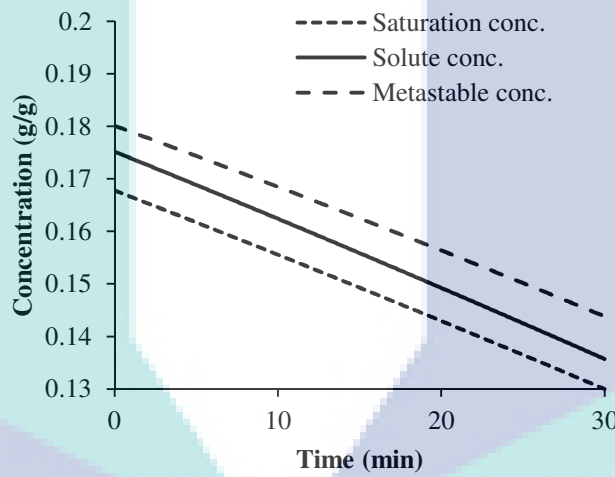


Figure 4.4 Potassium sulphate concentration profiles under open-loop condition

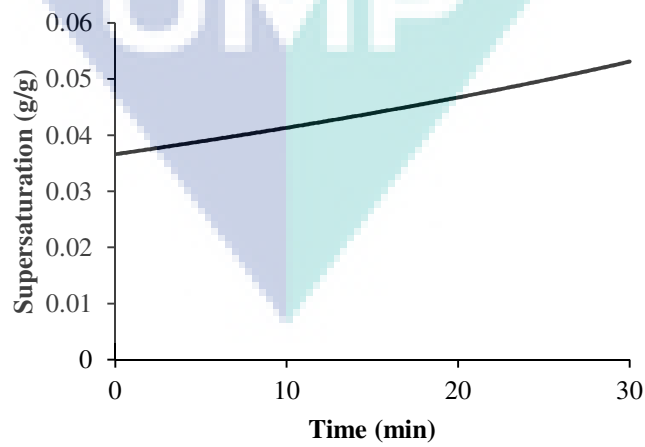


Figure 4.5 Supersaturation profiles under open-loop condition

Figure 4.4 also shows that the crystallization operation is operated within the metastable zone where the potassium sulphate concentration profile lies between the saturation concentration and metastable concentration. Meanwhile the relative supersaturation obtained is shown in Figure 4.5 where initially the relative supersaturation is 0.036 and starts to increase steadily up to 0.053. Based on Figures 4.4 and 4.5, it is clear indicated that the crystallization process occurs and the relative supersaturation level will drive the solute in the solution into seed crystal and grown based on nucleation and crystal growth kinetics. The final CSD obtained in this work is shown in Figure 4.6 where initially the seed of CSD as shown in Figure 4.2 at mean characteristic length of 275 μm has been grown into mean characteristic length of 512 μm which is matching with desired target set in product specification step. However there are two patterns of CSD behavior as shown in Figure 4.6 where the peak on the right is the crystals grown from initial seed. The other pattern indicates the crystals formed by secondary nucleation as shown on the left of Figure 4.6. Although the seed of CSD has been grown to achieve the desired target but the number of crystals produced from secondary nucleation is relatively high. This is due to the fact that the relative supersaturation is keeps increasing and thus the excessive nucleation is expected. The production of these new crystals at relatively low size is not preferable in the crystallization process because it will affect the downstream process such as fouling. In addition the final CSD obtained is in good agreement with the CSD from literature data which indicating the method of classes as a solution of PBE is indeed reliable.

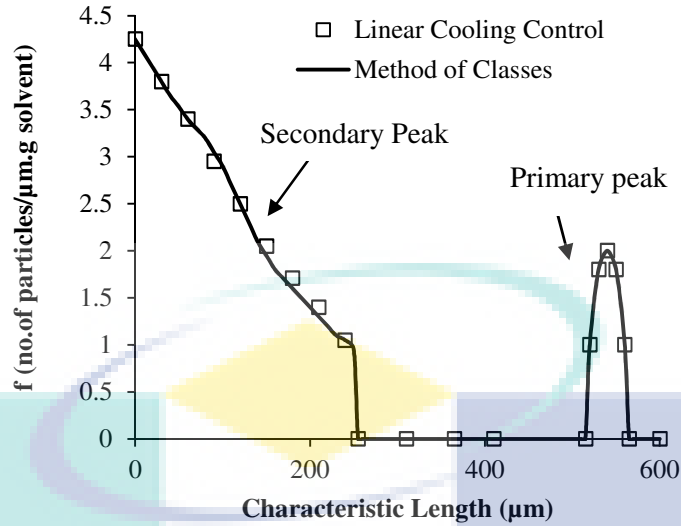


Figure 4.6 Comparison of CSD under method of classes with linear cooling control for potassium sulphate

In the work of Shi et al. (2006), the standard method of moments is also used for determining the total crystal particles using the zeroth moment and third moment for calculating the total crystal mass. Both properties can also be determined by using method of classes where the expressions relating both properties are shown in Table 4.1. For example the number of crystals produced from secondary nucleation is able to be determined by method of classes considering there is a clear gap between those two peaks as shown in Figure 4.6. The comparison of zeroth and third moments obtained using method of classes is shown in Figures 4.7 and 4.8. There will be two different profiles as shown in Figures 4.7 and 4.8. The first profiles is calculated based on initial seed of crystal and another profiles is determined based on crystal particles generated from secondary nucleation. Based on the simulation, the total number of crystal seeds remains constant at 70 until the end of operation as shown in Figure 4.7. This is due to the fact that no agglomeration and breakage is considered and thus the total number of crystal seeds is not changing. Meanwhile the total number of crystals formed from secondary nucleation at the end of operation is approximately 600 indicating the crystallisation process is also dominated by nucleation phenomena. Meanwhile the third moment for the seed is initially at 1.6×10^9 and is kept increasing to 9×10^9 . However there are no third moment at the beginning of the operation for nuclei particles but around 9×10^8 is obtained at the end of operation time. The third moment is related with the total crystal mass. Thus it is reasonable for the seed to have an initial mass and

the total crystal mass for the seed is expected to increase considering the seed will be grown into the larger size. Meanwhile initially there will be no crystal particles produced by secondary nucleation at the start of operation and the mass of crystal particles generated by secondary nucleation is then increased but at lower rate due to low size of nuclei crystal particles. Nevertheless, the model has been tested by comparing with the results of Shi et al. (2006) and a good agreement has been achieved between both methods in terms of the zeroth moment and third moment indicating that the method of classes is feasible to be used either for constructing the CSD and for calculating the physical properties of crystal particles.

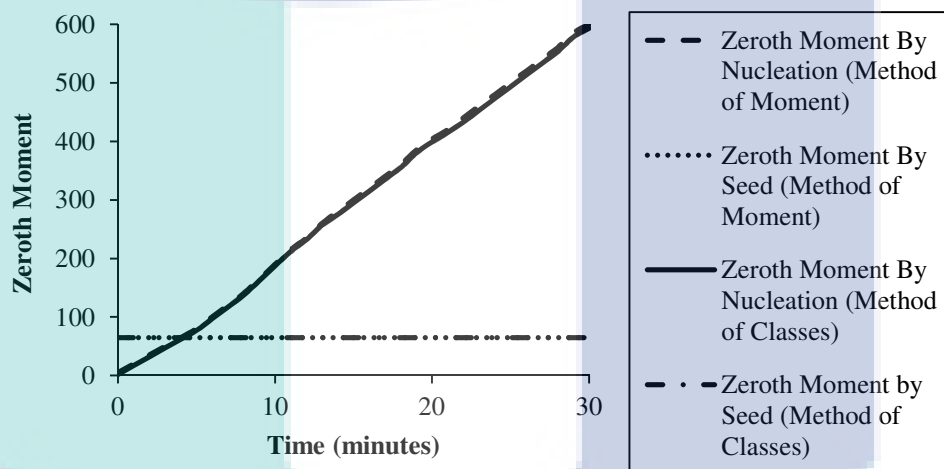


Figure 4.7 Comparison standard method of moments (Shi et al., 2006) and method of classes for zeroth moment (This work)

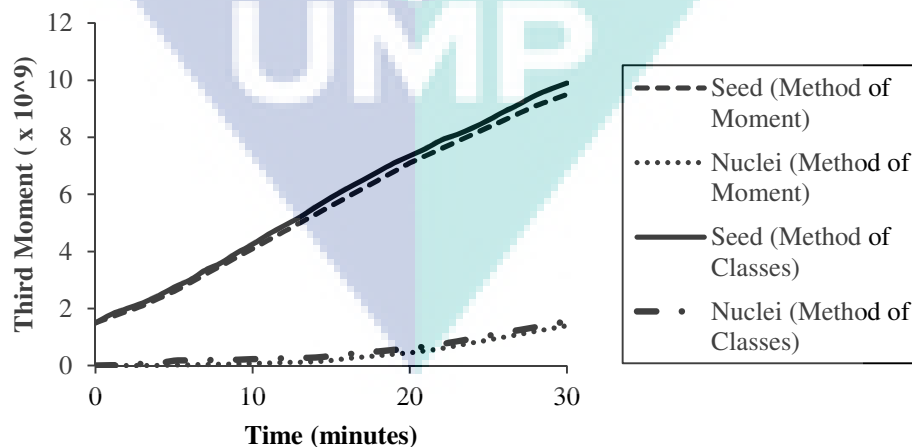


Figure 4.8 Comparison standard method of moments (Shi et al., 2006) and method of classes for third moment (This work)

4.2.6 Set-point Generation (Step 6)

Based on open-loop simulation in Step 5, it is clearly seen that the final CSD is matching the desired target CSD using the linear cooling profiles. However the main drawback using the linear cooling profiles is its inability to control the supersaturation level which contributes to the excessive nucleation. In this step, the set-point for the controller to be used in the closed-loop simulation is generated using extended analytical CSD estimator where the set-point is created on the basis of constant supersaturation. Based on the characteristic selection in Step 2, this is seeded operation, the effect of agglomeration and breakage is neglected and size independent crystal growth where the temperature dependence is included in the kinetic of this process. Therefore the analytical CSD estimator selected based on the characteristic selection is shown in Table 4.4.

Table 4.4 Analytical CSD estimator equation for potassium sulphate crystallization

| Characteristic | | Analytical model equations |
|--------------------------|---|--|
| Size independent growth: | Temperature dependence: (Arrhenius Equation) $G_x = k_g e^{\frac{-E_g}{RT}} S^g$ | Final CSD: $f_{n,i} = f_{n0,i} \quad i = 1, 2, \dots, N$ Final characteristic length: $L_{x,i} = L_{x0,i} + k_g e^{\frac{-E_g}{RT}} S_{sp}^g t_c, \quad i = 1, 2, \dots, N$ |

In order to demonstrate the application of this analytical CSD estimator, the target CSD, initial seed distribution and the kinetic growth parameters as shown in Figures 4.1 to 4.2 and Table 4.3 are employed. Theoretically the initial seed distribution acts as a starting point where the seed is grown until it reaches the final CSD, which in the ideal case should be as close as possible to the target CSD. It is important to remark that although arbitrary target CSD can be chosen but the same distribution functions for initial seed and target CSD need to be used. The target CSD may not be attained if different distribution function is used for initial seed and target CSD. The model-based optimization problem in Equations (2.16)-(2.19) is then solved using a sequential quadratic programming (SQP) based solver in order to obtain the optimal set-point. The optimal set-point consisting of the supersaturation set-point of 0.042 g/g that is to be maintained and the total crystallisation time of 30 minutes are obtained.

4.2.7 Closed-loop Simulation (Step 7)

A closed-loop simulation is then performed where a proportional-integral (PI) controller has been employed in order to maintain the potassium sulphate concentration at the desired set-point where the generated optimal set-point is used as a supersaturation set-point for the controller and inlet water temperature as the manipulated variable. The diagram for potassium sulphate crystallization is shown in Figure 4.9. The concentration is monitored by ATR-FTIR and the temperature is monitored by a thermocouple. The inlet water temperature is manipulated by blending hot and cold water. Meanwhile the CSD is also monitored by Malvern mastersizer. In order to calculate the controller parameters for PI controller, dynamic response from open-loop simulation is performed. Based on dynamic response, the process reaction curve in the form of first order plus time delay is constructed. Then the values of K_c and τ_I are calculated using Internal Model Control (IMC) tuning method (Samad et al., 2011; Nagy et al., 2008). Here the calculated values of K_c and τ_I are 60 and 6×10^{-5} respectively.

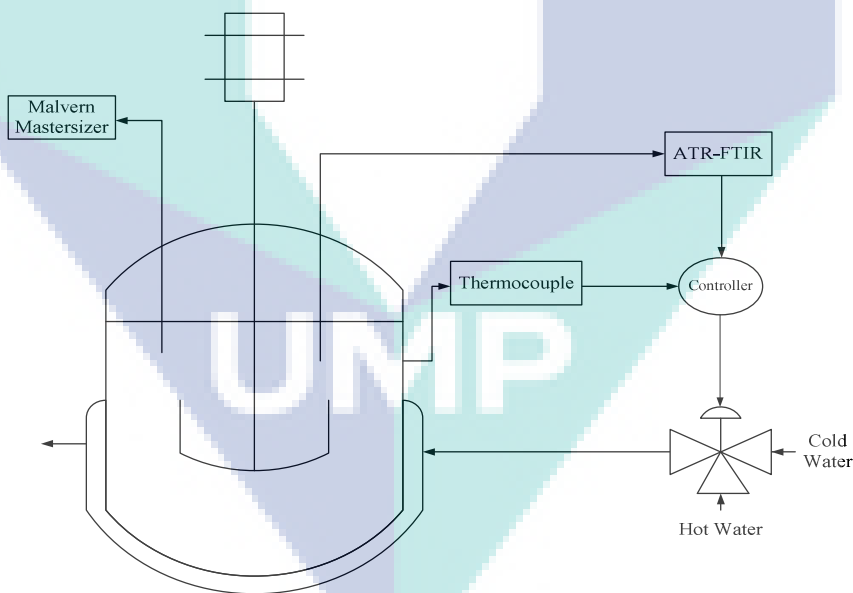


Figure 4.9 Potassium sulphate crystallization diagram

Based on the closed-loop simulation results, it can be concluded that the potassium sulphate concentration initially started at 0.1742 g/g was successfully maintained at the set-point using the PI controller in Figure 4.10. Approximately 0.1367 g/g of potassium sulphate concentration remains by the end of the operation as shown in

Figure 4.10. Figure 4.11 shows the temperature profiles obtained from closed-loop simulation where temperature initially decreased linearly from 323.15 K to 318.15 K and then further decreased steadily to the 303.15 K at 30 minutes. Meanwhile the level of relative supersaturation is shown in Figure 4.12 where in the beginning of the operation the relative supersaturation is 0.04327 and is decreased steadily to the set-point of 0.042. This is due to the effects of temperature drop based on linear profile where the PI controller acts aggressively to maintain the supersaturation at set-point of 0.042 which results into decrement of supersaturation level. Once the temperature profiles decreased steadily then the level of supersaturation is then maintained by PI controller until the end of operation. Figure 4.13 shows the total crystal mass obtained for this case study where initially 5 g of crystals seed has been increased to approximately 390 g by the end of the operation. In this work the total operation time is set at 30 minutes for model validation purpose. However the operation time could be extended. For potassium sulphate crystallization, if the total operation time is extended, the total crystal mass will be increased due to the decrease of solute concentration and maintained once the solute concentration reach saturation concentration line.

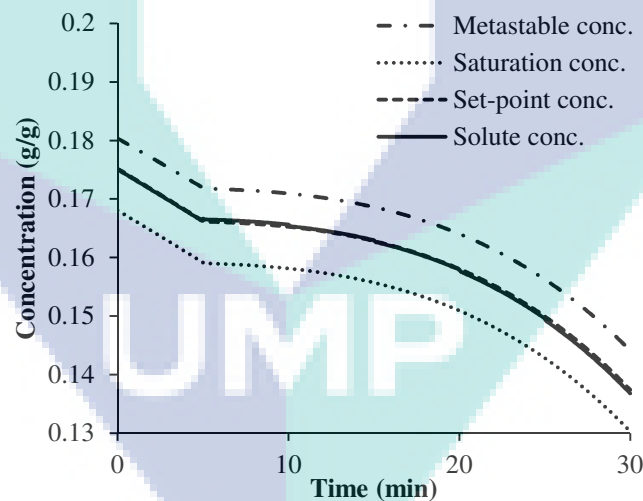


Figure 4.10 Potassium sulphate concentration profiles in the closed-loop simulation

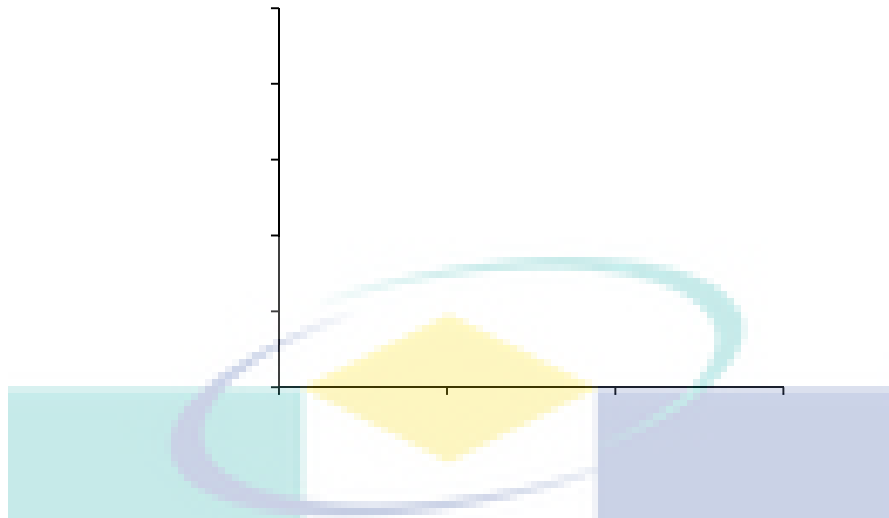


Figure 4.11 Solution temperature profiles in the closed-loop simulation

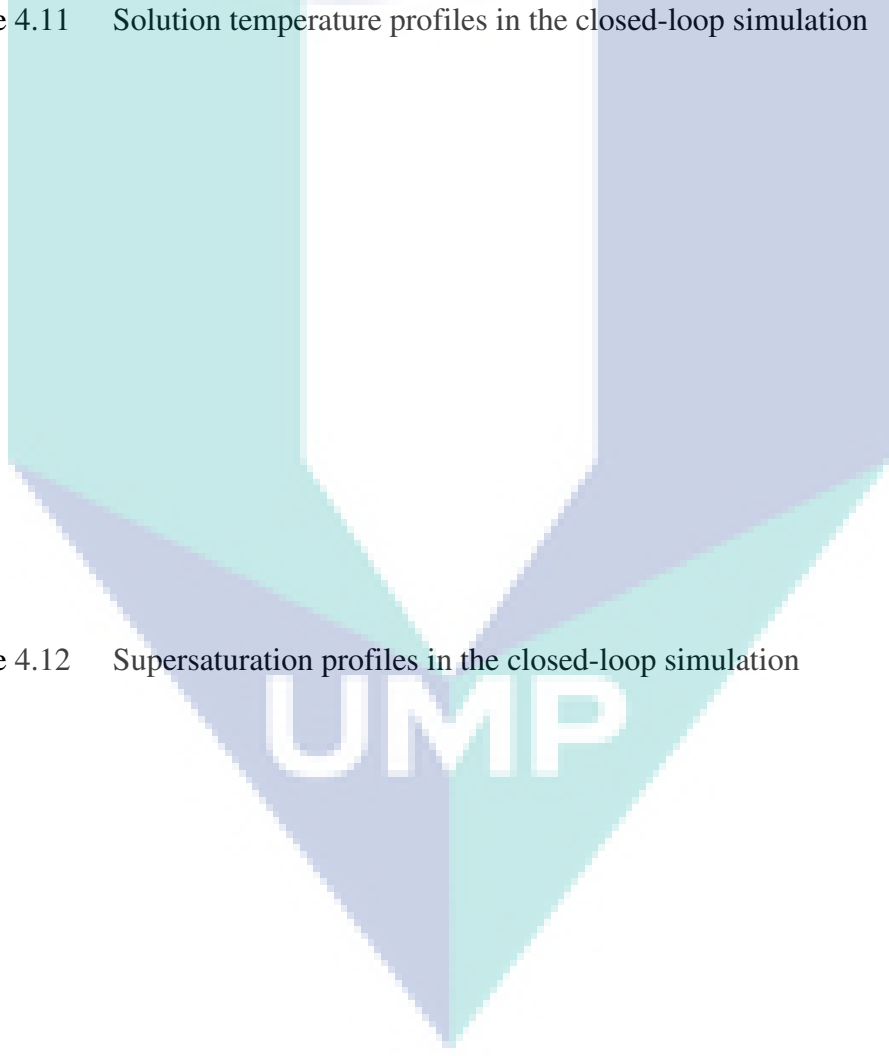
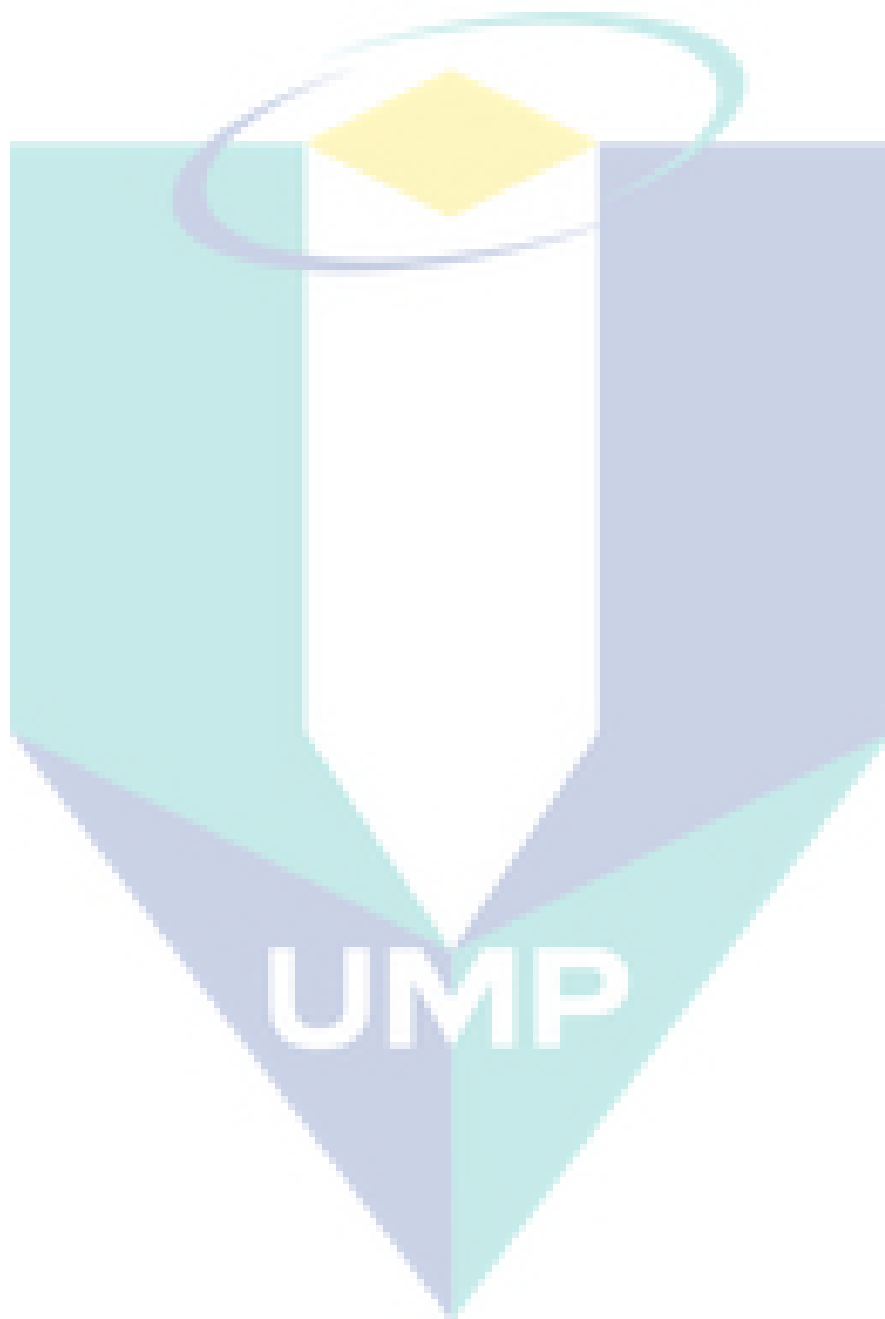
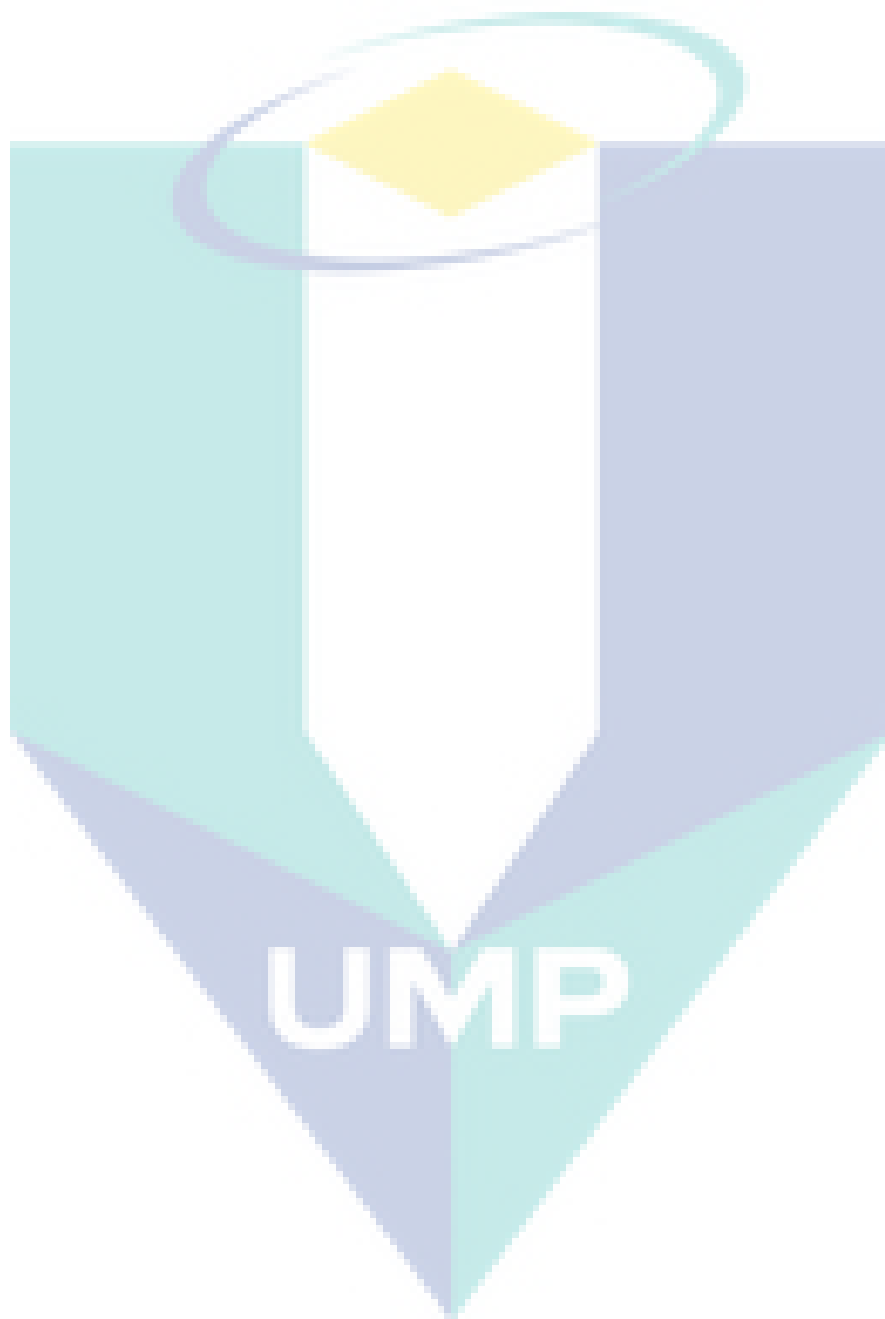
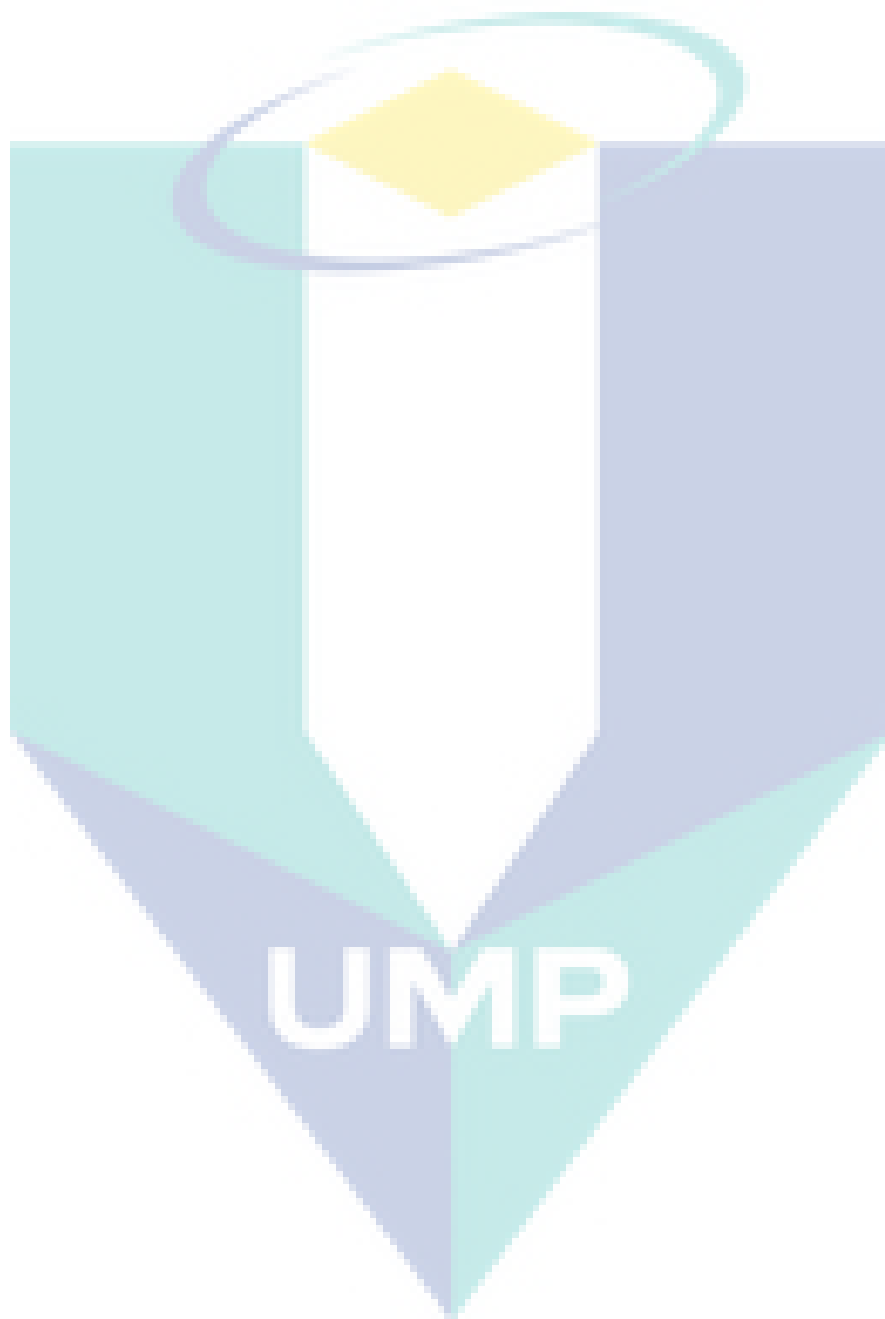


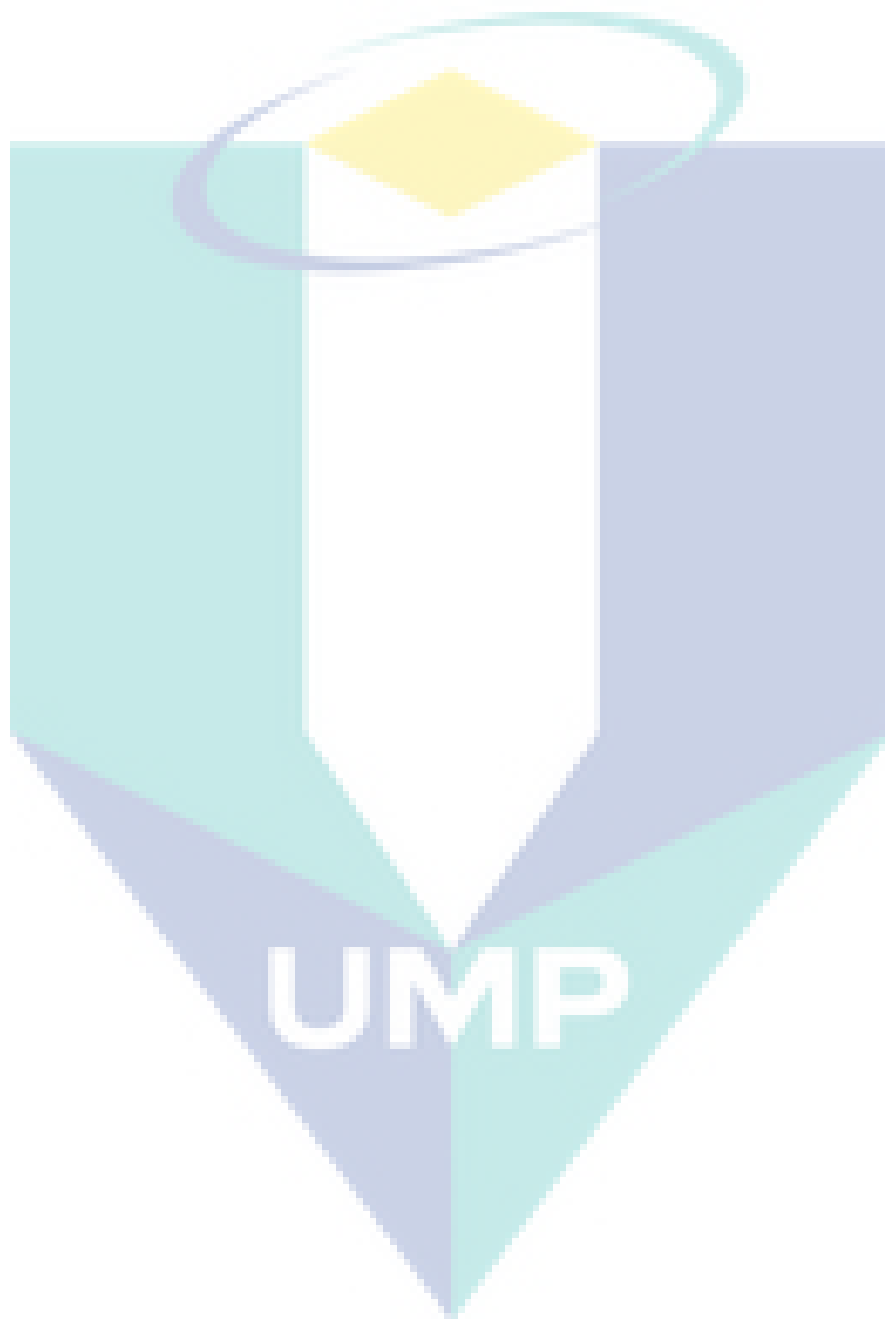
Figure 4.12 Supersaturation profiles in the closed-loop simulation

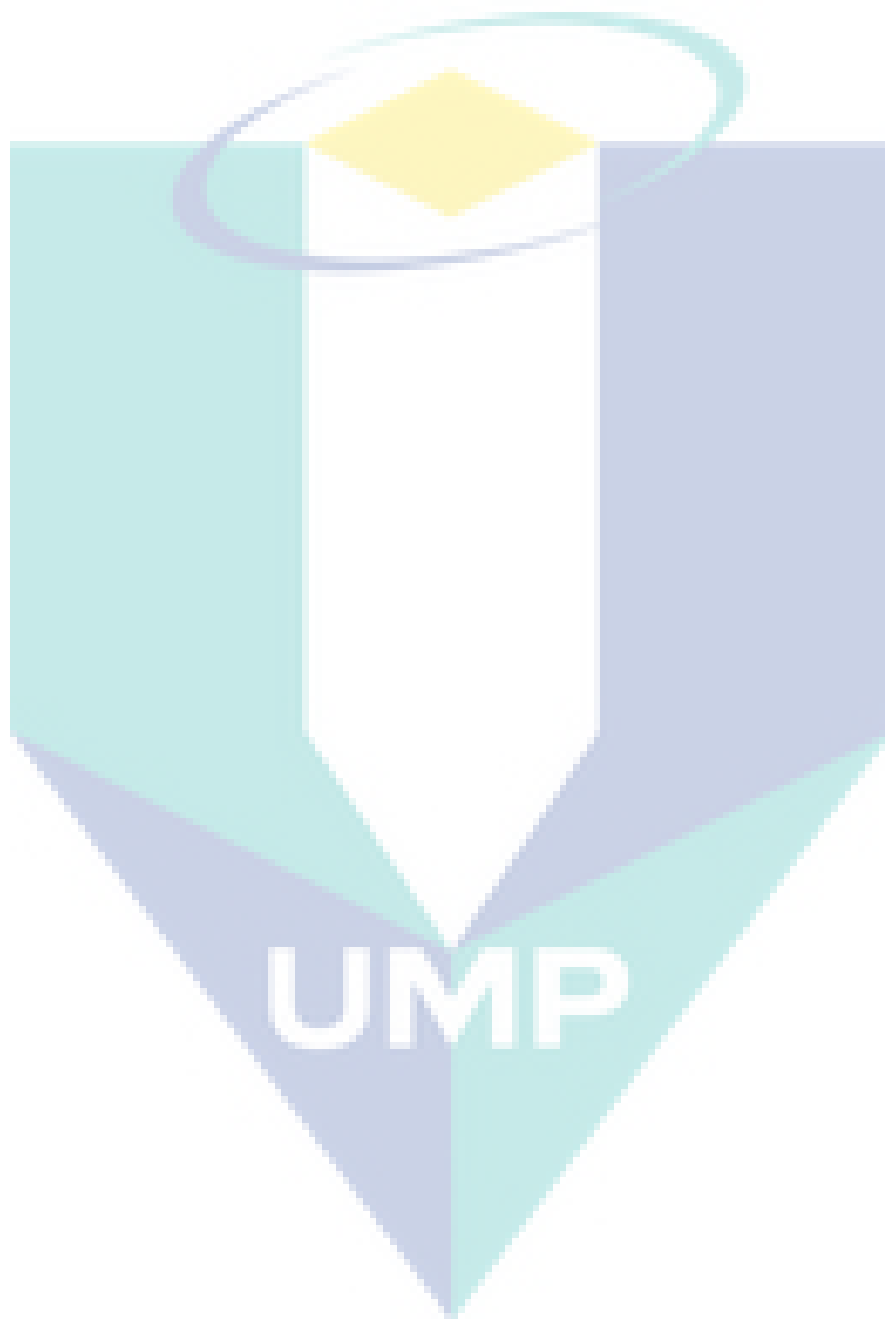
Figure 4.13 Total crystal mass obtained in the closed-loop simulation

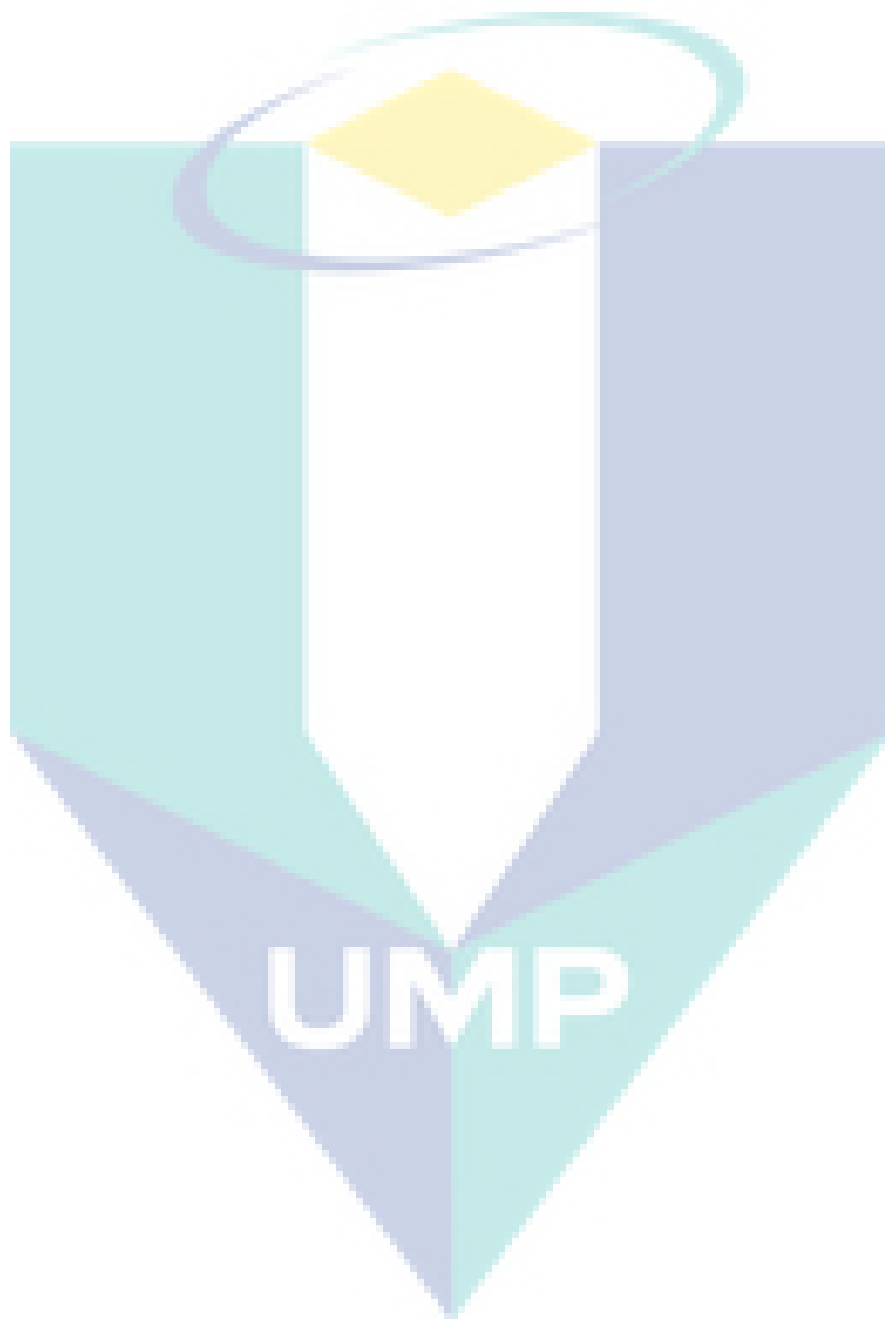


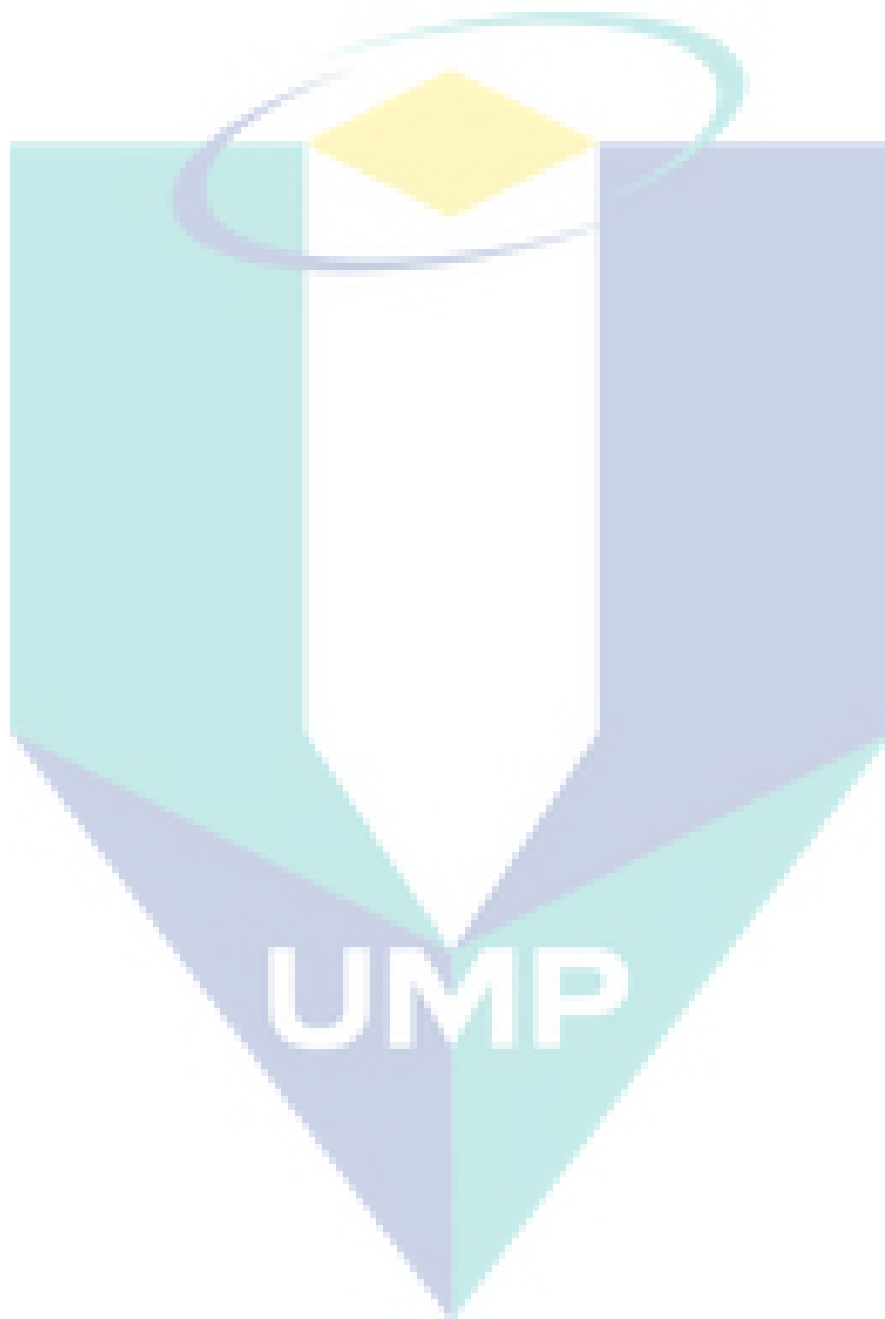


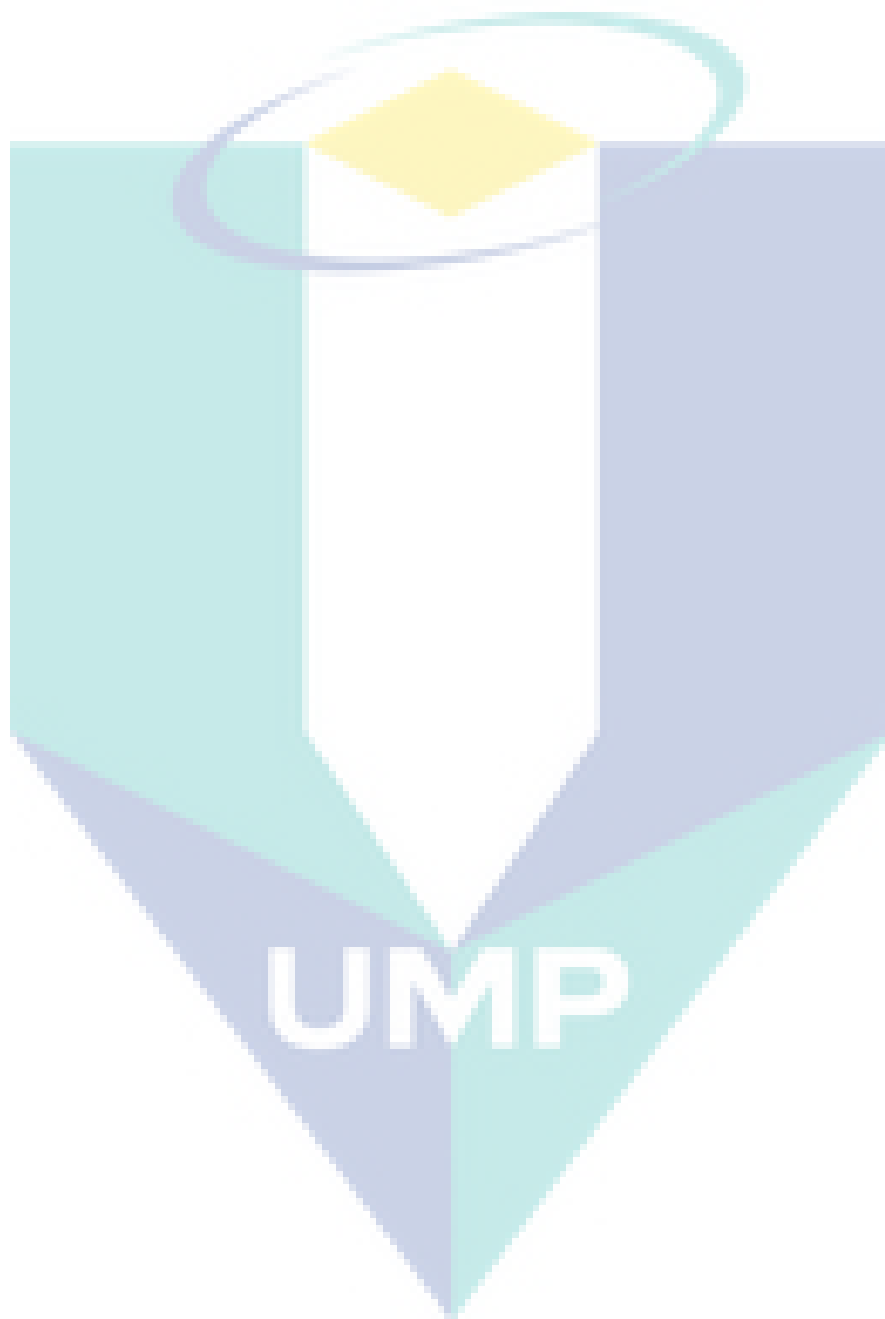












The evaluation of output uncertainties based on the Monte Carlo simulations are then implemented based on 125 number of sampling. Figures 4.19 - 4.22 show the closed-loop simulation results for potassium sulphate crystallization process obtained from Monte Carlo simulation. As shown in Figure 4.19, it is clear the input uncertainties in nucleation and crystal growth rate are affecting the behaviour of temperature. Initially the effect of input uncertainties is very minimum where only a small variation of temperature is observed but the spread of temperature ranging from 301 K to 305 K is obtained at final crystallization time due to the input uncertainties.

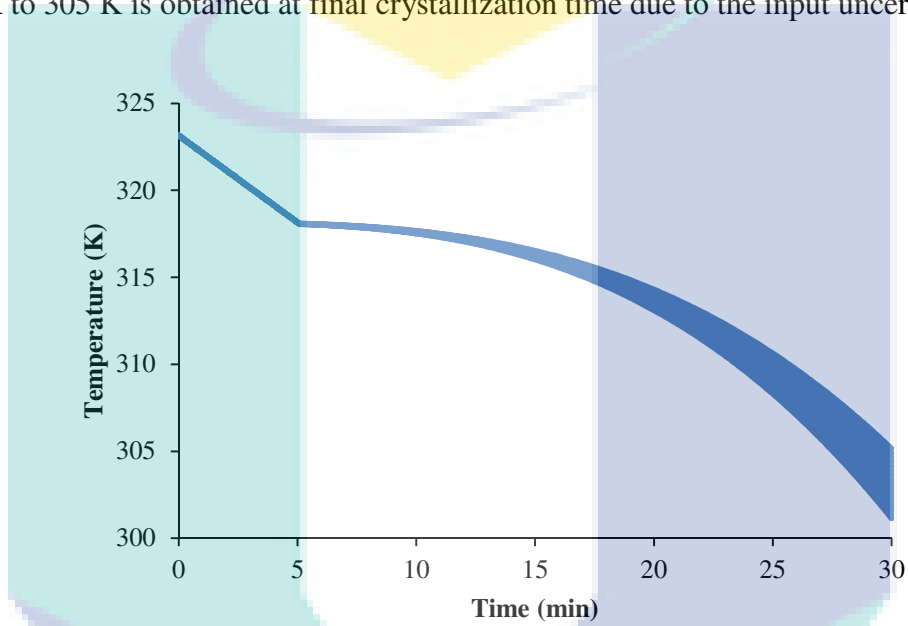


Figure 4.19 Effects of input uncertainties on the temperature for potassium sulphate crystallization

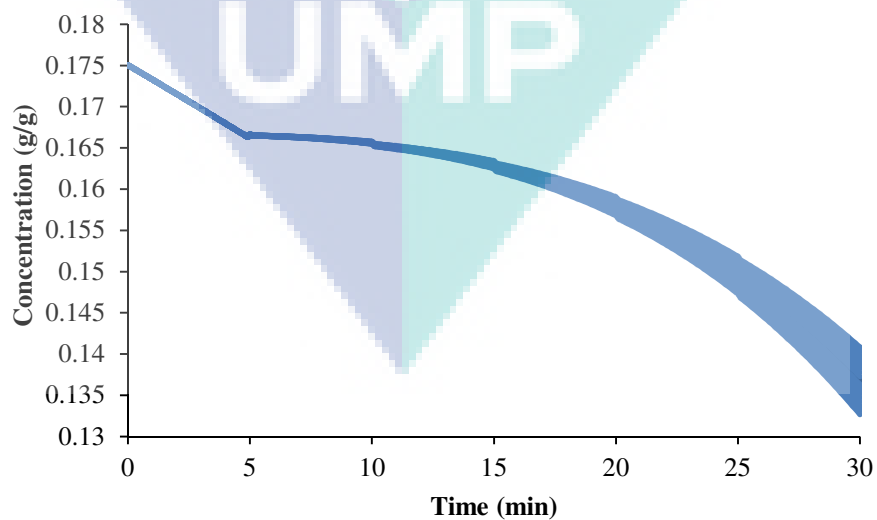


Figure 4.20 Effects of input uncertainties on the concentration for potassium sulphate crystallization

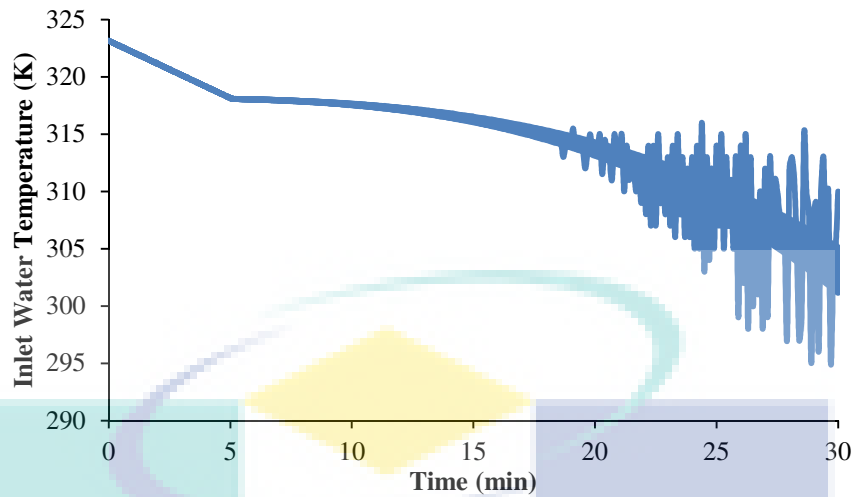


Figure 4.21 Effects of input uncertainties on the inlet water temperature for potassium sulphate crystallization

The effects of input uncertainties on the potassium sulphate concentration follows the same pattern as temperature behavior as shown in Figure 4.20. Based on the spread of potassium sulphate concentration, the impact of input uncertainties is at minimum at the beginning of operation and become dominant by the end of crystallization operation. In this case study, the supersaturation set-point is depending on the potassium sulphate concentration and saturation concentration (solubility) where the saturation concentration is depending on the temperature based on the polynomial expression. Since the input uncertainties are affecting the temperature then the saturation concentration is also changing which ultimately affecting the supersaturation level. In order to maintain the supersaturation set-point, the PI controller is acting aggressively by manipulating the inlet water temperature as shown in Figure 4.21. Figure 4.21 shows the profiles of inlet water temperature where it has been manipulated smoothly in the beginning of operation and then acted vigorously due to the aggressiveness of PI controller to deal with the effects of input uncertainties. As consequence, the high uncertainties is obtained on the CSD where it can be clearly seen the variability of the CSD as shown in Figure 4.22. Based on Table 4.1, the CSD is formed based on population balance equation (PBE) where the nucleation and crystal growth rate are two phenomena involved for CSD construction. Since the input uncertainties are introduced based on these two phenomena, therefore it is understandable the high uncertainty is dominant on the final CSD. Although the PI controller is acting aggressively for maintaining the supersaturation set-point but the effects of input uncertainties on the

CSD are too dominant by judging the wide spread of final CSD as shown in Figure 4.22.

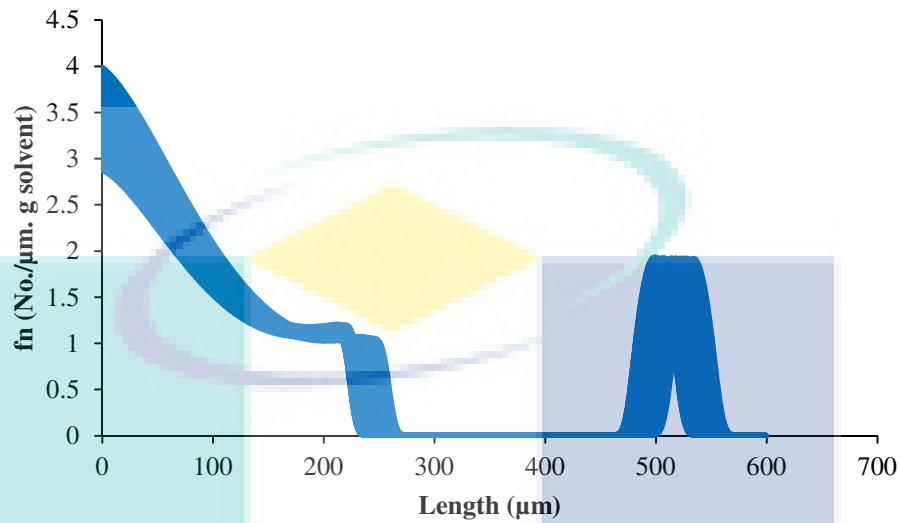


Figure 4.22 Effects of input uncertainties on the CSD for potassium sulphate crystallization.

Based on the Monte Carlo simulation results, it is shown that the effects of input uncertainties are low on the potassium sulphate crystallization and temperature but become superior on the final CSD. Since the final CSD is the main product of crystallization process, therefore there is a need to reduce the variability of the CSD. One of the ways to minimize the effect of input uncertainties is to perform controller tuning in order to get the new parameters for the PI controller. Controller tuning refers to the calculation of new tuning parameters in order to achieve the best performance of the controller. In this work, the adjustment is conducted by determining the new controller parameters which consists of proportional gain (K_c) and integral time (τ_i) values. The new PI controller parameters calculated using Internal Model Control (IMC) tuning method is shown in Table 4.8.

Table 4.8 New PI controller parameters for potassium sulphate crystallization

| | Original tuning parameters | New parameters after retuning |
|-----------------------------|----------------------------|-------------------------------|
| Proportional gain (K_c) | 60 | 70 |
| Integral time (τ_i) | 6×10^{-5} | 0.0035 |

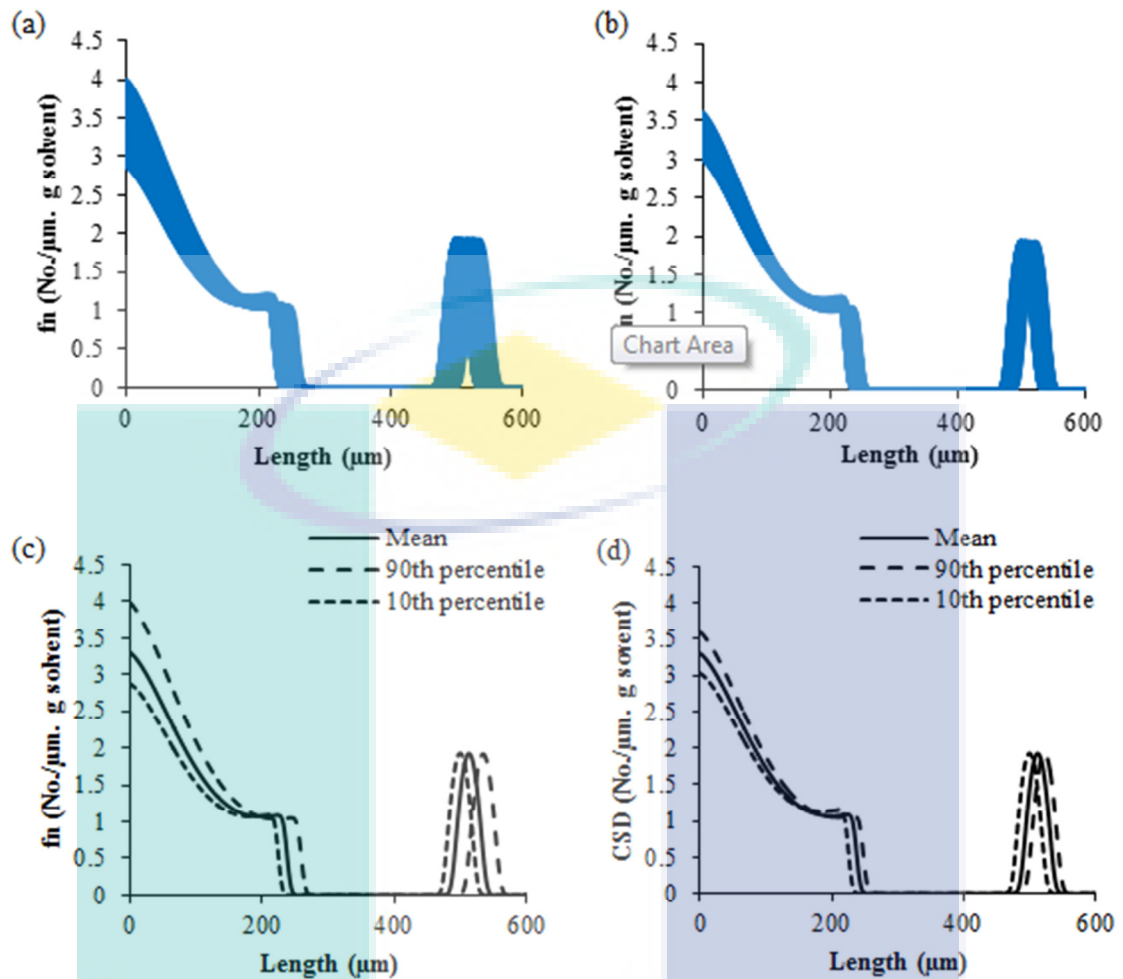


Figure 4.23 Effects of input uncertainties on (a) CSD obtained from old controller parameter, (b) CSD obtained from new controller parameter, (c) CSD representation from old controller parameter and (d) CSD representation from new controller parameter using mean, 10th percentile and 90th percentile

Based on the new controller tuning parameters, the Monte Carlo simulation is performed again and the final CSD obtained is evaluated. Figure 4.23(a) and (b) shows the final CSD obtained using old and new controller parameters. It can be clearly seen the impact of uncertainty is greatly reduced when using a new controller parameter. This indicates that the PI controller using new controller parameter is able to counteract the effect of input uncertainties and retuning the controller is able to minimize the variability in the final CSD. The representation of uncertainty in terms of mean, 10th and 90th percentile values of the final CSD obtained from Monte Carlo simulations is shown in Figure 4.23(c) and (d). The presence of uncertainty is clearly shown in Figure 4.23(c) where the 10th and 90th percentile is further away from the mean of final CSD obtained from old controller parameter. After the retuning the PI controller, the 10th and

90th percentile is very close to the mean indicating that the uncertainty for CSD is minimized and less variability of final CSD is achieved. Based on the uncertainty analysis, it can be concluded that the PI controller is robust enough to counteract the impact of input uncertainties in the nucleation and crystal growth rate model and retuning of controller is the useful way to reduce the effect of input uncertainties on the model output.

4.3 Application of Model-based Framework: Sucrose Crystallization Process

For the second case study, sucrose crystallization process is selected to demonstrate the target CSD for the case of agglomeration-breakage phenomena is achieved using the application of the model-based framework.

4.3.1 Problem Definition (Step 1)

In this case study the objective is set to achieve the desired target CSD for sucrose crystallization process in the case of agglomeration and breakage. The target CSD to be achieved is shown in Equations (4.6) and (4.7) which is based on the uniform distribution. Figure 4.24 shows the generated target CSD where the mean of characteristic length of CSD is 395 μm and the highest peak of CSD is 2.12 no. of particles/ μm . g solvent.

For $370 \mu\text{m} \leq L \leq 420 \mu\text{m}$:

$$f(L,0) = 0.0035(420 - L)(L - 370) \quad 4.6$$

For $L < 370 \mu\text{m}$, $L > 420 \mu\text{m}$:

$$f(L,0) = 0 \quad 4.7$$

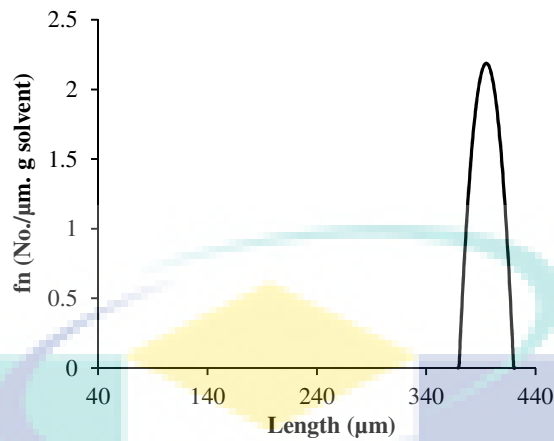


Figure 4.24 Target CSD for sucrose crystallization

4.3.2 Process and Product Specifications (Step 2)

For the process specification, the operation for sucrose crystallization is assumed for size independent growth with covering the effects of the agitation rate and the effects of agglomeration and breakage phenomena is also considered. The sucrose acts as the solute and the solvent selected is water for this process. The final CSD as shown in Figure 4.24 is the main target to be achieved for product specification.

4.3.3 Development of Mathematical Model (Step 3)

For the development of the mathematical model, the PBE model using method of classes is used where the production-reduction term (α) as suggested by Quintana-Hernández et al. (2004) is employed for representing the effects of agglomeration and breakage. For the purpose of constructing the CSD using PBE, 600 number of equations in method of classes are used using 1 μm size of class (ΔC_l). The solute concentration, energy balance and cooling jacket energy balance are also constructed in the same way as potassium sulphate crystallization. In terms of constitutive equations, the effect of agitation rate is included in the nucleation and crystal growth rate. The list of model equations for the sucrose crystallization process is shown in Table 4.9. Meanwhile the known variables for this mathematical model is shown in Table 4.10 which has been adopted from Quintana-Hernández et al. (2004).

Table 4.9 List of model equations for the one-dimensional model for sucrose crystallization

| Types | Equations |
|---|--|
| Population balance equation (size independent growth) | $\frac{dN_1}{dt} + \frac{G_x}{2\Delta Cl} N_1 = B_{nuc} + \alpha, i = 1$ $\frac{dN_i}{dt} + \frac{G_x}{2\Delta Cl} N_i + \frac{G_x}{2\Delta Cl} N_{i-1} = \alpha, 1 \leq i \leq n$ $\frac{dN_n}{dt} + \frac{G_x}{2\Delta Cl} N_n - \frac{G_x}{2\Delta Cl} N_{n-1} = \alpha, i = n$ |
| Solute concentration | $\frac{dc}{dt} = -\frac{\rho_c k_v V}{m_w} \left(\sum_{i=1}^n S_{xi}^3 \frac{dN_i}{dt} \right)$ |
| Energy balance | $\rho V c_p \frac{dT}{dt} = -H_c \rho_c k_v V \left(\sum_{i=1}^n S_{xi}^3 \frac{dN_i}{dt} \right) - U_1 A_1 (T - T_w)$ |
| Cooling jacket energy balance | $\rho_w V_w c_{pw} \frac{dT_w}{dt} = \rho_w F_{win} c_{pw} (T_{win} - T_w) + U_1 A_1 (T - T_w) + U_2 A_2 (T_{ex} - T_w)$ |
| Saturation concentration | $c^{sat} = 6.29 \times 10^{-2} + 2.46 \times 10^{-3} T - 7.14 \times 10^{-6} T^2$ |
| Supersaturation | $S = \frac{c - c^{sat}}{c^{sat}}$ |
| Nucleation | $B_{nuc} = k_b S^b M_c^j N_{rpm}^p$ |
| Crystal growth rate | $G_x = k_g S^g N_{rpm}^q$ |
| Characteristic size | $S_{xi} = \frac{L_{xi} - L_{xi-1}}{2}$ |
| Total crystal mass | $M_c = \rho_c k_v \left(\sum_{i=1}^n S_{xi}^3 N_i \right)$ |
| Crystal size distribution | $f_n(L_{xi}) = \frac{(N_i / \Delta Cl_i) + (N_{i+1} / \Delta Cl_{i+1})}{2}$ |
| Production reduction-term | $\alpha = k_a S^a M_c^k N_{rpm}^r$ |
| Mean size diameter | $D[4,3] = \frac{\sum_i^N S_i^4 N_i}{\sum_i^N S_i^3 N_i}$ |

Source: Quintana-Hernández et al. (2004)

Table 4.10 Parameter values for sucrose crystallization

| Parameter | Value | Units |
|---|---------|-----------------------|
| Heat capacity of solution, C_{ps} | 2.4687 | J/g°C |
| Density of crystals, ρ_c | 1.588 | g/cm ³ |
| Magma volume, V | 2230 | cm ³ |
| Heat capacity of water, C_{pw} | 4.18 | J/g°C |
| Volume of water, V_w | 820 | cm ³ |
| Exterior temperature, T_{ex} | 29 | °C |
| Inlet water flow rate, F_{win} | 4200 | cm ³ /min |
| Mass of water, M_w | 800 | g |
| Mass of solvent, M_s | 2528 | g |
| Volumetric shape factor, k_v | $\pi/6$ | - |
| Initial temperature, T_o | 70 | °C |
| Density of water, ρ_w | 1.0 | g/cm ³ |
| Overall heat transfer coefficient (internal), U_1 | 1800 | kJ/m ² h K |
| Total heat-transfer surface area (internal), A_1 | 0.25 | m ² |
| Overall heat transfer coefficient (external), U_2 | 2300 | kJ/m ² h K |
| Total heat-transfer surface area (external), A_2 | 0.45 | m ² |

Source: Quintana-hernandez et al. (2004)

4.3.4 Model Identification (Step 4)

For the model identification step, the experimental datas for temperature, sucrose concentration, mean size diameter, agitation rate, supersaturation and total crystal mass are available (adopted from Quintana-hernandez et al., 2004). These experimental datas can be used to estimate the kinetic parameters of nucleation, crystal growth rate and production-reduction term. The total kinetic parameters to be estimated is 11 parameters which consists of 4 parameters (k_b, b, j, p) in nucleation, 3 parameters (k_g, g, q) in crystal growth and 4 parameters (k_a, a, k, r) in production-reduction term respectively. The objective function developed for model identification is shown in Equation (4.8).

$$\begin{aligned}
F_{obj} = \min_{\theta} & \left\{ w_T \sum_{i=1}^n \left(\frac{T_{calculated} - T_{exp}}{T_{exp}} \right)^2 + w_c \sum_{i=1}^n \left(\frac{c_{calculated} - c_{exp}}{c_{exp}} \right)^2 \right. \\
& + w_D \sum_{i=1}^n \left(\frac{D_{calculated} - D_{exp}}{D_{exp}} \right)^2 + w_{Nrpm} \sum_{i=1}^n \left(\frac{Nrpm_{calculated} - Nrpm_{exp}}{Nrpm_{exp}} \right)^2 \\
& \left. + w_S \sum_{i=1}^n \left(\frac{S_{calculated} - S_{exp}}{S_{exp}} \right)^2 + w_{Mc} \sum_{i=1}^n \left(\frac{Mc_{calculated} - Mc_{exp}}{Mc_{exp}} \right)^2 \right\} \quad 4.8
\end{aligned}$$

Subject to : All model equations in Table 4.9 and $\theta_{min} \leq \theta \leq \theta_{max}$

Where $\theta = [k_b, b, j, p, k_g, g, q, k_a, a, k, r]$ is the set of parameters for the nucleation, crystal growth and production-reduction kinetic models, θ_{min} and θ_{max} are the specified lower and upper bounds for each parameter respectively. The objective function used in this work is based on the minimization of error between calculated data from mathematical model and experimental data for temperature, concentration, agitation rate, mean size diameter, supersaturation and total crystal mass. The weightage of 0.6 is set for temperature (w_T), for the sucrose concentration the weightage (w_c) used is 0.3, 0.4 is the weightage used for mean size diameter (w_D), the weightage of agitation rate (w_{Nrpm}) is 0.5 and finally the weightages of supersaturation and total crystal mass are specified at 0.4 respectively. Based on the simulation performed in Matlab software, the objective function for parameter regression is 2.3×10^{-06} which is acceptable tolerance for minimizing the error between experimental and calculated data. Tables 4.11 to 4.13 show the estimated kinetic parameters for sucrose crystallization with the confidence interval for each parameters. The estimated values obtained in this work is in good agreement with the values from literature indicating a good prediction has been obtained from model identification.

Table 4.11 Estimated nucleation kinetic parameters for sucrose crystallization

| Parameters | k_b | B | j | p |
|---|--------|--------|--------|-------|
| Literature values (Quintana- Hernandez et al., 2004) | 85.7 | 0.01 | 0.005 | 0.05 |
| This work | 82.4 | 0.0106 | 0.0044 | 0.048 |
| Confidence interval | 7.1743 | 0.0024 | 0.0008 | 0.004 |

Table 4.12 Estimated crystal growth kinetic parameters for sucrose crystallization

| Parameter | k_g | g | q |
|---|----------|-------|-------|
| Literature values (Quintana- Hernandez et al., 2004) | 0.000133 | 1.00 | 0.5 |
| This work | 0.000101 | 1.00 | 0.5 |
| Confidence interval | 0.000051 | 0.001 | 0.015 |

Table 4.13 Estimated production-reduction kinetic parameters for sucrose crystallization

| Parameter | k_a | a | k | r |
|---|-------|-------|------|--------|
| Literature values (Quintana- Hernandez et al., 2004) | 1.00 | 0.1 | 0.09 | 0.001 |
| This work | 1.00 | 0.085 | 0.11 | 0.001 |
| Confidence interval | 0.01 | 0.012 | 0.03 | 0.0005 |

4.3.5 Open-loop Simulation (Step 5)

The open-loop simulation is performed for model validation using the same conditions and assumptions from Quintana-hernandez et al., (2004). In this work the PBE is solved using the method of classes and method of moments is employed for solving the PBE in the literature. The agitation rate for this simulation is set to be fixed at 600 rpm for 20 minutes and then the agitation rate is decreased linearly to 100 rpm. The open-loop simulation results for sucrose crystallization are shown in Figure 4.25. For the sucrose crystallization, the temperature is cooled down from 70 °C to 40 °C based on the natural cooling profile. Although the temperature is already dropped but the sucrose concentration profiles is still maintained at the beginning of the operation. This is due to the fact that this is the unseeded operation where there is no crystal particles presence at the initial crystallization operation. Therefore the crystal particles are generated by nucleation phenomena known as crystal nuclei. However most of the crystal nuclei generated from nucleation kinetic is not stable and will dissolve back to the solution which explains the unchanged sucrose concentration profiles in the beginning of the operation. The sucrose concentration is starting to decrease at time 23.4 minutes where the crystal nuclei then start to grow due to the crystal growth rate phenomena until the end of the operation. This time is obtained from model simulation based on the decrement value of sucrose from 3.16 g sucrose/g water to 3.15 g sucrose/g water. Due to the crystal growth, more solute in the sucrose concentration is transferred

into the solid crystal particles which contributes to the decrement of sucrose concentration. In the end of the operation, 2.33 g sucrose/g water was achieved from initially 3.16 g sucrose/g water.

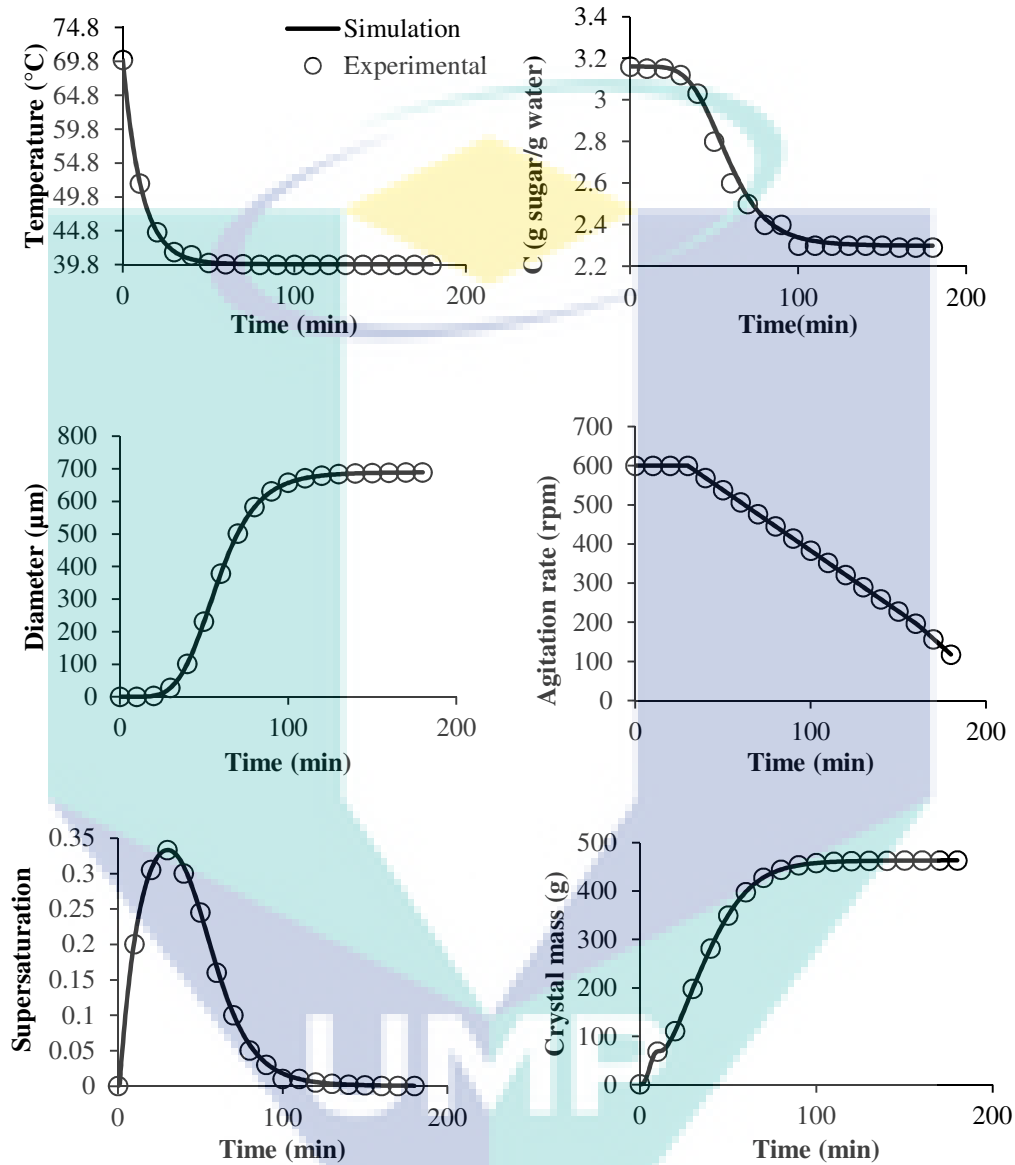


Figure 4.25 (a) Temperature (b) Concentration (c) Mean size diameter (d) Agitation rate (e) Supersaturation (f) Total crystal mass profile of sucrose in water.

As shown in Figure 4.25, a high supersaturation is obtained in the beginning of the operation and low/none supersaturation is observed by the end of the operation. Since temperature is dropped rapidly, the saturation concentration is also decreased. However the sucrose concentration is still maintained which contributes to the high supersaturation of this operation. Due to the high supersaturation, an excessive nucleation is expected and at the same time the crystal growth rate is also high which

necessitating the growth of crystal nuclei. However at the time of 100 minutes onwards, the temperature is starting to maintain at 40°C until the end of the operation and the level of supersaturation is decreasing quickly and approaching zero supersaturation level. This indicates that the sucrose concentration is reaching the saturated condition and no crystal particles will be produced and grown under this condition. This is the main weakness of natural cooling profile where the crystal particles can not be grown into desired crystal size due to the insufficient crystal growth rate. In addition a production of high crystal particles at relatively low size is also obtained which is not preferable in the crystallization process. Based on this simulation, approximately 460 g of the total crystal mass and 670 μm of mean size diameter were obtained. Although this is the unseeded operation but both total crystal mass and mean size diameter obtained is relatively high. This is due to the effects of agglomeration and breakage based on production-reduction term. In this operation, the agitation rate is decreased linearly in order to reduce the breakage of crystals and at the same time there will be a condition where the crystal particles is merging with another crystal particles due to the agglomeration. Increasing trends for both total crystal mass and mean size diameter are also observed which it can be concluded that this crystallization operation is dominated by agglomeration rather than breakage. Based on the simulation results of temperature, sucrose concentration, mean size diameter, agitation rate, supersaturation and total crystal mass profile, it shows that both simulation and experimental data are in good agreement indicating thereby a reliable and validated model are achieved.

The main weakness of the method of moments is its inability to generate the crystal size distribution in the form of crystal population density. Usually the CSD generated from method of moments is represented as mean size diameter as shown in Figure 4.25. Although approximately 670 μm of mean size diameter is obtained from open-loop simulation, this amount is calculated based on the overall summation of the crystal particles for all sizes. Therefore it is difficult to identify the exact size of crystal particles. In this work, the PBE is solved by using the method of classes. The mean size diameter obtained from the method of classes is in accordance with the mean size diameter generated from method of moments as shown in Figure 4.25. Therefore it is possible to identify the distribution of crystal particles at the various characteristic lengths (size). The CSD obtained using method of classes is shown in Figure 4.26 where the CSD is scattered at various characteristic length ranging from 0 μm to 1500

μm . However it is important to note that the CSD obtained in Figure 4.26 is not favourable in the crystallization process. This is because the crystal particles are not uniform and scattered at various characteristic length which makes it harder for the separation process. In order to overcome this problem, seeding can be introduced into the operation.

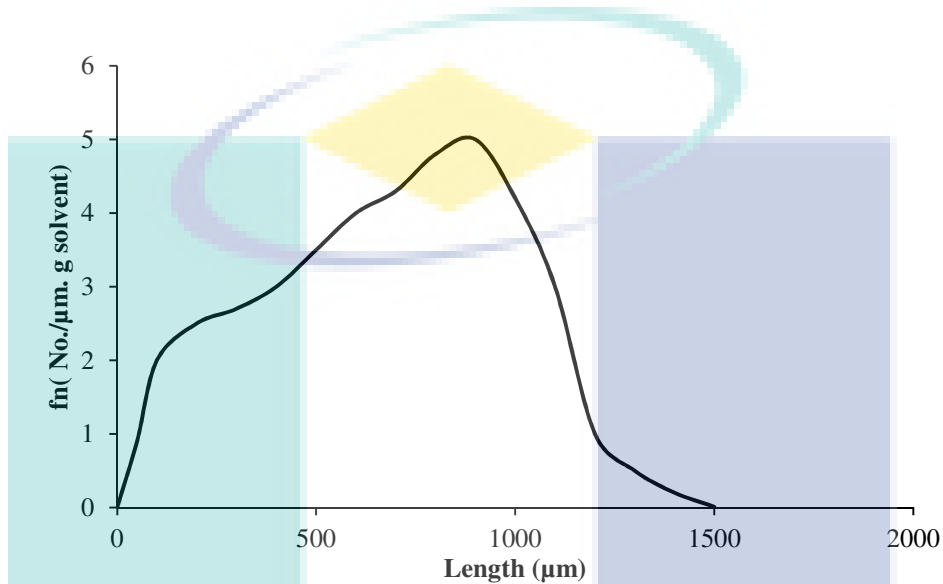


Figure 4.26 Crystal size distribution at final time of 180 minutes

4.3.6 Set-point Generation (Step 6)

In order to improve the CSD obtained from open-loop simulation, a seeding operation and different cooling strategy are then necessary. In this step, the cooling strategy can be generated using analytical CSD estimator. For the case size independent crystal growth with agitation rate and covering the effects of agglomeration and breakage, the expressions of the analytical CSD estimator is shown in Table 4.14.

Table 4.14 Analytical CSD estimator for sucrose crystallization

| Characteristic | New invention | Analytical model equations |
|---|--|--|
| Size independent growth (With agglomeration and breakage) | Temperature independence: $G_x = k_{gx} S^{gx} N_{rpm}^r$ | Final CSD: $f_{n,i} = f_{n0,i} + k_a S_{sp}^{gx} M_c^k N_{rpm}^r \quad i = 1, 2, \dots, N$ Final characteristic length: $L_{x,i} = L_{x0,i} + k_{gx} S_{sp}^{gx} N_{rpm}^q t_c, \quad i = 1, 2, \dots, N$ |

For the seeded operation, the initial seed of CSD is specified based on Equations (4.9) to (4.10) where Figure 4.27 shows the generated initial seed of CSD. Usually, in the case of size independent growth where the effects of both agglomeration and breakage are neglected, the peak and the curve shape of the initial and final CSD are similar except the mean of the characteristic length is increased due to the size independent growth effects (Samad et al., 2013). However, in this case study with the incorporation of agglomeration and breakage, both the curve shape of CSD and characteristic length are changed. Based on the open-loop simulation, it has been observed that the agglomeration is superior than breakage and thereby an increment of size is expected. For this reason, the peak of the target CSD should be higher than the peak of the initial CSD. For the purpose of this simulation, the highest peak for the initial seed is 2/μm.g solvent at a mean characteristic length of 275 μm meanwhile for the target CSD is 2.12/μm.g solvent at mean characteristic length of 395 μm. Notes that different peak and mean characteristic length can be chosen for achieving the target CSD.

For $250 \mu\text{m} \leq L \leq 300 \mu\text{m}$:

$$f(L,0) = 0.0032(300 - L)(L - 250) \quad 4.9$$

For $L < 250 \mu\text{m}, L > 300 \mu\text{m}$:

$$f(L,0) = 0 \quad 4.10$$

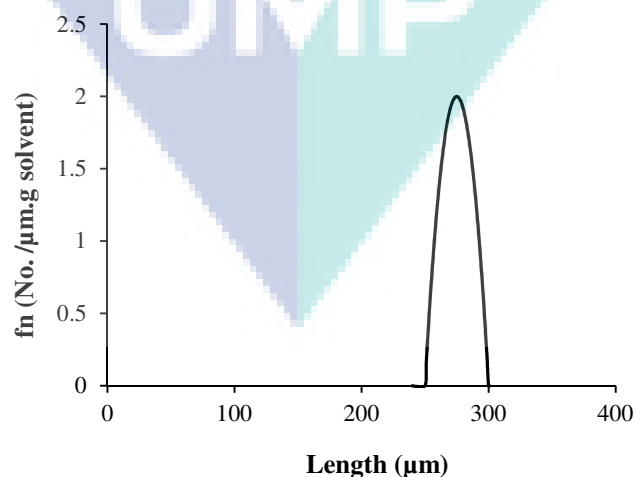


Figure 4.27 Initial seed distribution for sucrose crystallization

A model-based optimization approach as shown in Equations (2.16) to (2.19) is then used to optimize the supersaturation set-point and the total crystallization time in order to achieve the desired target CSD. The objective is to minimize the sum of squares of the relative errors between the desired target CSD and a predicted CSD obtained through the analytical CSD estimator. The set-point generated from the model-based optimization is shown in Table 4.15 where in this case, 3 different set-points are proposed to achieve the target CSD.

Table 4.15 Supersaturation set-point values for the seeded sucrose batch cooling crystallizer

| Time (min) | Supersaturation set-point (g/g) |
|------------|---------------------------------|
| 150 | 0.0352 |
| 180 | 0.0312 |
| 210 | 0.0281 |

4.3.7 Closed-loop Simulation (Step 7)

The next step concerns on the closed-loop simulation where controller performance is evaluated for maintaining the set-point at its trajectory. For this purpose, all of the generated set-points as shown in Table 4.15 will be tested in the closed-loop simulation in order to prove the target CSD can be obtained if it is successfully maintained in the specified trajectory. Similarly as previous case study, a PI controller has been considered to maintain the sucrose concentration at the desired set-point by manipulating inlet water temperature. The diagram for sucrose crystallization is shown in Figure 4.28. The concentration is monitored by ATR-FTIR and the temperature is monitored by a thermocouple. The inlet water temperature is manipulated by blending hot and cold water. Meanwhile the CSD is also monitored by Malvern mastersizer. In order to calculate the controller parameters for PI controller, dynamic response from open-loop simulation is performed. Based on dynamic response, the process reaction curve in the form of first order plus time delay is constructed. Then the values of K_c and τ_I are calculated using Internal Model Control (IMC) tuning method (Samad et al., 2011; Nagy et al., 2008). Here the calculated values of K_c and τ_I are 60 and 0.16 respectively.

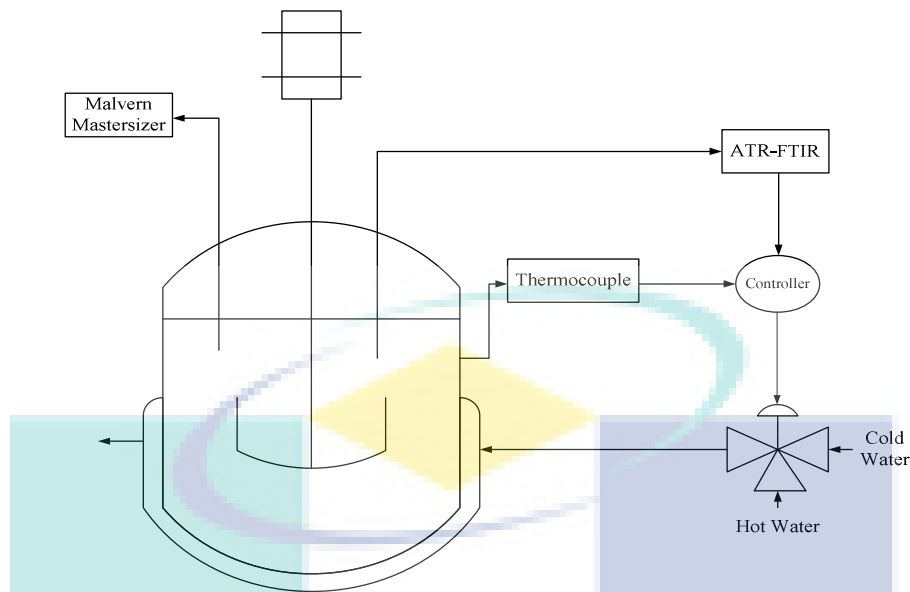


Figure 4.28 Sucrose crystallization diagram

The closed-loop simulation results obtained are shown in Figure 4.29. The sucrose concentration profiles for all closed-loop simulation were successfully maintained at the required set-point until the end of the operation indicating a reliable performance for PI controller. The sucrose concentration initially at 3.22 g sucrose/g water is decreased steadily to 2.40 g sucrose/g water at the end of operation time of 150 minutes, 180 minutes, and 210 minutes respectively. Figure 4.30 shows the cooling strategies used for the closed-loop simulation where the temperature in the crystallization process is cooled down from 67 °C to 40 °C. All of the temperatures profiles have a same pattern but is decreased at different rate based on the operation time. It can be observed that the sucrose concentration is depends on the temperature where the sucrose concentration is decreased when the temperature is also decreased due to the need to achieve the desired supersaturation level.

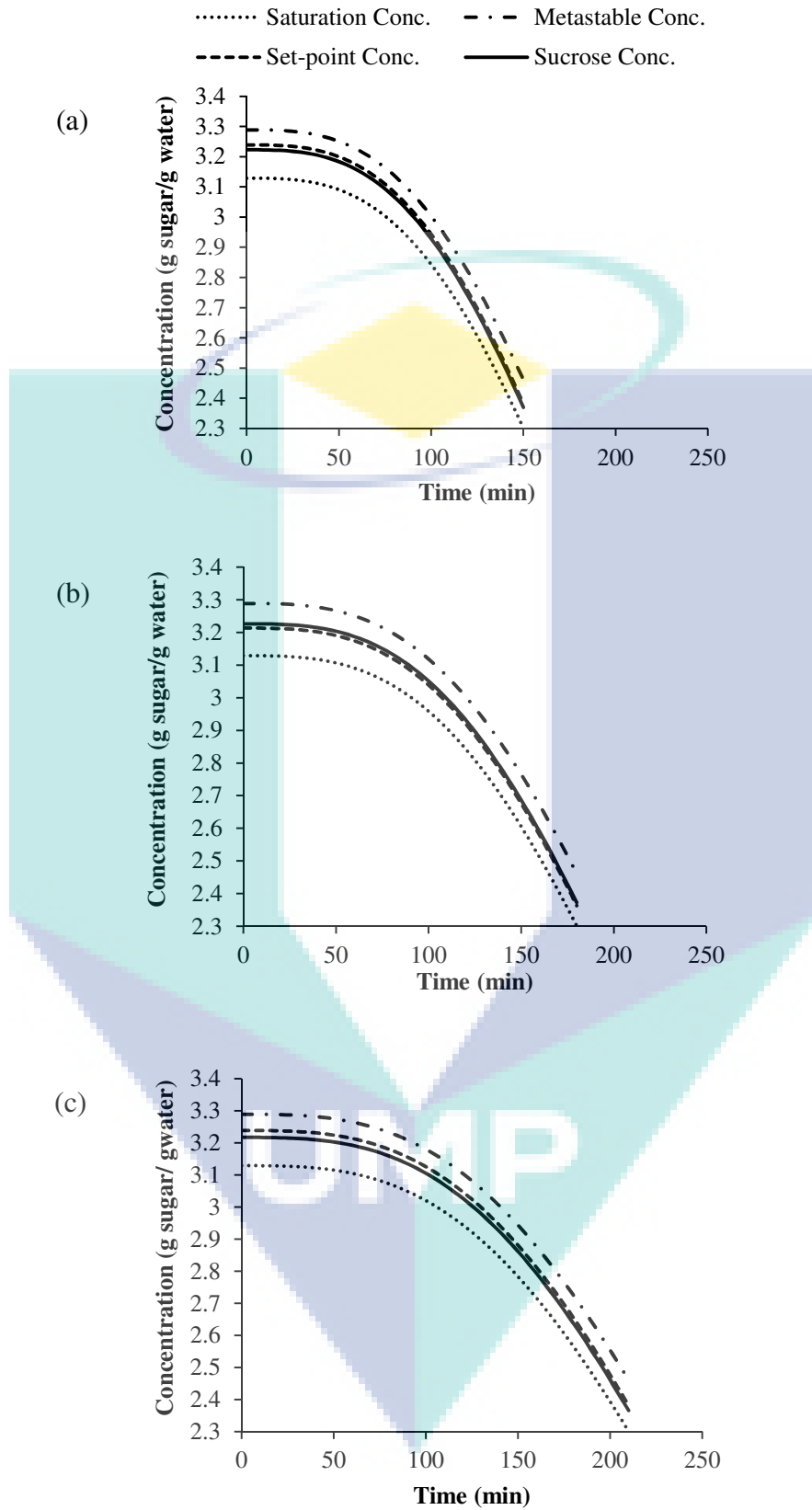


Figure 4.29 Sucrose concentration profiles in the closed-loop simulation for operational time of (a) 150 min, (b) 180 min, (c) 210 min.

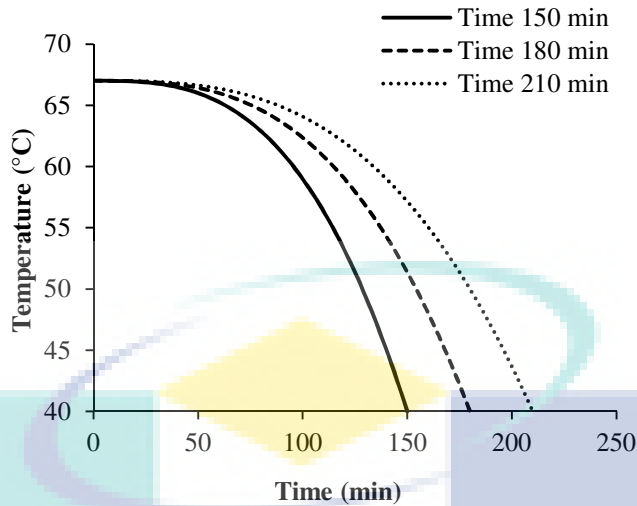


Figure 4.30 Temperature profiles of sucrose crystallization

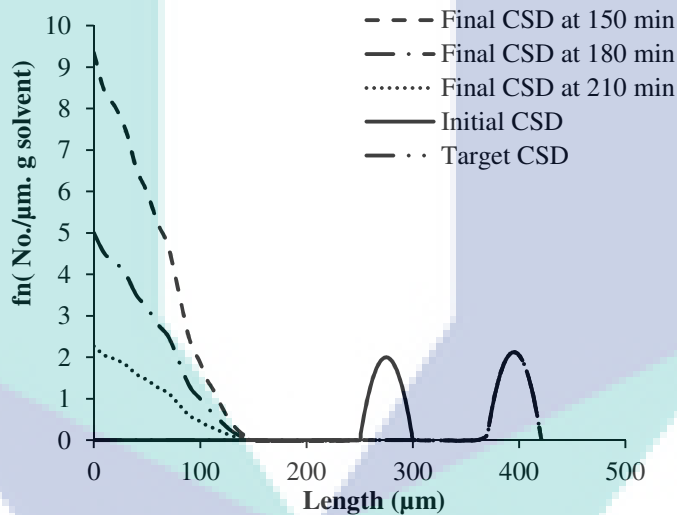


Figure 4.31 Final CSD of sucrose crystallization based on different operation times

Figure 4.31 shows the initial seed and final CSD obtained based on three different set-points for sucrose crystallization process. All of the closed-loop simulation using three different set-points are successfully reaching the desired target CSD where it is matching the shape of target CSD, target mean characteristic length of 395 μm and the peak of CSD around 2.12 no./ μm per gram of solvent. It is proven that the seeded formation for final CSD are tends to agglomerate rather than breakage due to the higher peak of crystal size distribution value obtained compare to initial peak of 2 no./ μm per gram of solvent. Usually the form of the peak remains the same in the case of nucleation and crystal growth only. For the case of agglomeration and breakage, the

final peak obtained is higher than the initial peak. This means that the number of particles is reduced but the characteristic length is increased. Due to agglomeration, particles tend to merge with other particles which explain the reduction of number of particles. As consequence of agglomeration, the characteristic length of particles will be increased when the seed particles are merged with smaller particles. This explains why the peak of CSD for agglomeration and breakage is higher than the initial peak of CSD. However, the secondary peak is also appeared in the final CSD for all set-points due to the nucleation effects that cannot be captured by the analytical estimator. As shown in Figure 4.31, the highest secondary peak was obtained when operating the crystallization process for 150 minutes (supersaturation set-point of 0.0352). Although the target CSD was achieved when operating at this condition however the drawback is higher secondary peak was obtained. This is due to the supersaturation set-point at 0.0352 operated closer to the metastable limit and thus more secondary nucleation has occurred in the operation. The secondary nucleation is not favorable in the crystallization process because it will produces more crystal particles at lower characteristic length and will affecting the growth of crystal seed. Meanwhile supersaturation set-point of 0.0281 and total crystallization time of 210 minutes produce lower secondary peak but the total crystallization time for this operation is too long compared to the others. This is mainly because the crystallizer has been operated close to the saturation line, and under such conditions it will take a long time to achieve the target CSD. If the total crystallization time is taken into consideration then it will not be very practical since the operating costs typically increase the longer the batch runs. As an alternative set-point of 0.0312 at crystallization time of 180 minutes can be selected due to its reasonable operation time while the performance is still acceptable, producing a CSD that is close to the target CSD generated by the analytical CSD estimator. Figure 4.32 shows the close up of target and final CSD obtained for supersaturation set-point of 0.0321 and 180 minutes operation time. It is clearly shown that the final CSD has reach the target in the end of the operation indicating the generated set-point from the extended analytical CSD estimator is indeed reliable and the PI controller successfully maintained the operation at the generated set-point to achieve the target CSD.

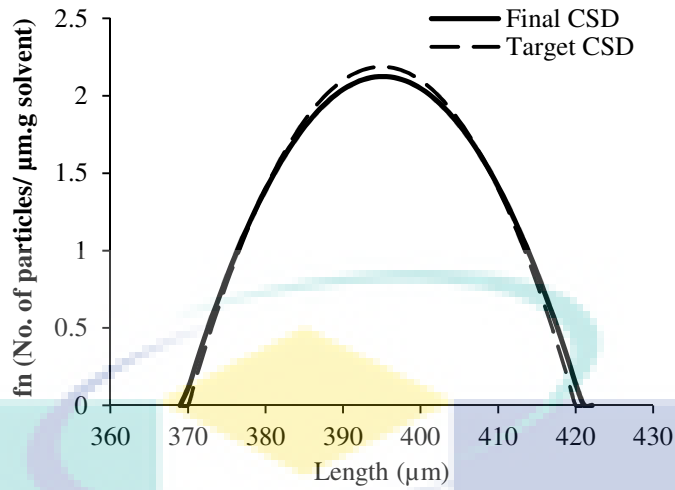


Figure 4.32 Final CSD of sucrose crystallization using 180 minutes operation times

Meanwhile the total mass of crystal particles is increased from 5 g to 590.79 g in Figure 4.33 and Figure 4.34 shows the mean size diameter for the sucrose crystallization process. The initial mean size diameter for seed crystals is 275 μm and the mean size is increased to 614 μm at the end of operation. This is due to the sucrose in the crystallization solution has been transferred into a seed crystal based on the effect of crystal growth phenomena and thus resulting into the increment of the total crystal mass and the mean size diameter of crystal particles.

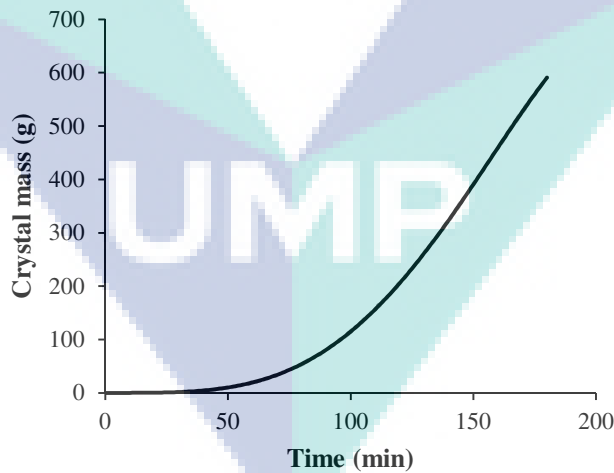


Figure 4.33 Total crystal mass obtained for sucrose crystallization

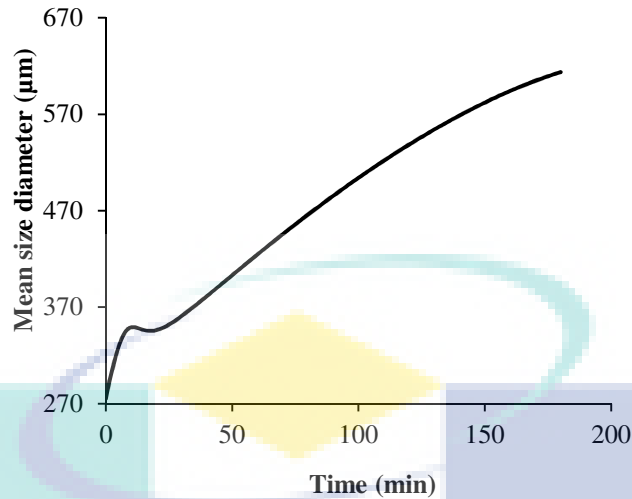


Figure 4.34 Mean size diameter for sucrose crystallization

4.3.8 Robustness Analysis (Step 8)

The PI controller developed for sucrose crystallization is tested for its robustness based on its ability to track the changes of set-point, to handle the disturbances introduced in the process and to deal with the presence of input uncertainties in the uncertainty analysis. The robustness analysis is performed on the closed-loop simulation using crystallization time of 180 minutes.

4.3.8.1 Set-point Tracking and Disturbance Rejection

In the test of set-point tracking, 3 different set-points consisting of 0.042 g/g, 0.00165 g/g and 0.048 g/g are introduced at operational time of 50 minutes, 100 minutes and 140 minutes respectively. Meanwhile for disturbance rejection test, the inlet water flow rate (F_{win}) is decreased by 5% at 54 minutes, increased by 5% at 87 minutes and increased by 7.5% at 140 minutes. Figures 4.35 shows the performance of PI controller during the set-point tracking. Based on the testing, the PI controller reacts well on the change of set-point. However it is noted that the PI controller is a little bit slow to react at time of 111 minutes and 150 minutes when the set-point is changed. The similar situation is also observed during the disturbance rejection test as shown in Figure 4.36 where the PI controller is reacting slowly at time of 87 minutes and 140 minutes. Once the inlet water flow rate (F_{win}) to the crystallization process is altered, the temperature profiles is also changed which contributing to the change of set-point.

Although the PI controller manage to adapt the new set-point but a delay in reacting is observed. This is possibly due to the fact that the value of the integral time constant parameter used in the PI controller is too low for this process which contributes to the slower response during the changes. In overall it can be concluded that the performance of PI controller in the sucrose crystallization process is satisfactory in terms of maintaining the crystallization operation at its set-point. However in some conditions as shown in Figures 4.35 and 4.36, a slower response of PI controller is observed.

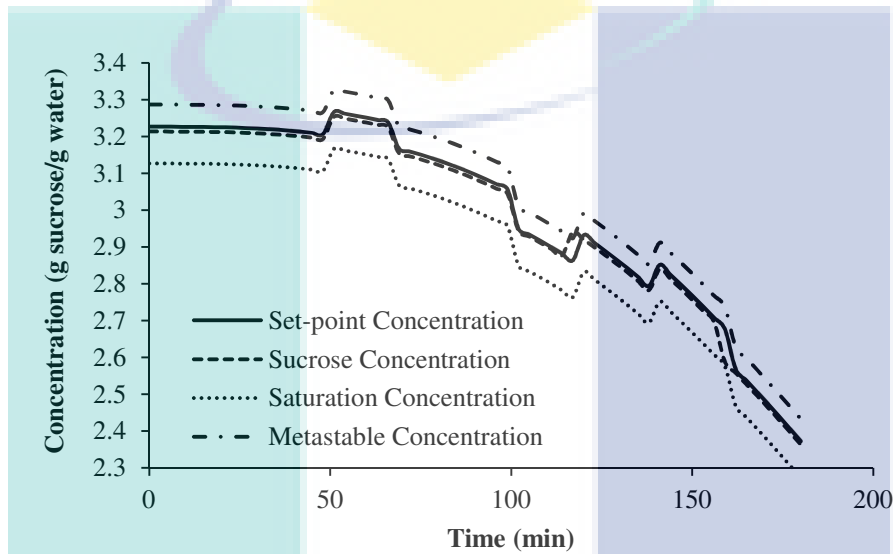


Figure 4.35 Performance of PI controller based on set-point tracking in sucrose crystallization process

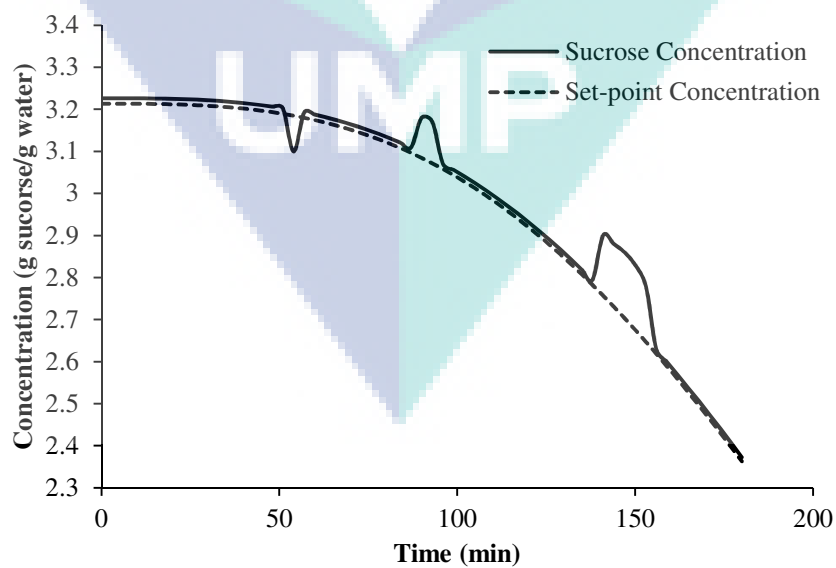


Figure 4.36 Performance of PI controller based on disturbance rejection in sucrose crystallization process

4.3.8.2 Uncertainty Analysis

In the sucrose crystallization case study, eleven parameters (k_b , b , j , p , k_g , g , q , k_a , a , k , r) from the nucleation, crystal growth and production-reduction model equations are selected for performing uncertainty analysis. These parameters are chosen because all of the phenomena are dominant and have a direct influence on the CSD. The parameters estimated from model identification as shown in Tables 4.11-4.13 are used where the lower and upper bound values of each parameter are shown in Table 4.16.

Table 4.16 Input uncertainties for sucrose crystallization

| Parameters | Units | Values | Confidence interval | Lower bound | Upper bound |
|--|--|----------|---------------------|-------------|-------------|
| Nucleation rate constant, k_b | No. /cm ³ .min. (g/cm ³) ^j .(rpm) ^p | 82.4 | ±7.1743 | 75.2257 | 89.5743 |
| Nucleation order constant, b | Dimensionless | 0.0106 | ±0.0024 | 0.0082 | 0.013 |
| Mass order at nucleation, j | Dimensionless | 0.0044 | ±0.0008 | 0.0036 | 0.0052 |
| Agitation order at nucleation, p | Dimensionless | 0.048 | ±0.004 | 0.044 | 0.052 |
| Crystal growth rate, k_g | cm/min.(rpm) ^q | 0.000101 | ±0.000051 | 0.00005 | 0.000152 |
| Crystal growth order constant, g | Dimensionless | 1.00 | ±0.001 | 0.999 | 1.001 |
| Agitation order at crystal growth, q | Dimensionless | 0.5 | ±0.015 | 0.485 | 0.515 |
| Production-reduction rate constant, k_a | No. of particles/cm ³ .min. (g/cm ³) ^k .(rpm) ^r | 1.00 | ±0.01 | 1.01 | 0.99 |
| Production-reduction order constant, a | Dimensionless | 0.085 | ±0.012 | 0.073 | 0.097 |
| Mass order at production-reduction, k | Dimensionless | 0.11 | ±0.03 | 0.08 | 0.14 |
| Agitation order at production-reduction, r | Dimensionless | 0.001 | ±0.0005 | 0.0005 | 0.0015 |

The number of sampling needs to be specified for performing the Monte Carlo simulation. The repetitive test using 10, 50, 75, 100 and 125 samples have been implemented in order to obtain a suitable number of samples which can be obtained based on the lowest Monte Carlo errors as reported by Samad et al. (2013). In this procedure, there are three sub-steps that must be taken into account. The Monte Carlo error calculated for each different number of samples is shown in Table 4.17. As the number of sampling is increased, it is shown that the Monte Carlo error is decreased. In this case the 125 number of samples shows the lowest Monte Carlo error. The Monte Carlo errors can be further decreased by increasing the number of samples to 150 or 200 number of samples but the errors obtained in the case of 100 and 125 number of samples are relatively similar and thus insignificant decrement of Monte Carlo error is expected if the number of samples to 150 or 200 number of samples are used. Therefore the evaluation of input uncertainties on the output prediction is performed based on 125 number of sampling.

Table 4.17 Monte Carlo error for different number of samples in the sucrose crystallization case study

| No. of samples | 10 | 50 | 75 | 100 | 125 |
|-----------------------|-----------|-----------|-----------|------------|------------|
| Mean | 3.1911 | 3.0517 | 2.9546 | 2.9060 | 2.8815 |
| Standard deviation | 0.2433 | 0.3553 | 0.3575 | 0.3596 | 0.3647 |
| Monte Carlo error | 0.0769 | 0.0502 | 0.0412 | 0.0359 | 0.03236 |

The effect of input uncertainties on the temperature and sucrose concentration based on 125 number of sampling are shown in Figures 4.37 and 4.38 where both figures show the profiles of temperature and sucrose concentration based on 125 number of Monte Carlo simulations. Based on Figures 4.37 and 4.38, it is clearly shown that the input uncertainties affecting the temperature and sucrose concentration. For both profiles, the impact of input uncertainties is almost negligible at the beginning of operation but tends to increase by the end of the operation. It has been observed the temperature initially started at 67 °C and cooled down in the range of 35 to 45 °C by the end of operation. Meanwhile a variation in the range of 2.34 to 2.5 g sucrose/g water is obtained at the end of crystallization time as consequence of input uncertainties. Since the temperature profiles is changed then the PI controller needs to be very efficient in order to maintain the level of supersaturation. In this Monte Carlo simulation, the

supersaturation set-point is fixed at 0.0312 g/g for all 125 number of sampling. Thus a PI controller used for maintaining the sucrose concentration is acting aggressively towards the end of the crystallization operation in order to follow the specified supersaturation set-point which explains the variation of sucrose concentration is obtained. This can be seen in the profiles of inlet water temperature as shown in Figure 4.39 where the inlet water temperature has been manipulated vigorously by PI controller in order to deal the effects of input uncertainties.

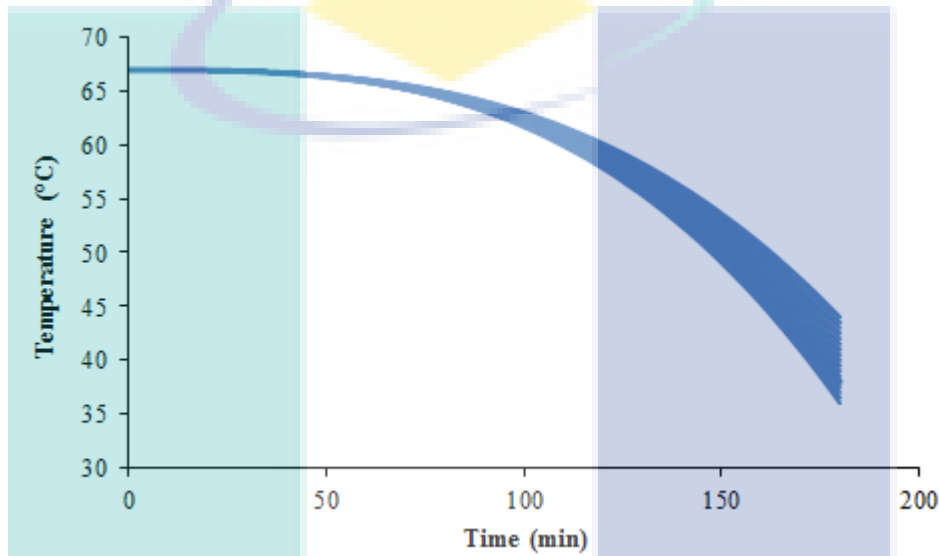


Figure 4.37 Effects of input uncertainties on the temperature for sucrose crystallization

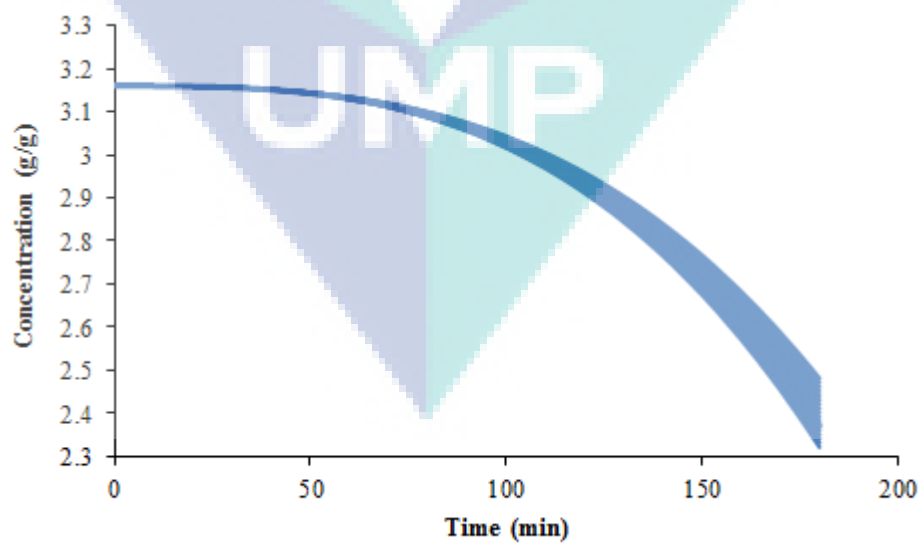


Figure 4.38 Effects of input uncertainties on the concentration for sucrose crystallization

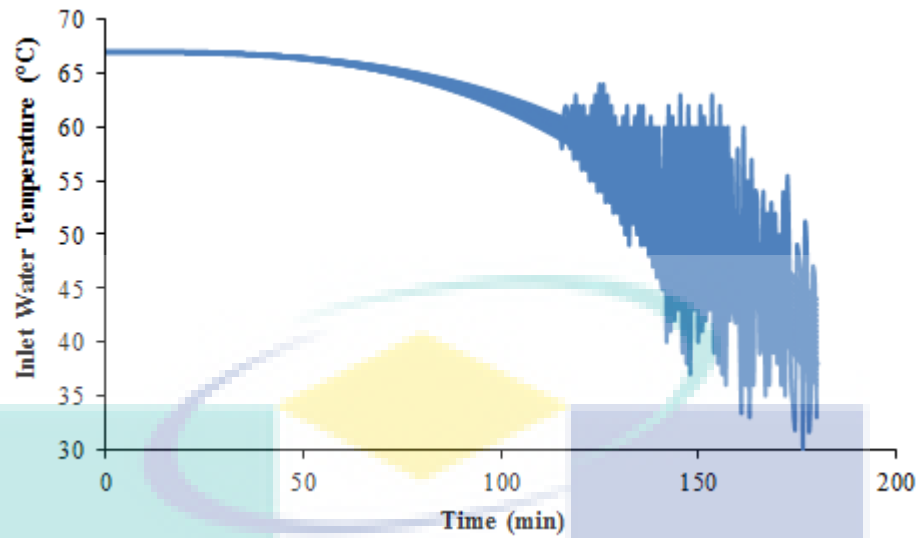


Figure 4.39 Effects of input uncertainties on the inlet water temperature for sucrose crystallization

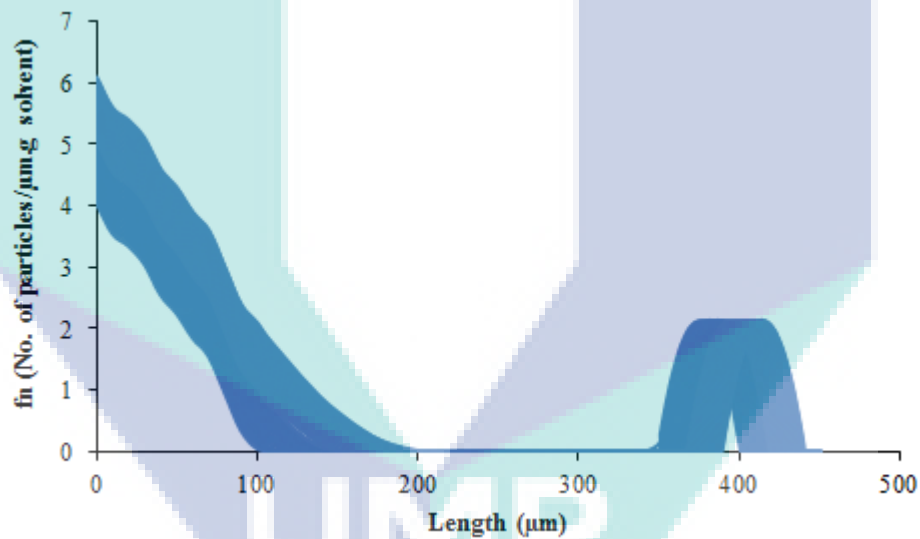


Figure 4.40 Effects of input uncertainties on the CSD for sucrose crystallization

The impact of input uncertainties on the CSD is evaluated as shown in Figure 4.40. High uncertainty is observed on the CSD obtained at final crystallization time. Based on the closed-loop simulation, the final CSD obtained is matching the specified target at the peak of 2.12 no./ μm per gram of solvent and mean characteristic length of 395 μm . However, due to the effect of input uncertainties, the CSD is varied in the range of mean characteristic length of 375 μm to 425 μm . In addition the variability of the secondary peak is also large due to the secondary nucleation. Therefore it is clearly

indicated the impact of input uncertainties is very high on the CSD. This is absolutely true considering the input uncertainties involving the nucleation, crystal growth and production-reduction phenomena are part of the PBE model equations for constructing the CSD. Therefore a different set of parameters for nucleation, crystal growth and production-reduction models are directly contributing to the variability of the CSD. Although the PI controller is performed aggressively to minimize the effect of input uncertainties, but the PI controller only able to directly influence the sucrose concentration and temperature profiles. In this case, a low uncertainty level is observed based on the temperature and sucrose concentration due to the PI controller action but it is still contributing to the high impact of uncertainty on the CSD. In order to further reduce the uncertainty level on the CSD, the PI controller needs to be retuned again for reducing or eliminating the effects of input uncertainties on the temperature and sucrose concentration. The new PI controller parameters after retuning is shown in Table 4.18.

Table 4.18 New PI controller parameters for sucrose crystallization

| | Original tuning parameters | New parameters after retuning |
|-----------------------------|----------------------------|-------------------------------|
| Proportional gain (K_c) | 60 | 70 |
| Integral time (τ_i) | 0.16 | 0.042 |

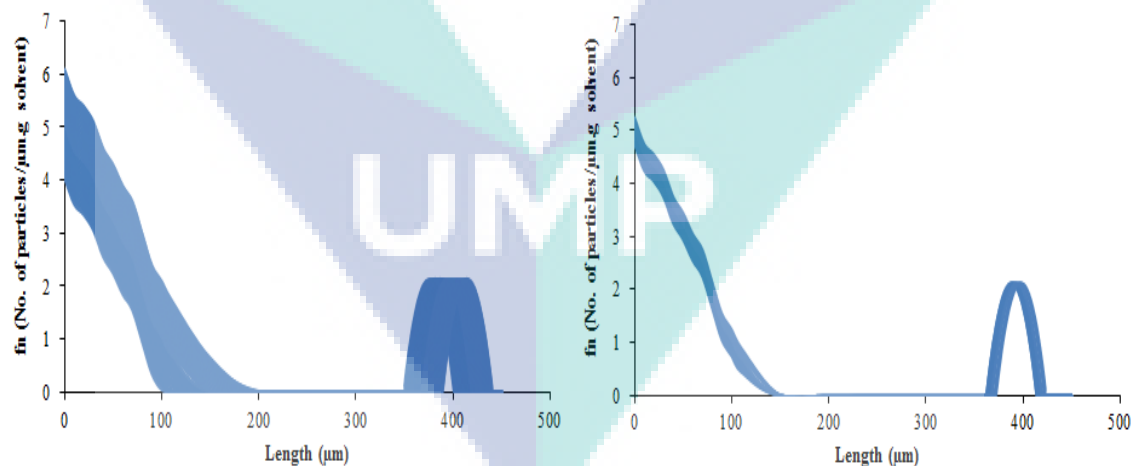


Figure 4.41 Effects of input uncertainties on the CSD for sucrose crystallization before (left) and after retuning (right)

Based on the new PI controller parameters, the Monte Carlo simulation is performed again using 125 number of sampling. The result of Monte Carlo simulation is shown in Figure 4.41 where it is clearly shown the impact of input uncertainties on the CSD has

been minimized. Based on the comparison between before and after retuning, the variability of the product CSD is greatly reduced. In addition the secondary peak obtained after retuning the PI controller parameters shows a significant decrement in terms of variability. The small spread in the CSD as shown in Figure 4.39 indicates the PI controller ability to minimize the effect of input uncertainties. The impact of input uncertainties is further evaluated in terms of mean, 10th percentile and 90th percentile as shown in Figure 4.42. The 10th percentile and 90th percentile is selected because it is realistic representation for evaluating the data. Before retuning the PI controller, the 10th and 90th percentile is further away from the mean of CSD (Figure 4.42(left)) and this distance has been reduced after retuning the PI controller where the 10th and 90th percentile is now very close to the mean of CSD indicating a low extent of uncertainty as shown in Figure 4.42(right). Therefore it can be concluded that the PI controller developed for sucrose concentration is robust enough to maintain the supersaturation at the specified set-point and achieving the target CSD under the presence of input uncertainties.

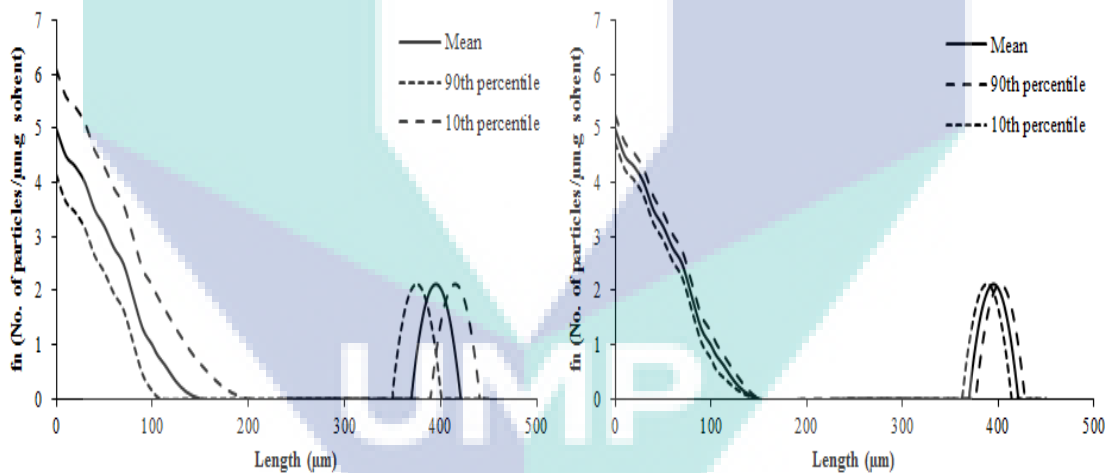


Figure 4.42 Evaluation of input uncertainties on the CSD for sucrose crystallization in terms of mean, 10th percentile and 90th percentile before (left) and after (right) retuning

4.4 Concluding Remarks

The application of the systematic model-based framework for robust supersaturation control has been highlighted through the potassium sulphate and sucrose crystallization case study where the objective is to achieve the desired target

CSD. Through the framework, the necessary mathematical model for both case studies are generated and the model identification for estimating the necessary kinetic parameters are performed. A good agreement has been achieved during open-loop simulation involving both case studies indicating the estimated parameters are reliable. The set-point needed to achieve the desired target CSD has been generated using analytical CSD estimator where through closed-loop simulation, a PI controller is successfully maintaining the operation at its set-point and ultimately producing the desired target of CSD for potassium sulphate and sucrose crystallization case study. This indicates the extended analytical CSD estimator for covering the effects of temperature dependence (in the case of potassium sulphate crystallization) and the effects of agglomeration and breakage (in the case of sucrose crystallization) is able to generate the necessary set-point that guarantees the production of target CSD. In addition the robustness of PI controller is evaluated on two approaches namely the set-point tracking and disturbance rejection as well as uncertainty analysis. In the test of set-point tracking and disturbance rejection, the PI controller performs very well on both case studies but in the uncertainty analysis, the PI controller is not fully able to counteract the input uncertainties and as consequence the variability of the CSD is obtained in potassium sulphate and sucrose case studies. However the impact of input uncertainties are greatly reduced once the PI controller undergoes retuning process. After retuning, the variability of the CSD has been greatly reduced where the 10th percentile and 90th percentile obtained is very close to the mean of the CSD for potassium sulphate and sucrose case studies. This indicates a robust PI controller has been successfully developed for maintaining the operation at various set-points and able to counteract the effect of input uncertainties and retuning the controller is able to minimize the variability in the final CSD.

CHAPTER 5

CONCLUSIONS

5.1 Conclusions

A systematic model-based framework for robust supersaturation control in batch cooling crystallization process has been successfully developed in this work. The main conclusions that have been obtained are summarized as follows:

- a) The developed framework is a step-by-step procedure and it consists of eight main steps. Every steps in this framework has its specific purpose and procedure in order to allow an efficient and structured way to cover a wide range of crystallization operation.
- b) The mathematical model development is proposed in the framework in order to cover a wide range of crystallization operation. For example it is possible to develop a crystallization operation involving the phenomena of nucleation, crystal growth, agglomeration and breakage. Therefore it is possible to study the crystallization operation with or without agglomeration and breakage. For agglomeration and breakage, a production-reduction term is adopted from Quintana-hernandez et al. (2004) to study the effects of agglomeration and breakage on the crystal product. For the PBE solution, the method of classes is employed to represent the crystal product. The application of method of classes is highlighted in the potassium sulphate and sucrose crystallization case studies where this method is capable to generate similar results as method of moments. In addition the use of method of classes overcome the limitation of method of moments in constructing the crystal size distribution (CSD).

- c) The model identification is also included as one of the feature in this framework. Through this framework, it is possible to predict the kinetic parameters of nucleation, crystal growth and production-reduction term. However the use of the model identification is depending on the experimental data of temperature, concentration, total crystal mass, supersaturation or crystal particles. For simplification, experimental data of temperature and concentration must be available for parameter estimation. The ability of the model identification is illustrated in the case of potassium sulphate and sucrose crystallization. Based on the estimation for potassium sulphate crystallization, the 6 kinetic parameters for nucleation and crystal growth obtained from model identification is matching with the literature data. Meanwhile 11 kinetic parameters of nucleation, crystal growth and production-reduction term predicted by model identification is also in good agreement with the literature data indicating a reliable prediction has been obtained. In addition the confidence intervals also calculated for each parameters in both case studies which subsequently be used during uncertainty analysis.
- d) The original analytical CSD estimator for predicting the necessary set-point has been extended in this work to cover the effects of agglomeration and breakage as well as temperature dependence in the kinetic of crystal growth rate. The requirement to use this estimator is the information on initial seed of CSD and target CSD must be available. In addition the kinetic parameters of crystal growth and production-reduction needs to be available as well. For illustrating the application of this estimator, target CSDs for potassium sulphate and sucrose have been specified in this work. Through the information of initial seed of CSD, target CSD and the kinetic parameters obtained from model identification, the optimal set-point has been generated for both case studies through model-based optimization approach.
- e) Through this framework, the crystallization model can be simulated under open- and closed-loop operation. Under open-loop condition, the crystallization operation can be studied in terms of the behavior of concentration, temperature and crystal properties based on natural cooling profile. Meanwhile a PI controller is used to maintain the operation based on set-point generated from

analytical CSD estimator. Therefore the comparison between open-loop and closed-loop can be made and of course a further improvement in terms of crystallization operation and crystal particles can be observed under closed-loop condition. In this work, the open-loop simulation is used for model validation in order to validate the predicted kinetic parameters and for understanding the crystallization operation. Based on this understanding, the closed-loop simulation is applied where it is concluded that the PI controller is successfully maintaining the operation at the generated set-points. The most important finding is the final CSD obtained is matching with the specified target CSD for potassium sulphate and sucrose crystallization indicating the ability of analytical CSD estimator for generating the required set-point which guarantees the target CSD.

- f) The robustness of controller is performed based on two different analysis. The first analysis concerns with the ability of controller to adapt set-point tracking and to reject the disturbance. For both case studies, it has been proven that the PI controller is managed to perform adequately during set-point tracking and disturbance rejection. Therefore the PI controller performance is further tested in uncertainty analysis. In the uncertainty analysis, 6 parameters of nucleation and crystal growth have been identified as input uncertainties in potassium sulphate crystallization. For sucrose crystallization, 11 parameters of nucleation, crystal growth and production-reduction term have been employed. Based on the Monte Carlo simulation, a low uncertainty has been obtained in temperature and concentration profiles but a high extent of uncertainty is achieved in the product CSD. Therefore the PI controller underwent retuning process to increase its robustness. Finally the variability of the CSD has been successfully reduced using the new tuning controller parameters indicating a robust PI controller has been obtained for both potassium sulphate and sucrose crystallization case studies.

5.2 Recommendations for Future Work

The application of the systematic model-based framework in this work has been successfully highlighted through potassium sulphate and sucrose crystallization processes where the robust PI control has been developed to maintain the operation at

the set-point generated by extended analytical CSD estimator and a minimum variation of product CSD has been achieved under input uncertainties. However there are still room for further improvements. The recommendations for future work are summarized as follows:

- a) In this research, all of this work carried out based on the simulation work only. Although it has been proven the simulation is able to represent the required crystallization operation, but it still required the data from experiment. Therefore it would be good to perform the experimental work in order to further verify the strategy proposed in this work particularly the CSD production.
- b) The procedure proposed in this work is implemented based on the crystallization operated on the batch mode. In some of the chemical or pharmaceutical industries, a continuous operation or batch-to-batch operation is preferred. In order to cover this operation, some of the step in the framework for example mathematical model or set-point generation by analytical CSD estimator need to be extended. This is also some recommendations for the future work where this extension enables flexibility of the framework to deal with the changes of operational mode.
- c) In the uncertainty analysis, the input uncertainties considered include the kinetic parameters of nucleation, crystal growth and production-reduction term. Other than kinetic parameters, the initial seed distribution can be used as source of input uncertainties. Usually the initial seed distribution during experimental work is prepared based on the sieving process where it can be contributed to some extent of uncertainties. Therefore it would be interesting to investigate the effect of initial seed distribution on the final CSD in the uncertainty analysis.

REFERENCES

- Aamir, E. (2010). *Population balance model-based optimal control of batch crystallisation processes for systematic crystal size distribution design*. © Erum Aamir.
- Abbas, A., & Romagnoli, J. A. (2007). Multiscale modeling, simulation and validation of batch cooling crystallization. *Separation and Purification Technology*, 53(2), 153-163.
- Amini, Y., Gerdroodbary, M.B., Pishvaie, M.R., Moradi, R. & Monfared, S. M. (2016). Optimal control of batch cooling crystallizer by using genetic algorithm. *Case Studies in Thermal Engineering*, 8, 300-310.
- Aoun, M., Plasari, E., David, R., & Villiermaux, J. (1999). A simultaneous determination of nucleation and growth rates from batch spontaneous precipitation. *Chemical Engineering Science*, 54(9), 1161-1180.
- Artusio, F., & Pisano, R. (2018). Surface induced crystallization of pharmaceuticals and biopharmaceuticals: A review. *International Journal of Pharmaceutics*, 547(1-2), 190-208.
- Acevedo, D., Jarmer, D. J., Burcham, C. L., Polster C. S. & Nagy, Z. K. (2018). A continuous multi-stage mixed-suspension mixed-product removal crystallization system with fines dissolution. *Chemical Engineering Research and Design*, 135, 112-120.
- Baino, F., & Fiume, E. (2018). Quantifying the effect of particle size on the crystallization of 45S5 bioactive glass. *Materials Letters*, 224, 54-58.
- Bhoi, S., Lenka, M., & Sarkar, D. (2017). Particle engineering by optimization for the unseeded batch cooling crystallization. *Crystallization Engineering Communication*, 19, 6373-6382.
- Bohlin, M., & Rasmuson, A. C. (1992). Application of controlled cooling and seeding in batch crystallization. *The Canadian Journal of Chemical Engineering*, 70(1), 120-126.
- Borsos, Á., & Lakatos, B. G. (2012). Simulation and analysis of crystallization of high aspect ratio crystals with fragmentation. *Chemical Engineering Science*, 53, 231-239.
- Canning, T., & Randolph, A. (1967). Some aspects of crystallization theory: Systems that violate McCabe's delta L law. *AIChE Journal*, 13(1), 5-10.

- Cao, Y., Acevedo, D., Nagy, Z. K. & Laird, C. D. (2017). Real time feasible multi-objective optimization based nonlinear model predictive control of particle size and shape in a batch crystallization process. *Control Engineering Practice*, 69, 1-8.
- Cubillas, P., & Anderson, M. W. (2010). Synthesis mechanism: crystal growth and nucleation. *Zeolites and Catalysis: Synthesis, Reactions and Applications*, 1-55.
- De Yoreo, J. J., & Vekilov, P. G. (2003). Principles of crystal nucleation and growth. *Reviews in Mineralogy and Geochemistry*, 54(1), 57-93.
- Derdour, L, Reckamp, J.M., & Pink, C. (2017). Development of reactive slurry salt crystallization to improve solid properties and process performance and scalability. *Chemical Engineering Research & Design*, 121, 207-218.
- Dirksen, J., & Ring, T. (1991). Fundamentals of crystallization: kinetic effects on particle size distributions and morphology. *Chemical Engineering Science*, 46(10), 2389-2427.
- Ditl. P., Beranek. L., Rieger. F., (1996). Simulation of a stirred sugar boiling pan, *Zuckerindustrie* 115(8), 667-676.
- Dunuwila, D. D., & Berglund, K. A. (1997). ATR FTIR spectroscopy for in situ measurement of supersaturation. *Journal of Crystal Growth*, 179(1), 185-193.
- Eek, R. A. (1995). *Control and dynamic modelling of industrial suspension crystallizers*: Technische Universiteit Delft.
- Everett. J., (1976). Effects of supersaturation and temperature on nucleation and crystal growth in a MSMPR crystallizer. Retrospective Theses and Dissertations. Helt Iowa State University. Page 6213.
- Forgione, M., Birpoutsoukis, G., Bombois, X., Mesbah, A., Daudey, P.J. & Van den Hof, P. M. J. (2015). Batch-to-batch model improvement for cooling crystallization. *Control Engineering Practice*, 41, 72-82.
- Fujiwara, M., Nagy, Z. K., Chew, J. W., & Braatz, R. D. (2005). First-principles and direct design approaches for the control of pharmaceutical crystallization. *Journal of Process Control*, 15, 493-504.
- Fujiwara, M., Chow, P. S., Ma, D. L., & Braatz, R. D. (2002). Paracetamol crystallization using laser backscattering and ATR-FTIR spectroscopy: metastability, agglomeration, and control. *Crystal Growth & Design*, 2(5), 363-370.

- Gao, Z., Rohani, S., Gong, J., & Wang, J. (2017). Recent development in crystallization process: Toward the pharmaceutical industry. *Engineering*, 3(3), 343-353.
- Geankoplis, C. (2003). *Transport processes and separation process principles (includes unit operations)*: Prentice Hall Press.
- Gernaey, K. V., Cervera-Padrell, A. E., & Woodley, J. M. (2012). A perspective on PSE in pharmaceutical process development and innovation. *Computers & Chemical Engineering*, 42, 15-29.
- Ghadipasha, N., Romagnoli, J. A., Tronci, S., & Baratti, R. (2018). A model-based approach for controlling particle size distribution in combined cooling-antisolvent crystallization processes. *Chemical Engineering Science*, 190, 260-272.
- Gimbutu, J., Nagy, Z. K., & Rielly, C. D. (2009). Simultaneous quadrature method of moments for the solution of population balance equations, using a differential algebraic equation framework. *Industrial & Engineering Chemistry Research*, 48(16), 7798-7812.
- Giulietti, M., Seckler, M., Derenzo, S., Ré, M., & Cekinski, E. (2001). Industrial crystallization and precipitation from solutions: state of the technique. *Brazilian Journal of Chemical Engineering*, 18(4), 423-440.
- Gunawan, R., Fusman, I., & Braatz, R. D. (2004). High resolution algorithms for multidimensional population balance equations. *AIChE Journal*, 50(11), 2738-2749.
- Helton, J. C., & Davis, F. J. (2003). Latin hypercube sampling and the propagation of uncertainty in analyses of complex systems. *Reliability Engineering & System Safety*, 81(1), 23-69.
- Hemalatha, K., Nagveni, P., Kumar, P. N., & Rani, K. Y. (2018). Multiobjective optimization and experimental validation for batch cooling crystallization of citric acid anhydrate. *Computers & Chemical Engineering*, 112, 292-303.
- Hojjati, H., & Rohani, S. (2005). Cooling and seeding effect on supersaturation and final crystal size distribution (CSD) of ammonium sulphate in a batch crystallizer. *Chemical Engineering and Processing: Process Intensification*, 44(9), 949-957.
- Hu, Q., Rohani, S., & Jutan, A. (2005). Modelling and optimization of seeded batch crystallizers. *Computers & Chemical Engineering*, 29(4), 911-918.

- Hulburt, H. M., & Katz, S. (1964). Some problems in particle technology: A statistical mechanical formulation. *Chemical Engineering Science*, 19(8), 555-574.
- Iman, R. L., & Conover, W.-J. (1982). A distribution-free approach to inducing rank correlation among input variables. *Communications in Statistics-Simulation and Computation*, 11(3), 311-334.
- Ji, X., Curcio, E., Al Obaidani, S., Di Profio, G., Fontananova, E., & Drioli, E. (2010). Membrane distillation-crystallization of seawater reverse osmosis brines. *Separation and Purification Technology*, 71(1), 76-82.
- Jones, A. G., & Mullin, J. (1974). Programmed cooling crystallization of potassium sulphate solutions. *Chemical Engineering Science*, 29(1), 105-118.
- Jones, F., Piana, S., & Gale, J. (2008). Understanding the kinetics of barium sulfate precipitation from water and water-methanol solutions. *Crystal Growth and Design*, 8(3), 817-822.
- Konstantakou, M., Perganti, D., Falaras, P. & Stergiopoulos, T. (2017). Anti-solvent crystallization strategies for highly efficient perovskite solar cells. *Crystals*, 7(10), 1-21.
- Laloue, N., Couenne, F., Le Gorrec, Y., Kohl, M., Tanguy, D., & Tayakout-Fayolle, M. (2007). Dynamic modeling of a batch crystallization process: A stochastic approach for agglomeration and attrition process. *Chemical Engineering Science*, 62(23), 6604-6614.
- Lenka, M., & Sarkar, D. (2018). Combined cooling and antisolvent crystallization of l-asparagine monohydrate. *Powder Technology*, 334, 106-116.
- Marchal, P., David, R., Klein, P. & Villermaux, J. (1988). Crystallization and precipitation engineering - I. An efficient method for solving population balance in crystallization with agglomeration. *Chemical Engineering Science*, 43(1), 59-67.
- Mersmann, A. (1995). Crystallization technology handbook. *Drying Technology*, 13(4), 1037-1038.
- Mesters, J. R. (2007). Practical protein crystallization *Principles of Protein X-Ray Crystallography* (pp. 297-304): Springer.
- Myerson, A. (2002). *Handbook of industrial crystallization*: Butterworth-Heinemann.
- Nagy, Z., & Aamir, E. (2012). Systematic design of supersaturation controlled crystallization processes for shaping the crystal size distribution using an analytical estimator. *Chemical Engineering Science*, 84, 656-670.

- Nagy, Z. K., Chew, J. W., Fujiwara, M., & Braatz, R. D. (2008). Comparative performance of concentration and temperature controlled batch crystallizations. *Journal of Process Control*, 18(3), 399-407.
- Nakamura, K., Sora, Y., Yoshikawa, H. Y., Hosokawa, Y., Murai, R., Adachi, H., Mori, Y., Sasaki, T., & Masuhara, H. (2007). Femtosecond laser-induced crystallization of protein in gel medium. *Applied Surface Science*, 253(15), 6425-6429.
- Paengjuntuek, W., Kittisupakorn, P., & Arpornwichanop, A. (2008). Optimization and nonlinear control of a batch crystallization process. *Journal of the Chinese Institute of Chemical Engineers*, 39(3), 249-256.
- Park, M.-W., & Yeo, S.-D. (2012). Antisolvent crystallization of carbamazepine from organic solutions. *Chemical Engineering Research and Design*, 90(12), 2202-2208.
- Perez-Calvo, J-F, Kadam, S.S. & Kramer, H.J.M. (2016). Determination of kinetics in batch cooling crystallization processes-A sequential parameter estimation approach. *AIChE Journal*. 62, 3992-4012.
- Powell. K.A., Croker. D.M., Rielly. C.D., Nagy. Z.K., (2016). PAT-based design of agrochemical co-crystallization processes. *Chemical Engineering Science*. 152, 95-108.
- Puel, F., Fevotte, G., & Klein, J. (2003). Simulation and analysis of industrial crystallization processes through multidimensional population balance equations. Part 2: a study of semi-batch crystallization. *Chemical Engineering Science*, 58(16), 3729-3740.
- Quintana-Hernández, P., Bolaños-Reynoso, E., Miranda-Castro, B., & Salcedo-Estrada, L. (2004). Mathematical modeling and kinetic parameter estimation in batch crystallization. *AIChE Journal*, 50(7), 1407-1417.
- Rao. C.N.R., Muller., Cheetham. A.K., (2007). Retrieved from Nanomaterials Chemistry, Copyright 8.
- Saengchan, A., Kittisupakorn, P., Paengjuntuek, W. & Arpornwichanop, A. (2011). Improvement of batch crystallization control under uncertain kinetic parameters by model predictive control. *Journal of Industrial and Engineering Chemistry*, 17, 430-438.

- Samad, N. A. F. A., & Saleh, S. (2016). Reducing the effect of input uncertainties using model predictive control for crystallization process. *ARPJ Journal of Engineering and Applied Sciences*, 11(4), 2660-2667.
- Samad, N. A. F. A., Sin, G., Gernaey, K. V., & Gani, R. (2013). A systematic framework for design of process monitoring and control (PAT) systems for crystallization processes. *Computers & Chemical Engineering*, 54, 8-23.
- Samad, N. A. F. A., Singh, R., Sin, G., Gernaey, K. V., & Gani, R. (2011). A generic multi-dimensional model-based system for batch cooling crystallization processes. *Computers & Chemical Engineering*, 35(5), 828-843.
- Shi, D., El-Farra, N. H., Li, M., Mhaskar, P., & Christofides, P. D. (2006). Predictive control of particle size distribution in particulate processes. *Chemical Engineering Science*, 61(1), 268-281.
- Shiau, L.-D., & Lu, T.-S. (2004). Programmed cooling of a batch crystallizer in the presence of growth rate dispersion. *Journal of the Chinese Institute of Chemical Engineers*, 35(6), 677-682.
- Simone, E., Szilagy, B., & Nagy, Z. K. (2017). Systematic model identification and optimization-based active polymorphic control of crystallization processes. *Chemical Engineering Science*, 174, 374-386.
- Sin, G., Gernaey, K. V., Neumann, M. B., van Loosdrecht, M. C., & Gujer, W. (2009). Uncertainty analysis in WWTP model applications: a critical discussion using an example from design. *Water Research*, 43(11), 2894-2906.
- Spina, R., Spekowius, M., & Hopmann, C. (2018). Simulation of crystallization of isotactic polypropylene with different shear regimes. *Thermochimica Acta*, 659, 44-54.
- Vetter, T., Burcham, C. L., & Doherty, M. F. (2014). Regions of attainable particle sizes in continuous and batch crystallization processes. *Chemical Engineering Science*, 106, 167-180.
- Wang, H., & Ward, J. D. (2016). Dynamics and control of continuous reactive crystallization processes. *Journal of the Taiwan Institute of Chemical Engineers*, 65, 28-42.
- Wang, J., Li, F., & Lakerveld, R. (2018). Process intensification for pharmaceutical crystallization. *Chemical Engineering and Processing - Process Intensification*, 127, 111-126.

- Wang, L., & Dong, C. M. (2006). Synthesis, crystallization kinetics, and spherulitic growth of linear and star-shaped poly (L-lactide) s with different numbers of arms. *Journal of Polymer Science Part A: Polymer Chemistry*, 44(7), 2226-2236.
- Wang, T., Lu, H., Wang, J., Yan, X., & Hao, H. (2018). Recent progress of continuous crystallization. *Journal of Industrial and Engineering Chemistry*, 54, 14-29.
- Wibowo, C., Kelkar, V. V., Samant, K. D., Schroer, J. W., & Ng, K. M. (2006). Development of reactive crystallization processes. *Integrated Chemical Processes: Synthesis, Operation, Analysis, and Control*, 339-358.
- Widenski, D., Abbas, A., & Romagnoli, J. (2010). Comparison of different solubility equations for modeling in cooling crystallization. *Chemical Engineering and Processing: Process Intensification*, 49(12), 1284-1297.
- Wohlgemuth, K., & Schembecker, G. (2013). Modeling induced nucleation processes during batch cooling crystallization: A sequential parameter determination procedure. *Computers & Chemical Engineering*, 52, 216-229.
- Yang, G., Li, X., & Qian, Y. (2014). A real time updated model predictive control strategy for batch processes based on state estimation. *Computers & Chemical Engineering*, 33, 22-42.
- Yamba, O.A., Steinbuch M., Landlust J., Wildenberg J., & Backx T, (2008). Cooling crystallization, PID and MPC Control. 144, 463-474.
- Zarabad, M. S., & Rezvani, M. (2018). Time-temperature-transformation diagrams for crystallization of the oxyfluoride glass system. *Results in Physics*, 10, 356-359.
- Zhang, D., Xu, S., Du, S., Wang, J., & Gong, J. (2017). Progress of pharmaceutical continuous crystallization. *Green Chemical Engineering Review*, 3(3), 354-364.
- Zumstein, R., & Rousseau, R. (1987). Growth rate dispersion in batch crystallization with transient conditions. *AIChE journal*, 33(11), 1921-1925.

APPENDIX A LIST OF PUBLICATIONS

A-1 Journals

- Zahari, Z.M., Saleh, S. & Samad, N.A.F.A. (2018). Reducing the effect of input uncertainties on the crystal size distribution in the case of agglomeration and breakage for batch cooling crystallization process. *Journal of Chemical and Biochemical Engineering Quarterly (Submitted)*.
- Zahari, Z.M., Saleh, S. & Samad, N.A.F.A. (2018). A systematic model-based framework of supersaturation controlled crystallization process for achieving the target crystal size distribution. *Computer and Chemical Engineering (Submitted)*.
- Zahari, Z.M., Adnan, S.Z., Kanthasamy, R., Saleh, S. & Samad, N.A.F.A. (2018). Supersaturation control using analytical crystal size distribution estimator for temperature dependent in nucleation and crystal growth phenomena. *IOP Conference Series: Materials Science and Engineering*, 318: 012013.
- Zahari, Z.M., Saleh, S. & Samad, N.A.F.A. (2017). Achieving the target crystal size distribution in the case of agglomeration and breakage for batch cooling crystallization process. *Chemical Engineering Transaction*, 56: 205–210.
- Zahari, Z.M., Saleh, S. & Samad, N.A.F.A. (2017). Achieving the target crystal size distribution in the case of agglomeration and breakage for batch cooling crystallization process. *Australian Journal of Basic and Applied Sciences*, 11(3): 128–136.

A-2 Conferences (Oral Presentation)

- Zahari, Z.M., Adnan, S.Z., Kanthasamy, R., Saleh, S. & Samad, N.A.F.A. (2017). Supersaturation control using analytical crystal size distribution estimator for temperature dependent in nucleation and crystal growth phenomena. *Malaysian Universities Conference on Engineering and Technology (MUCET 2017)*.
- Zahari, Z.M., Saleh, S. & Samad, N.A.F.A. (2016). Achieving the target crystal size distribution in the case of agglomeration and breakage for batch cooling crystallization process. *Regional Conference on Chemical Engineering (RCChE 2016)*.

Zahari, Z.M., Saleh, S. & Samad, N.A.F.A. (2016). Achieving the target crystal size distribution in the case of agglomeration and breakage for batch cooling crystallization process. *International Conference of Chemical Engineering and Industrial Biotechnology (ICCEIB 2016)*.

